NASA CONTRACTOR REPORT

NASA CR-2365

NASA CR-2365

FINITE-DIFFERENCE SOLUTION FOR TURBULENT SWIRLING COMPRESSIBLE FLOW IN AXISYMMETRIC DUCTS WITH STRUTS

by O. L. Anderson

Prepared by
UNITED AIRCRAFT CORPORATION
East Hartford, Conn. 06108
for Lewis Research Center

NATIONAL AERONAUTICS AND SPACE ADMINISTRATION • WASHINGTON, D. C. • FEBRUARY 1974

1. Report No.	2. Government Accession No.	3. Recipient's Catalog No.
NASA CR-2365		

4. Title and Subtitle	5. Report Date
FINITE-DIFFERENCE SOLUTION FOR TURBULENT SWIRLING COMPRESSIBLE FLOW IN AXISYMMETRIC DUCTS WITH STRUTS	February 1974
	6. Performing Organization Code

7. Author(s)	8. Performing Organization Report No.
O. L. Anderson	L911211-1
	10. Work Unit No.

9. Performing Organization Name and Address	11. Contract or Grant No.
United Aircraft Corporation 400 Main Street East Hartford, Connecticut 06108	NAS 3-15402
	13. Type of Report and Period Covered
12. Sponsoring Agency Name and Address	Contractor Report
National Aeronautics and Space Administration Washington, D. C. 20546	14. Sponsoring Agency Code

15. Supplementary Notes

Final Report. Project Manager, Bernhard H. Anderson, Wind Tunnel and Flight Division, NASA Lewis Research Center, Cleveland, Ohio

16. Abstract

A finite-difference procedure for computing the turbulent, swirling, compressible flow in axisymmetric ducts is described. Arbitrary distributions of heat and mass transfer at the boundaries can be treated, and the effects of struts, inlet guide vanes, and flow straightening vanes can be calculated. The calculation procedure is programmed in FORTRAN IV and has operated successfully on the UNIVAC 1108, IBM 360, and CDC6600 computers. The analysis which forms the basis of the procedure, a detailed description of the computer program, and the input/output formats are presented. The results of sample calculations performed with the computer program are compared with experimental data.

17. Key Words (Suggested by Author(s))	18. Distribution Statement
Propulsion Diffusers Finite difference solution	Unclassified - unlimited

19. Security Classif. (of this report)	20. Security Classif. (of this page)	21. No. of Pages	22. Price*
Unclassified	Unclassified	152	Domestic, $4.75 Foreign, $7.25

* For sale by the National Technical Information Service, Springfield, Virginia 22151

TABLE OF CONTENTS

SUMMARY

A finite-difference procedure for computing the turbulent, swirling, compressible flow in axisymmetric ducts is described. Arbitrary distributions of heat and mass transfer at the boundaries can be treated and the effects of struts, inlet guide vanes, and flow straightening vanes can be calculated. The calculation procedure is programmed in FØRTRAN IV and has operated successfully on the UNIVAC 1108, IBM 360, and CDC6600 computers. The analysis which forms the basis of the procedure, a detailed description of the computer program, and the input/output formats are presented. The results of sample calculations performed with the computer program are compared with experimental data.

2.0 INTRODUCTION

A continuing problem in the development of air breathing propulsion systems is the design of efficient subsonic diffusers. Not only is the engineer faced with building an efficient diffuser, but frequently he must tailor the exit flow within certain physical constraints imposed by the propulsion engine. This task has proven extremely difficult in the past since the engineer has been forced to rely on empirical design methods based on correlations of limited experimental data. Diffuser performance maps based on empirical correlations have been published by Reneau (Ref. 1) for incompressible two-dimensional flow and by Sovran (Ref. 2) for incompressible annular flow. These performance maps generally correlate pressure rise coefficient with area ratio and length and serve as useful design tools within the class of geometries tested. In addition, regions of stall on the performance map have been defined by Fox (Ref. 3) for two-dimensional diffusers and by Howard (Ref. 4) for annular diffusers. Thus, reasonable bounds have been set for the design of unstalled diffusers. Sovran (Ref. 2) has developed a correlation for pressure rise coefficient as a function of inlet blockage due to boundary layer displacement, thus adding a new parameter to the correlations. The effect of inlet Mach number has been examined by Runstadler (Ref. 5) for two-dimensional diffusers and performance maps published. Comparable performance maps for annular diffusers apparently have not been published.

Even with the large effort that has been expended in the past in the development of empirical diffuser design methods, sufficiently generalized methods have not been forthcoming. Considering the vast number of geometric parameters, such as area ratio, length, wall curvature, and support struts, together with the physical flow parameters, such as Mach number, Reynolds number, swirl angle, and inlet flow distortion, it is evident that the development of such methods will be extremely time consuming and very costly. Clearly, the availability of accurate analytical design tools would enable the engineer to arrive at an efficient design for a specialized diffuser in a much shorter period of time at less cost while at the same time providing a better understanding of the diffuser flow processes.

The development of analytical diffuser design methods has generally not kept pace with empirical studies. The conventional solutions, such as that used by Sovran (Ref. 2), divide the flow field into an irrotational free-stream flow and a boundary layer flow. These methods, which require an iteration between the potential flow pressure field and the boundary layer displacement thickness, frequently fail to converge when the boundary layers merge and cannot account for such problems as inlet swirl and flow distortion. Recently, however, Anderson introduced a new method (Refs. 6 and 7) for solving the diffuser flow problem. This method involves numerically solving the equations of motion for the entire flow in the diffuser thereby enabling compatibility between the inviscid flow and boundary layer to be achieved without the need for matching a boundary layer solution to an inviscid flow

solution. The method provides the accurate analytical design tool required to define optimum diffuser designs for a wide range of applications in a short period of time at a minimum of cost. Good agreement in the prediction of pressure rise coefficient and stall has been demonstrated for both straight-wall and curved-wall unseparated diffusers. In addition, Anderson has demonstrated the applicability of the method to the treatment of the effects of inlet distortion and inlet swirl.

This user's manual describes an extension of the method of Ref. 6, to enable the calculation of swirling, turbulent compressible flows in axisymmetric ducts. A generalization of the method to include treatment of arbitrary distributions of heat and mass transfer at the boundaries and the effects of struts or blades in the diffuser passage is also described.

3.0 ANALYSIS

The present analysis represents an extension to compressible flow of the analysis presented in Refs. 6 and 7 for computing incompressible swirling flows in axisymmetric ducts. The unique feature of the analysis is that a conceptual division of the flow into an inviscid, irrotational flow and boundary layer is not made but rather the analysis solves for the entire flow across the duct at each streamwise station. The problems of matching solutions for the inviscid flow and boundary layer are thereby eliminated and no difficulties exist when the boundary layers on the duct walls merge. The analysis supposes that the streamlines of the actual flow through the duct will not be appreciably different from the potential flow streamlines; an assumption which from simple physical considerations must remain valid for internal duct flows with only small regions of separation. Thus it is possible to make boundary layer-type approximations, such as supposing the transverse velocity is small, in a coordinate system based upon the stream function and velocity potential of the potential flow. In this manner, the viscous effects can be treated as a perturbation upon the inviscid field and, as such, governed by a parabolic partial differential equation. The elliptic properties of the flow (i.e., downstream conditions affecting the upstream flow), are retained through the choice of the potential flow streamlines as the coordinate system for the parabolic partial differential equation. Included in the present analysis is the capability for treating the effect of struts, inlet guide vanes, and flow straightening vanes, as well as the effect of distributed wall bleed.

A description of the various components of the analysis is presented in the following subsections.

3.1 Streamline Coordinate System

The orthogonal streamline coordinate system used in the present analysis is a simplified version of the coordinate system described in Ref. 7. The coordinate system of Ref. 7 was obtained from the solution of the plane potential flow through the duct in question where the stream function formed the normal coordinate and the velocity potential S formed the streamwise coordinate. Rotation of this solution about the axis of symmetry provides the third coordinate (see Fig. 3.1.1). As demonstrated in Ref. 7, use of this coordinate system provides a means of reducing the general equations of motion for the diffuser from an elliptic set of equations to a parabolic set of equations by making the well-justified assumption, for unstalled diffusers, that the flow normal to the streamwise coordinate is small. A second advantage is that since the equations of motion are written in generalized curvilinear coordinates, more general curved wall duct geometries can be treated.

The stream function η and velocity potential S used to generate this potential flow coordinate system satisfy Laplace's equation, that is

$$\frac{\partial^2 \eta}{\partial R^2} + \frac{\partial^2 \eta}{\partial Z^2} = 0 \tag{3.1.1}$$

$$\frac{\partial^2 S}{\partial R^2} + \frac{\partial^2 S}{\partial Z^2} = 0 \tag{3.1.2}$$

In addition to the wall boundary condition, $\eta = 0$ along the inner wall and $\eta = 1$ along the outer wall, the condition of no normal pressure gradients at the inlet and exit of the duct ($\partial V/\partial \eta = 0$) must be satisfied where V is the potential flow velocity or metric scale coefficient. Thus from orthogonality conditions, the angle that the potential flow streamline makes with the axis of symmetry (see Fig. 3.1.1) becomes

$$\cos\theta = V \frac{\partial R}{\partial \eta} = V \frac{\partial Z}{\partial S} \tag{3.1.3}$$

$$\sin\theta = V \frac{\partial R}{\partial S} = -V \frac{\partial Z}{\partial \eta} \tag{3.1.4}$$

The curvature of the coordinates are given by

$$\frac{1}{\rho_s} = -\frac{\partial V}{\partial n} \tag{3.1.5}$$

$$\frac{1}{\rho_n} = -\frac{\partial V}{\partial s} \tag{3.1.6}$$

Distances along the three coordinates are determined from the metric scale coefficients.

$$Y = \int \frac{dn}{V} \tag{3.1.7}$$

$$X = \int \frac{ds}{V} \tag{3.1.8}$$

$$R\phi = \int R\,d\phi \tag{3.1.9}$$

It should be noted that this coordinate system is not the only orthogonal coordinate system that can be constructed from the plane potential flow solution. The solution is made unique only with the boundary condition $dV/dn = 0$ at the inlet and exit of the duct. This boundary condition, as shown in Ref. 7, implies a zero normal static pressure gradient at the inlet and exit of the duct in the absence of swirl. Ducts with normal pressure gradients at the inlet and exit can be treated by extending the duct with the required curvature.

Because of the requirement that the n and s coordinates be accurately determined up to third derivatives, extreme care must be exercised in obtaining the potential flow solution by numerically solving Eqs. (3.1.1) and (3.1.2) as described in Ref. 7. In addition, such a numerical solution requires significant computer time. Accordingly, for the present analysis a method of approximating the potential flow coordinate system which yields accurate coordinate derivatives and saves computer

time was used. This approximate method has proven adequate providing the diffuser wall does not have rapid changes in wall curvature or large diffusion angles. Since these conditions would generally lead to separation, which the analysis is presently not capable of handling, use of this approximate method represents little additional sacrifice in generality. The approximate potential flow coordinate system is obtained as follows.

Assuming that the curvatures are small, it is possible to construct a circular arc of radius $\bar{\rho}_n$ (see Fig. 3.1.2), such that it satisfies the orthogonality relations, Eqs. (3.1.3) and (3.1.4), on the duct walls and mean line. Then from Eq. (3.1.5)

$$\frac{\partial V}{\partial n} = (V_T - V_H) = -\frac{1}{\bar{\rho}_s} \tag{3.1.10}$$

and

$$V = \frac{V_T + V_H}{2} + (V_T - V_H)(n - 1/2) = V_M - \frac{n - 1/2}{\bar{\rho}_s} \tag{3.1.11}$$

The radius of the circular arc, from Eq. (3.1.6), is given by

$$\frac{1}{\bar{\rho}_n} = -\frac{\partial V_M}{\partial S} \tag{3.1.12}$$

where second order terms in $1/\bar{\rho}_s$ are neglected. The distances along the arc, which approximates a potential line is given by

$$Y = \bar{\rho}_s \, \theta \tag{3.1.13}$$

and the distance along the chord in terms of the diffusion angle θ is,

$$Y = 2\,\bar{\rho}_s \, \sin \theta/2 \simeq Y - O(\theta^3) \tag{3.1.14}$$

Hence for small diffusion angles, $\theta << 1$, the distance along the arc can be represented by the distance along the chord line. The potential line must now satisfy the orthogonality relations. On the wall, from Eqs. (3.1.3) and (3.1.8),

$$\frac{1}{V} = \frac{1}{\sqrt{1+\left(\frac{dR}{dt}\right)^2}} \frac{dZ}{dS} = \frac{dX}{dS} \tag{3.1.15}$$

Hence, for two adjacent potential lines

$$\frac{V_H}{V_T} = \frac{\Delta X_T}{\Delta X_H} \tag{3.1.16}$$

and from Eq. (3.1.7)

$$Y_M \, Y_T = 1 \tag{3.1.17}$$

The metric scale coefficient can be found from Eqs. (3.1.16) and (3.1.17), once the potential lines are determined. These potential lines are described by chord lines (see Fig. 3.1.2) which are perpendicular to the mean line of the duct

$$R_M = (R_H + R_T)/2 \tag{3.1.18}$$

satisfying the relation

$$\frac{dR_M}{dZ} = \frac{1}{2}\left[\frac{dR_H}{dZ} + \frac{dR_T}{dZ}\right] = -\frac{Z_T - Z_H}{R_T - R_H} \tag{3.1.19}$$

In summary, the streamline coordinate system is constructed by first locating the chord lines according to Eq. (3.1.19), calculating the metric scale coefficients along the wall from Eqs. (3.1.16), (3.1.17), and, finally, determining the curvatures from Eqs. (3.1.10) and (3.1.12).

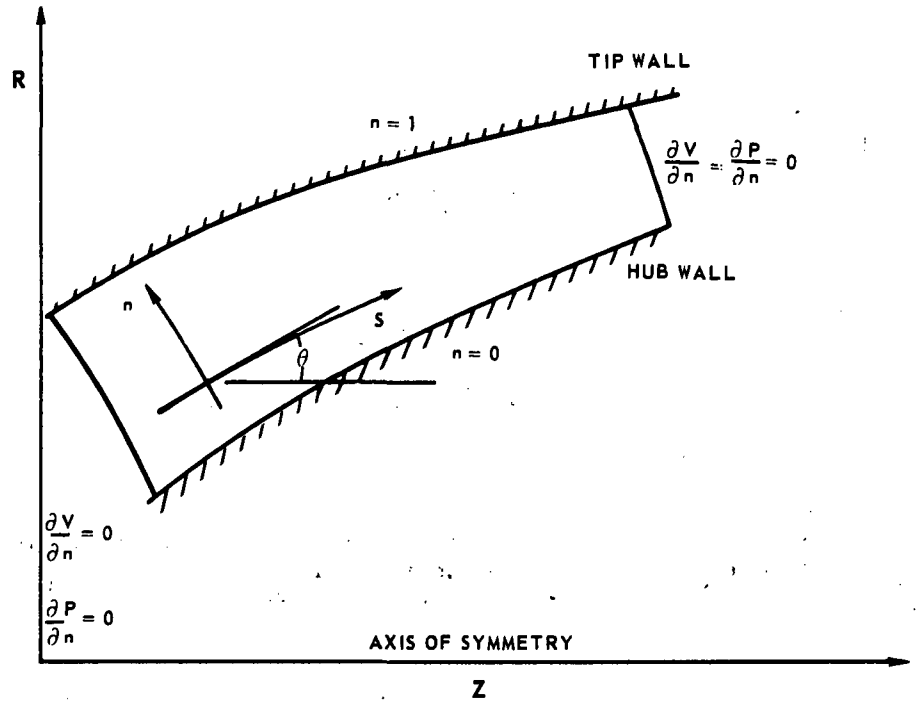

FIG. 3.1.1–ORTHOGONAL STREAMLINE COORDINATE SYSTEM.

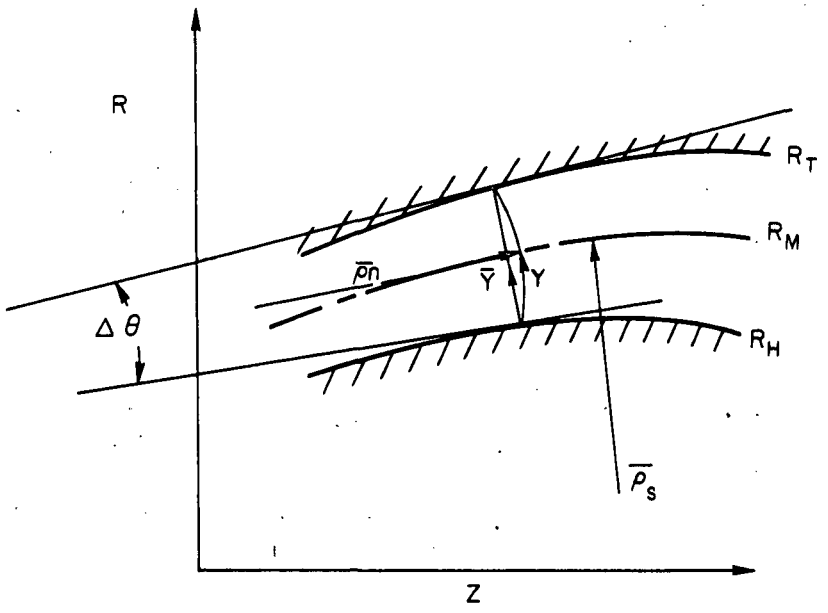

FIG. 3.1.2-CONSTRUCTION OF STREAMLINE COORDINATES.

3.2 Equations of Motion

The equations of motion for a compressible flow in a general orthogonal curvilinear coordinate system have been derived by Pai (Ref. 8). Substitution of the metric scale coefficients (1/V, 1/V, R) into the equations derived in Ref. 8 produce the following equations of motion in the streamline coordinate system described in Section 3.1.

Continuity Equation

$$\frac{\partial \rho}{\partial t} + \frac{V^2}{r}\left[\frac{\partial}{\partial S}\left(\frac{r\rho u_s}{V}\right) + \frac{\partial}{\partial n}\left(\frac{r\rho u_n}{V}\right) + \frac{\partial}{\partial \phi}\left(\frac{u_\phi}{V^2}\right)\right] = 0 \qquad (3.2.1)$$

s Momentum Equation

$$\rho\frac{\partial u_s}{\partial t} + \rho u_s V\frac{\partial u_s}{\partial S} + \rho u_n V\frac{\partial u_s}{\partial n} + \frac{\rho u_\phi}{r}\frac{\partial u_s}{\partial \phi} - \frac{\rho u_n^2}{\rho_n}$$

$$-\frac{\rho u_\phi^2}{r}\sin\theta + \frac{\rho u_s u_n}{\rho_s} = -\frac{V\partial P}{\partial S} + \frac{V^2}{r}\left[\frac{\partial}{\partial S}\left(\frac{r\tau_{ss}}{V}\right)\right. \qquad (3.2.2)$$

$$\left. + \frac{\partial}{\partial n}\left(\frac{r\tau_{sn}}{V}\right) + \frac{\partial}{\partial \phi}\left(\frac{\tau_{s\phi}}{V^2}\right)\right] - \frac{\tau_{nn}}{\rho_n} - \frac{\tau_{\phi\phi}}{r}\sin\theta + \frac{\tau_{sn}}{\rho_s}$$

n Momentum Equation

$$\rho\frac{\partial u_n}{\partial t} + \rho u_s V\frac{\partial u_n}{\partial S} + \rho u_n V\frac{\partial u_n}{\partial n} + \frac{\rho u_\phi}{r}\frac{\partial u_n}{\partial \phi} - \frac{\rho u_s^2}{\rho_s}$$

$$-\frac{\rho u_\phi^2}{r}\cos\theta + \rho\frac{u_s u_n}{\rho_n} = -V\frac{\partial P}{\partial n} + \frac{V^2}{r}\left[\frac{\partial}{\partial S}\left(\frac{r\tau_{ns}}{V}\right)\right. \qquad (3.2.3)$$

$$\left. + \frac{\partial}{\partial n}\left(\frac{r\tau_{nn}}{V}\right) + \frac{\partial}{\partial \phi}\left(\frac{\tau_{n\phi}}{V}\right)\right] - \frac{\tau_{ss}}{\rho_s} - \frac{\tau_{\phi\phi}}{r}\cos\theta + \frac{\tau_{sn}}{\rho_n}$$

ϕ Momentum Equation

$$\rho \frac{\partial u_\phi}{\partial t} + \rho u_s V \frac{\partial u_\phi}{\partial S} + \rho u_n V \frac{\partial u_\phi}{\partial n} + \rho \frac{u_\phi}{r} \frac{\partial u_\phi}{\partial \phi} + \rho \frac{u_n u_\phi}{r}$$

$$\cos\theta + \rho \frac{u_s u_\phi}{r} \sin\theta = -\frac{1}{r} \frac{\partial P}{\partial \phi} + \frac{V^2}{r} \left[\frac{\partial}{\partial S} \left(\frac{r\tau_{s\phi}}{V} \right) \right. \tag{3.2.4}$$

$$\left. + \frac{\partial}{\partial n} \left(\frac{r\tau_{n\phi}}{V} \right) + \frac{\partial}{\partial \phi} \left(\frac{\tau_{\phi\phi}}{V^2} \right) \right] + \frac{\tau_{n\phi}}{r} \cos\theta + \frac{\tau_{s\phi}}{r} \sin\theta$$

Energy Equation

$$\rho T \left\{ \frac{\partial I}{\partial t} + u_s V \frac{\partial I}{\partial S} + u_n V \frac{\partial I}{\partial n} + \frac{u_\phi}{r} \frac{\partial I}{\partial \phi} \right\}$$

$$= \frac{V^2}{r} \left[\frac{\partial}{\partial S} \left(\frac{r q_n}{V} \right) + \frac{\partial}{\partial n} \left(\frac{r q_n}{V} \right) + \frac{\partial}{\partial \phi} \left(\frac{q_\phi}{V^2} \right) \right] + \frac{1}{2} \left\{ \tau_{nn}\, e_{nn} \right. \tag{3.2.5}$$

$$\left. + \tau_{ss}\, e_{ss} + \tau_{\phi\phi}\, e_{\phi\phi} \right\} + \tau_{ns}\, e_{ns} + \tau_{\phi n}\, e_{\phi n} + \tau_{\phi s}\, e_{\phi s}$$

Where the stress, strain, and heat flux vectors are given by

Strain

$$\frac{e_{ss}}{2} = V \frac{\partial u_s}{\partial S} - u_n \frac{\partial V}{\partial n} \tag{3.2.6}$$

$$\frac{e_{nn}}{2} = V \frac{\partial u_n}{\partial n} - u_s \frac{\partial V}{\partial S} \tag{3.2.7}$$

$$\frac{e_{\phi\phi}}{2} = \frac{1}{r} \frac{\partial u_\phi}{\partial \phi} + u_s \frac{V}{r} \frac{\partial r}{\partial S} + u_n \frac{V}{r} \frac{\partial r}{\partial n} \tag{3.2.8}$$

$$e_{n\phi} = r V \frac{\partial}{\partial n} \left(\frac{u_\phi}{r} \right) + \frac{1}{rV} \frac{\partial}{\partial \phi} (u_n V) \tag{3.2.9}$$

$$e_{s\phi} = \frac{1}{rV}\frac{\partial}{\partial \phi}(u_s V) + rV\frac{\partial}{\partial S}\left(\frac{u_\phi}{r}\right) \tag{3.2.10}$$

$$e_{ns} = \frac{\partial}{\partial S}(u_n V) + \frac{\partial}{\partial n}(u_s V) \tag{3.2.11}$$

Stress

$$\tau_{ss} = \mu e_{ss} - \rho \overline{u_s' u_s'} - \frac{2}{3}\mu\nabla \tag{3.2.12}$$

$$\tau_{nn} = \mu e_{nn} - \rho \overline{u_n' u_n'} - \frac{2}{3}\mu\nabla \tag{3.2.13}$$

$$\tau_{\phi\phi} = \mu e_{\phi\phi} - \rho \overline{u_\phi' u_\phi'} - \frac{2}{3}\mu\nabla \tag{3.2.14}$$

$$\tau_{n\phi} = \mu e_{n\phi} - \rho \overline{u_n' u_\phi'} \tag{3.2.15}$$

$$\tau_{s\phi} = \mu e_{s\phi} - \rho \overline{u_s' u_\phi'} \tag{3.2.16}$$

$$\tau_{sn} = \mu e_{sn} - \rho \overline{u_s' u_n'} \tag{3.2.17}$$

where the stresses include the Reynolds stresses and the dilitation ∇ is given by

$$\nabla = \frac{V^2}{r}\left[\frac{\partial}{\partial S}\left(\frac{r u_s}{V}\right) + \frac{\partial}{\partial n}\left(\frac{r u_n}{V}\right) + \frac{\partial}{\partial \phi}\left(\frac{u_\phi}{V^2}\right)\right] \tag{3.2.18}$$

Heat Flux

$$q_n = \frac{\mu_E}{P_{RE}} V \frac{\partial}{\partial n}(C_p T) \tag{3.2.19}$$

$$q_s = \frac{\mu_E}{P_{RE}} V \frac{\partial}{\partial S}(C_p T) \tag{3.2.20}$$

$$q_\phi = \frac{\mu_E}{P_{RE}} \frac{1}{r} \frac{\partial}{\partial \phi}(C_p T) \tag{3.2.21}$$

Since flow losses are of special interest in diffusers, the energy equation, in the present analysis, was written in terms of the entropy, that is

$$\rho T \frac{DI}{Dt} = \rho C_p \frac{DT}{Dt} - \frac{DP}{Dt} = Q + \Phi \tag{3.2.22}$$

It can be seen from Eq. (3.2.22) that the change in entropy is the small difference between two large terms and involves only dissipation and heat transfer. The thermodynamic variables can be recovered from the entropy by the relation

$$I - I_r = C_p \ln\left(\frac{I}{T_r}\right) - \ln\left(\frac{P}{P_r}\right) \tag{3.2.23}$$

With struts in steady flow, circumferential variations of the flow variables exist. In the present analysis, these variations were averaged according to the general relation

$$\bar{f}(n,s) = \frac{1}{\phi_2 - \phi_1} \int_{\phi_1}^{\phi_2} f(n,s,\phi)\, d\phi \tag{3.2.24}$$

Writing the dependent variables in terms of the mean $\bar{f}$ and deviation f' as (see Fig. 3.2.1)

$$f(n,s,\phi) = \bar{f}(n,s) + f(n,s,\phi) \tag{3.2.25}$$

and then integrating

$$\int_{\phi_1}^{\phi_2} \frac{\partial f}{\partial a}\, d\phi = \frac{\partial}{\partial a}\left[\frac{G}{R}\bar{f}\right] + f_1 \frac{\partial \phi_1}{\partial a} - f_2 \frac{\partial \phi_2}{\partial a} \tag{3.2.26}$$

$$\int_{\phi_1}^{\phi_2} \frac{\partial f}{\partial \phi}\, d\phi = f_2 - f_1 \tag{3.2.27}$$

where for the case of no struts

$$f_2 = f_1 \tag{3.2.28}$$

These above rules of averaging are similar to those used in obtaining the Reynolds stresses from the Navier-Stokes equations (Ref. 9) and are applied to the present equations of motion accordingly. With the assumption that

$$f'/\bar{f} << 1 \tag{3.2.29}$$

all double and triple correlations can be neglected except those terms involving the stresses in the strut boundary layers and the stresses produced by the mean flow which produce the annulus boundary layer. Since the equations of motion are written in a coordinate system approximating the real streamlines, the additional simplifying assumption can be made that

$$U_n / U_s << 1 \qquad (3.2.30)$$

and that only the shear stress terms Σ_{ns} and $\Sigma_{n\phi}$ and strain terms E_{ns} and $E_{n\phi}$ need be retained.

Application of the above averaging procedures and simplifications results in the following basic equations of motion in which H_S, H_ϕ are terms identified as strut forces and Φ_B as the dissipation function for the strut boundary layer.

Continuity Equation

$$\frac{\partial}{\partial \eta}\left(\frac{\partial \Psi}{\partial S}\right) - \frac{G}{V} U_s \frac{\partial P}{\partial S} - \frac{G}{V} P \frac{\partial U_s}{\partial S} = P U_s \frac{\partial}{\partial S}\left(\frac{G}{V}\right) \qquad (3.2.31)$$

S Momentum Equation

$$P U_s \frac{\partial U_s}{\partial S} - \frac{V}{G} \frac{\partial U_s}{\partial \eta} \frac{\partial \Psi}{\partial S} + \frac{1}{\gamma M_r^2} \frac{\partial \Pi}{\partial S} = \frac{V}{G} \frac{\partial}{\partial \eta}\left[\frac{G \Sigma_{ns}}{V}\right] - \frac{\Sigma_{ns}}{V} \frac{\partial V}{\partial \eta} + \frac{H_s}{V} + P \frac{U_\phi^2}{R} \frac{\partial R}{\partial S} \qquad (3.2.32)$$

ϕ Momentum Equation

$$P U_s \frac{\partial U_\phi}{\partial S} - \frac{V}{G} \frac{\partial U_\phi}{\partial \eta} \frac{\partial \Psi}{\partial S} = \frac{V}{G} \frac{\partial}{\partial \eta}\left[\frac{G \Sigma_{n\phi}}{V}\right] + \frac{\Sigma_{n\phi}}{R} \frac{\partial R}{\partial \eta} + \frac{H_\phi}{V} - P \frac{U_s U_\phi}{R} \frac{\partial R}{\partial S} \qquad (3.2.33)$$

η Momentum Equation

$$\frac{1}{\gamma M_r^2}\frac{\partial}{\partial \eta}\left(\frac{\partial \Pi}{\partial S}\right) + 2\frac{PU_s}{V}\frac{\partial V}{\partial \eta}\frac{\partial U_s}{\partial S} - 2\frac{PU_\phi}{R}\frac{\partial R}{\partial \eta}\frac{\partial U_\phi}{\partial S}$$

$$-\left[-\frac{1}{V}\frac{\partial V}{\partial \eta}U_s^2 + \frac{1}{R}\frac{\partial R}{\partial \eta}U_\phi^2\right]\frac{\partial P}{\partial S} = -PU_s^2\left[\frac{1}{V}\frac{\partial^2 V}{\partial \eta\,\partial S} - \frac{1}{V^2}\frac{\partial V}{\partial \eta}\frac{\partial V}{\partial S}\right] \tag{3.2.34}$$

$$+PU_\phi^2\left[\frac{1}{R}\frac{\partial^2 R}{\partial \eta\,\partial S} - \frac{1}{R^2}\frac{\partial R}{\partial \eta}\frac{\partial R}{\partial S}\right]$$

Energy Equation

$$PU_s\frac{\partial I}{\partial S} - \frac{V}{G}\frac{\partial I}{\partial \eta}\frac{\partial \Psi}{\partial S} = \frac{1}{V\Theta}\left\{\frac{-\gamma}{\partial - 1}\frac{V^2}{G}\frac{\partial}{\partial \eta}\left[\frac{GQ}{V}\right]\right. \tag{3.2.35}$$

$$\left. + \gamma M_r^2\left[\Sigma_{ns}E_{ns} + \Sigma_{n\phi}E_{n\phi} + \Phi_B\right]\right\}$$

where the stream function is expressed as

$$\frac{\partial \psi}{\partial n} = \frac{G}{V}PU_s \tag{3.2.36}$$

$$\frac{\partial \psi}{\partial s} = \frac{-G}{V}PU_n \tag{3.2.37}$$

and the gap G is expressed as

$$G = R(\phi_2 - \phi_1) \tag{3.2.38}$$

The continuity equation and the s and ϕ momentum equation and energy equation follow directly from the equations of motion in the streamline coordinate system. Equation (3.2.34) was obtained by differentiation of the n momentum equation given by

$$\frac{\partial \Pi}{\partial \eta} = \gamma M_r^2 \left\{ - \frac{P}{V} \frac{\partial V}{\partial \eta} U_s^2 + \frac{P}{R} \frac{\partial R}{\partial \eta} U_\phi^2 \right\} \tag{3.2.39}$$

Equation (3.2.39) illustrates the significance of the approximations used in the streamline coordinate system; namely that the pressure field and particularly the normal pressure gradient is determined by the radius of curvature of the streamline coordinate system rather than the radius of curvature of the real streamlines.

To complete the set of equations for the number of unknowns the equation of state, definition of entropy, and the definition of the stress strain relations and heat flux given below, are used. (The equation of state and entropy equation, (i.e., Eq. (3.2.23)), are differentiated in the s direction for direct application of the explicit numerical integration method.)

Equation of State

$$\frac{\partial \Pi}{\partial S} - P \frac{\partial \Theta}{\partial S} - \Theta \frac{\partial P}{\partial S} = 0 \tag{3.2.40}$$

Entropy Equation

$$\frac{\partial I}{\partial S} - \frac{\gamma}{\partial - 1} \frac{1}{\Theta} \frac{\partial \Theta}{\partial S} + \frac{1}{\Pi} \frac{\partial \Pi}{\partial S} = 0 \tag{3.2.41}$$

Stress, Strain Components, Heat Flux

$$E_{ns} = V \frac{\partial U_s}{\partial \eta} + U_s \frac{\partial V}{\partial \eta} \tag{3.2.42}$$

$$E_{n\phi} = V \frac{\partial U_\phi}{\partial \eta} - V \frac{U_\phi}{R} \frac{\partial R}{\partial \eta} \tag{3.2.43}$$

$$\sum_{ns} = \left(\frac{\mu_T}{\mu_r} \right) \frac{E_{ns}}{N_R} \tag{3.2.44}$$

$$\sum_{n\phi} = \left(\frac{\mu_E}{\mu_r}\right) \frac{E_{n\phi}}{N_R} \tag{3.2.45}$$

$$Q = -\frac{1}{N_R P_{RE}} \left(\frac{\mu_E}{\mu_r}\right) V \frac{\partial \Theta}{\partial n} \tag{3.2.46}$$

In addition the following thermodynamic relations such as the isentropic flow relations, and definitions of engineering parameters are used.

Thermodynamic Relations

$$\Pi = P\Theta \tag{3.2.47}$$

$$I = \frac{\gamma}{\gamma-1} \ln \Theta - \ln \Pi \tag{3.2.48}$$

$$M = M_r U/C \tag{3.2.49}$$

$$C = \sqrt{\Theta} \tag{3.2.50}$$

$$\frac{\Pi_0}{\Pi} = \left[1 + \frac{\gamma-1}{2} M^2\right]^{\frac{\gamma}{\gamma-1}} \tag{3.2.51}$$

$$\frac{\Theta_0}{\Theta} = 1 + \frac{\gamma-1}{2} M^2 \tag{3.2.52}$$

Additional Relations

$$C_f = \frac{2\sum}{P_\infty U_\infty^2} \qquad \text{(wall friction coefficient)} \qquad (3.2.53)$$

$$R_C = (\Theta_w/\Theta_\infty - 1) \Big/ \left(\frac{\gamma-1}{\alpha} M_\infty^2\right) \qquad \text{(recovery factor)} \qquad (3.2.54)$$

$$S_t = \frac{Q_w}{P_\infty U_\infty (\Theta_\infty - \Theta_A)} \qquad \text{(Stanton number)} \qquad (3.2.55)$$

$$S_t = C_f / (2S_A) \qquad \text{(Reynolds analogy factor)} \qquad (3.2.56)$$

These equations of motion form a complete set of equations for the solution of a flow problem provided a priori knowledge is obtained for the blade forces H_s, H_ϕ, and for the blade losses Φ_B. This information is obtained from the blade section lift and drag coefficients and is described in Section 3.3.

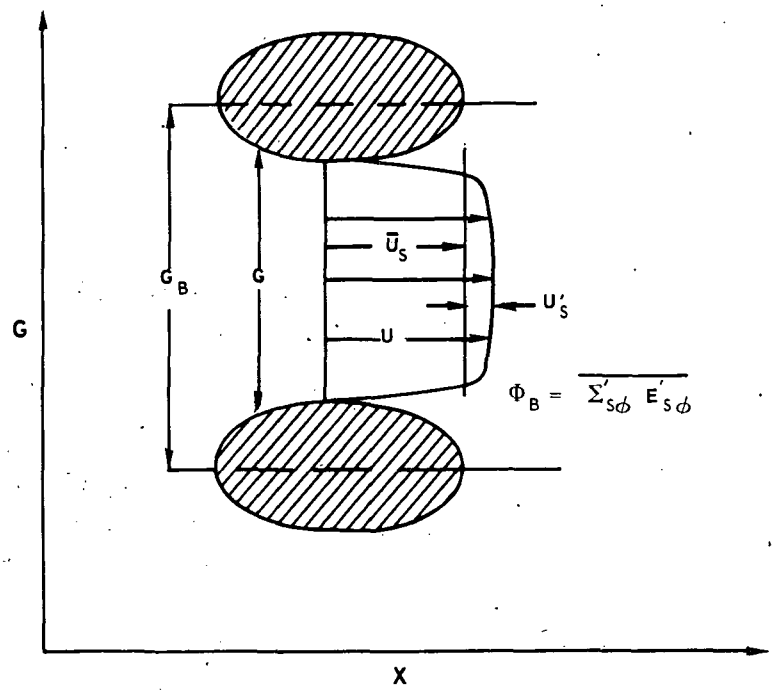

FIG. 3.2.1.-CIRCUMFERENTIAL AVERGE BETWEEN STRUTS.

3.3 Blade Element Forces and Losses

The blade element forces are obtained by collecting those terms from the equations of motion derived in Section 3.2 that do not cancel out at the strut surface. These terms are

$$f_s = \frac{rV}{g}\left[\left(P_2\frac{\partial\phi_2}{\partial S} - P_1\frac{\partial\phi_1}{\partial S}\right) - \left(\tau_{ss2}\frac{\partial\phi_2}{\partial S} - \tau_{ss1}\frac{\partial\phi_1}{\partial S}\right)\right. \tag{3.3.1}$$
$$\left. + \left(\tau_{sn2}\frac{\partial\phi_2}{\partial n} - \tau_{sn1}\frac{\partial\phi_1}{\partial n}\right) + \frac{\tau_{s\phi 2} - \tau_{s\phi 1}}{rV}\right]$$

$$f_n = \frac{rV}{g}\left[\left(P_2\frac{\partial\phi_2}{\partial n} - P_1\frac{\partial\phi_1}{\partial n}\right) - \left(\tau_{sn2}\frac{\partial\phi_2}{\partial s} - \tau_{sn1}\frac{\partial\phi_1}{\partial s}\right)\right. \tag{3.3.2}$$
$$\left. - \left(\tau_{nn2}\frac{\partial\phi_2}{\partial n} - \tau_{nn1}\frac{\partial\phi_1}{\partial n}\right) + \frac{\tau_{n\phi 2} - \tau_{n\phi 1}}{rV}\right]$$

$$f_\phi = \frac{rV}{g}\left[\frac{P_2 - P_1}{rV} - \left(\tau_{s\phi 2}\frac{\partial\phi_2}{\partial S} - \tau_{s\phi 1}\frac{\partial\phi_1}{\partial S}\right)\right. \tag{3.3.3}$$
$$\left. - \left(\tau_{n\phi 2}\frac{\partial\phi_2}{\partial n} - \tau_{n\phi 1}\frac{\partial\phi_1}{\partial n}\right) + \frac{\tau_{\phi\phi 2} - \tau_{\phi\phi 1}}{rV}\right]$$

It can be seen that these terms contain all the skin friction forces and the normal forces produced by the static pressure at the strut surface.

To demonstrate that the above terms are precisely the forces acting per unit volume on the flow, consider an element of volume (see Fig. 3.3.1) given by,

$$d\forall = g\frac{dS}{V}\frac{dn}{V} \tag{3.3.4}$$

and an element of area on surface (1) by

$$dA_1 = \frac{dS}{V}\frac{dn}{V}\sqrt{1+\left(rV\frac{\partial\phi_1}{\partial n}\right)^2}\ \sqrt{1+\left(rV\frac{\partial\phi_1}{\partial S}\right)^2} \tag{3.3.5}$$

such that the direction cosines of the blade surface vector, $\vec{\gamma}_1$, normal to the blade surface (1) are

$$\vec{\gamma}_1 \cdot \vec{i}_s = \frac{-rV\dfrac{\partial \phi_1}{\partial S}}{\sqrt{1+(rV\dfrac{\partial \phi_1}{\partial n})^2}\ \sqrt{1+(rV\dfrac{\partial \phi_1}{\partial S})^2}} \tag{3.3.6}$$

$$\vec{\gamma}_1 \cdot \vec{i}_\phi = \frac{1}{\sqrt{1+(rV\dfrac{\partial \phi_1}{\partial n})^2}\ \sqrt{1+(rV\dfrac{\partial \phi_1}{\partial S})^2}} \tag{3.3.7}$$

$$\vec{\gamma}_1 \cdot \vec{i}_n = \frac{-rV\dfrac{\partial \phi_1}{\partial n}}{\sqrt{1+(rV\dfrac{\partial \phi_1}{\partial n})^2}\ \sqrt{1+(rV\dfrac{\partial \phi_1}{\partial S})^2}} \tag{3.3.8}$$

Then the force acting on an area dA_1 for surface (1) is given by

$$\begin{aligned}\vec{f}_1 = &\left\{\left[(-P+\tau_{ss})\vec{i}_s + \tau_{sn}\vec{i}_n + \tau_{s\phi}\vec{i}_\phi\right]\cdot\vec{\gamma}_1\right\}\vec{i}_s \\ &+\left\{\left[\tau_{ns}\vec{i}_s + (-P+\tau_{nn})\vec{i}_n + \tau_{n\phi}\vec{i}_\phi\right]\cdot\vec{\gamma}_1\right\}\vec{i}_n \\ &+\left\{\tau_{\phi s}\vec{i}_s + \tau_{\phi n}\vec{i}_n + \tau_{\phi\phi}\vec{i}_\phi\right]\cdot\vec{\gamma}_1\right\}\vec{i}_\phi\end{aligned} \tag{3.3.9}$$

This produces a force per unit volume acting on the flow from both surfaces

$$\vec{f} = \frac{\vec{f}_2\, dA_2 - \vec{f}_1\, dA_1}{d\forall} \qquad f_s\vec{i}_s + f_n\vec{i}_n + f_\phi\vec{i}_\phi \tag{3.3.10}$$

where f_s, f_n, $f\phi$ are precisely the terms defined by Eqs. (3.3.1) through (3.3.3).

The total blade force is obtained by integrating over the volume to obtain

$$\vec{F} = \int_{\forall} \vec{f}\, g\, \frac{dn}{V}\, \frac{dS}{V} \tag{3.3.11}$$

Hence the blade force per unit span is given by

$$f = V \frac{\partial}{\partial n} \vec{F} = \int_s g \vec{f} \frac{dS}{V} \tag{3.3.12}$$

and the blade force per volume is related to the section blade force by

$$f = \frac{V}{g} \frac{\partial f}{\partial S} \tag{3.3.13}$$

In the present analysis provision is made for obtaining the blade force from either the section lift or drag coefficients of isolated airfoils (the case for struts with low solidity) or from loss coefficient and turning angle correlations (e.g., Refs. 10, 11, and 12) (the case of closely spaced struts or blades). Before the blade force can be obtained by either method it is first necessary to determine the streamwise static pressure differentiation (back pressure) across the struts, which can be significant, particularly if the flow is swirling. Since the back pressure depends upon knowledge of the blade forces, (however, an iteration between back pressure and blade forces) is required. This iterative solution is obtained in the following manner using methods developed in Ref. 12.

To develop the required iterative solution it is first necessary to develop relations for determining the blade forces f_s and $f\phi$ and the blade dissipation Φ_B (or, in dimensionless form, Ξ_s, Ξ_ϕ, and Φ_B) in terms of the flow variables entering (station 2) and leaving (station 3) the blade row (see Fig. 3.3.2). Considering the flow in a blade element strip $\Delta Y = \Delta n/V$, as shown in Fig. 3.3.2, and assuming that U_n is small, and the walls are adiabatic, the S and ϕ momentum equation, with the additional assumption that the shear stresses can be neglected, and the energy equation in dimensionless form (Eqs. (3.2.32), (3.2.33), and (3.2.35)) become

$$H_s = \frac{V}{\gamma M_r^2} \frac{\partial \Pi}{\partial S} + P U_s V \frac{\partial U_s}{\partial S} \tag{3.3.14}$$

$$H_\phi = P U_s V \frac{\partial U_\phi}{\partial S} \tag{3.3.15}$$

$$\Phi_B = \frac{\mathcal{M} P U_s}{\gamma M_r^2} V \frac{\partial (\Delta I_B)}{\partial S} \tag{3.3.16}$$

Allowing for small spanwise flows so that the back pressure can be in equilibrium, U_{s3} need not equal U_{s2}, and the solution for the blade element force will be a function of the mass flow ratio. Making the approximation

$$(PU_s)_A = \frac{(PU_s)_2 + (PU_s)_3}{2} \tag{3.3.17}$$

the forces H_s and H_ϕ may be integrated over the chord using Eq. (3.3.13), to yield

$$\Xi_s = G_B \int H_s \frac{dS}{V} = G_B \left\{ \frac{\Pi_3 - \Pi_2}{\gamma M_r^2} + \frac{(PU_s)_3 + (PU_s)_2}{2} \left[U_{s3} - U_{s2} \right] \right\} \tag{3.3.18}$$

$$\Xi_\phi = G_B \int H_\phi \frac{dS}{V} = G_B \frac{(PU_s)_3 + (PU_s)_2}{2} \left[U_{\phi 3} - U_{\phi 2} \right] \tag{3.3.19}$$

Differentiating Eqs. (3.3.18) and (3.3.19) yields for the local blade force

$$H_s = V \frac{\partial}{\partial S} \left(\frac{\Xi_s}{G} \right) \tag{3.3.20}$$

$$H_\phi = V \frac{\partial}{\partial S} \left(\frac{\Xi_\phi}{G} \right) \tag{3.3.21}$$

The blade dissipation function Φ_B can be determined from the entropy change through the blade row. Defining the loss coefficient as

$$Z_B = \frac{\Pi_{02} - \Pi_{03}}{\Pi_{02} - \Pi_2} \tag{3.3.22}$$

the entropy rise becomes, using the isentropic flow relations, Eqs. (3.2.51) and (3.2.52), as well as the assumption that the total temperature is conserved since no work is done,

$$\Delta I_B = -\ln\left\{\left(\frac{\Theta_2}{\Theta_{02}}\right)^{\frac{\gamma}{\gamma-1}}\left[\frac{\Pi_{02}}{\Pi_2} - Z_B\left(\frac{\Pi_{02}}{\Pi_0} - 1\right)\right]\right\} \tag{3.3.23}$$

From Eqs. (3.3.18), (3.3.19) and (3.3.23) H_s, H_ϕ, and Φ_B or Ξ_S, Ξ_ϕ, ΔI_B, are known in terms of the flow variables upstream and downstream of the strut. Having developed relations between the blade forces and dissipation function in terms of the upstream and downstream flow variables, it is now necessary to develop additional relations for computing the downstream flow variables given the upstream flow.

Assuming that the blade force in the annulus boundary layer is the same as the blade force at a distance from the wall equal to the displacement thickness of the boundary layer, the flow variables at station (2) and station (3) can be calculated as though the flow were inviscid. This is accomplished in the present analysis by setting all the flow variables in the annulus boundary layer between the wall and the boundary layer displacement height equal to their value at the displacement height, that is

$$\begin{aligned}
&\hat{\phi}(Y) = \phi(\delta^*) && \text{for} \quad 0 \le Y \le \delta^*_H \\
&\hat{\phi}(Y) = \phi(Y) && \delta^*_H < Y < Y_T - \delta^*_H \\
&\hat{\phi}(Y) = \phi(Y-\delta^*_T) && Y_T - \delta^*_T \le Y \le Y_T
\end{aligned} \tag{3.3.24}$$

The solution of this inviscid flow problem requires that the flow satisfy the equations of motion (Eqs. (3.2.31), (3.2.32), (3.2.33), (3.2.35), and (3.2.39)) with the viscous terms deleted. The S and ϕ momentum equations (Eqs. (3.2.32) and (3.2.33)) are satisfied by introducing lift and drag coefficient correlations, or turning angle and loss coefficient correlations depending on which is known.

If C_L and C_D are known then Ξ_s and Ξ_ϕ are determined by a simple resolution of forces

$$\Xi_\sigma = -G_B \hat{P}_2 \hat{U}_2^2 \sigma\left[-C_L \sin\hat{\alpha}_2 + C_D \cos\hat{\alpha}_2\right] \tag{3.2.25}$$

$$\Xi_\phi = -G_B \hat{P}_2 \hat{U}_2^2 \sigma\left[-C_L \cos\hat{\alpha}_2 + C_D \sin\hat{\alpha}_2\right] \tag{3.2.26}$$

and Eq. (3.3.18) and Eq. (3.3.19) may be used to solve for u_{s3} and $u_{\phi 3}$. The energy equation (Eq. (3.2.35)) in this case reduces simply to

$$\Theta_{03} = \Theta_{02} \tag{3.3.27}$$

since no work is done by the blades. The remaining equations to be solved are the continuity equation, Eq. (3.2.36), and the normal pressure gradient equation, Eq. (3.2.39), which are expressed as

$$\frac{\partial \Psi}{\partial \eta} = \frac{G P u_s}{V} \tag{3.3.28}$$

$$\frac{\partial \Pi}{\partial \eta} = \gamma M_r^2 \left\{ -\frac{1}{V} \frac{\partial V}{\partial \eta} P u_s^2 + \frac{1}{R} \frac{\partial R}{\partial \eta} P u_\phi^2 \right\} \tag{3.3.29}$$

If the exit flow angle α and loss coefficient Z_B are known, Eqs. (3.3.28) and (3.3.29) may be reduced to

$$\frac{\partial \Psi}{\partial \eta} = \frac{G \cos \alpha}{M_r V \sqrt{\Theta_0}} \Pi \left\{ \frac{2}{\gamma - 1} \left(\frac{\Pi_0}{\Pi} \right)^{\frac{\gamma - 1}{\gamma}} \left[\left(\frac{\Pi_0}{\Pi} \right)^{\frac{\gamma - 1}{\gamma}} - 1 \right] \right\} \tag{3.3.30}$$

$$\frac{\partial \Pi}{\partial \eta} = \gamma \left\{ -\frac{1}{V} \frac{\partial V}{\partial \eta} \cos^2 \alpha + \frac{1}{R} \frac{\partial R}{\partial \eta} \sin^2 \alpha \right\} \left\{ \frac{2\Pi}{\gamma - 1} \left[\left(\frac{\Pi_0}{\Pi} \right)^{\frac{\gamma - 1}{\gamma}} - 1 \right] \right\} \tag{3.3.31}$$

where Eq. (3.3.22) is used to determine Π_0 from Z_B.

It is evident from the above discussion that for both the case where C_L and C_D are specified and the case where α and Z_B are specified, there are two differential equations relating the blade foces and dissipation to the back pressure; that is, Eqs. (3.3.28) and (3.3.29), or Eqs. (3.3.30) and (3.3.31). These equations are solved iteratively using the boundary conditions.

(3.3.32)

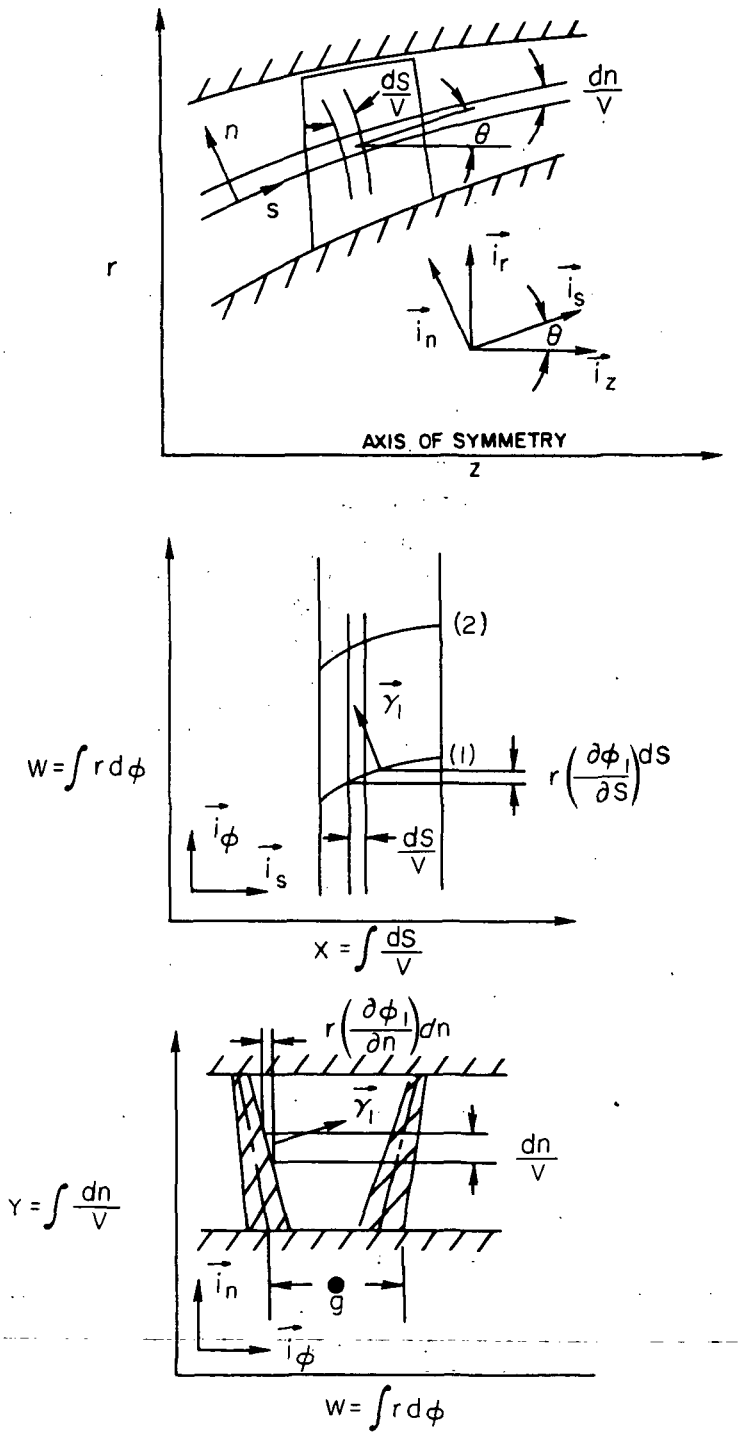

FIG. 3.3.1. – RESOLUTION OF BLADE FORCES.

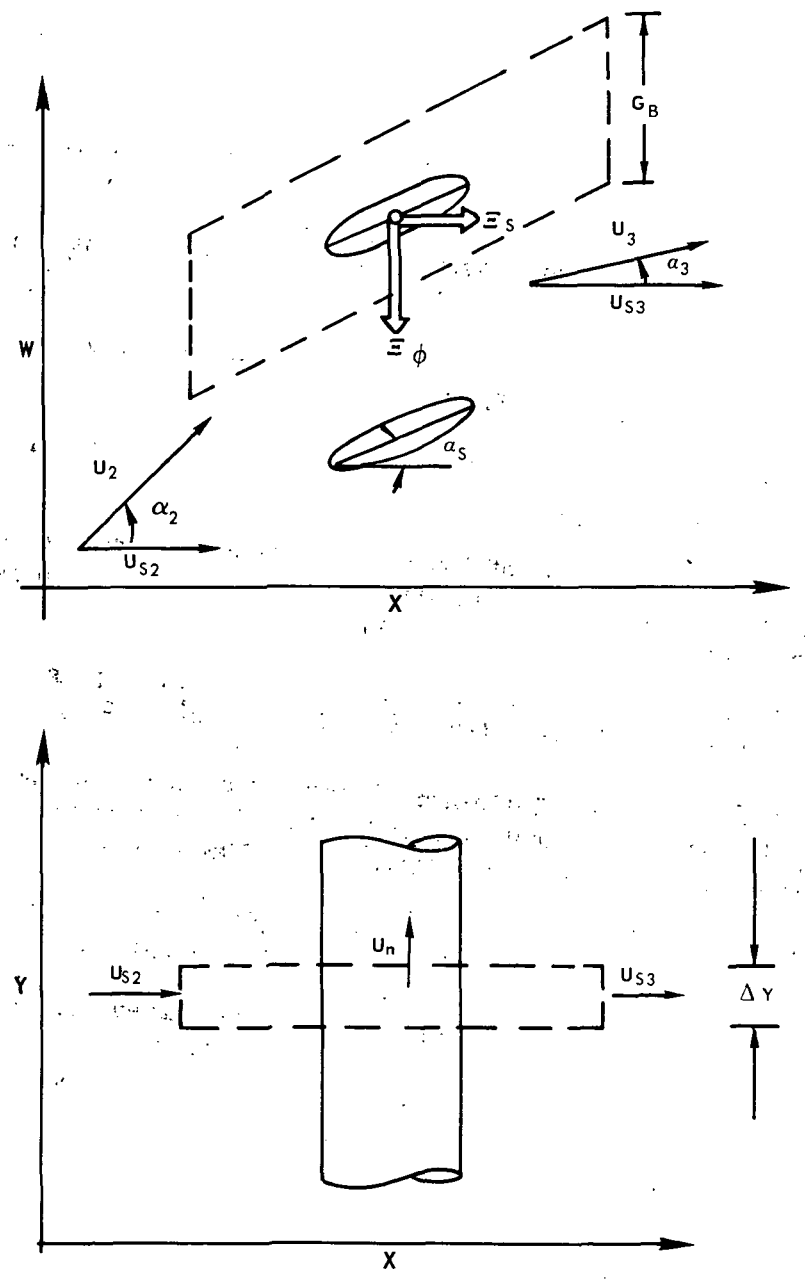

FIG. 3.3.2-BLADE ELEMENT FORCES.

3.4 Turbulence Model

The turbulence model used in the present analysis is the same as that used in Ref. 13 with the inner layer region governed by Prandtl's mixing length theory (Ref. 14) with a Van Driest damping factor and the outer layer region governed by an eddy viscosity model proposed by Clauser (Ref. 15). The inner layer solution is obtained analytically using the method of Spalding (Ref. 16) and the outer layer solution is obtained numerically.

Outer Layer Solution

For Clauser's eddy viscosity model, we have from Ref. 15

$$\mu_E = \chi \rho u_\infty \delta^* \tag{3.4.1}$$

where U_∞ is the velocity at the edge of the boundary layer and δ^* is the boundary layer displacement thickness. In dimensionless form the eddy viscosity can be written

$$\frac{\mu_E}{\mu} = \chi N_R P U_\infty \Delta^* \tag{3.4.2}$$

In the present analysis U_∞ is defined as the maximum velocity in the duct and the average velocity $\bar{U}$ and Δ^* are defined as

$$2, U_\infty \Delta^* = \int_0^1 (U_\infty - U) \frac{d\mathcal{R}}{V} = (U_\infty - \bar{U}) Y_T \tag{3.4.3}$$

Thus the outer layer eddy viscosity is (see Ref. 7),

$$\frac{\mu_E}{\mu} = \chi N_R P_\infty \frac{Y_T}{2} (U_\infty - \bar{U}) \tag{3.4.4}$$

where for thick boundary layers or for flows with radial total pressure distortion the mixing length is of the order of the duct width. For thin boundary layers, Eq. (3.4.4) reduces to Clauser's law of the wake model.

Inner Layer Solution

In the region near the wall, the independent variables and their derivatives change rapidly and numerical solution is difficult except with a large number of closely spaced mesh points. Using the numerical method chosen for the present analysis, the step size in the streamwise direction must be very small to obtain a stable numerical solution with a large number of closely spaced mesh points; thereby resulting in large computational time. However, Spalding (Ref. 16) has shown that the solution for the flow near the wall can be computed from analytical relations with reasonable accuracy. Therefore, Spalding's analytical method was used for the inner layer calculation, to enable larger step sizes to be employed in computing the diffuser flow. This method, however, may not work well for very high Mach number flows, or when the temperature and momentum displacement thicknesses are very different.

According to Ref. 16 the equations of motion for the inner layer in universal turbulent coordinates are given by,

$$\left(\frac{\mu_E}{\mu_W}\right)\frac{dU^+}{dY^+} = \tau^+ = 1 + P^+ Y^+ + M^+ U^+ \qquad (3.4.5)$$

$$\left(\frac{1}{P_{RE}}\ \frac{\mu_E}{\mu_W}\right)\frac{dH^+}{dY^+} = Q^+ = 1 + M^+ H^+ \qquad (3.4.6)$$

$$\left(\frac{1}{P_{RE}}\ \frac{\mu_E}{\mu_W}\right)\ \frac{dH_A^+}{dY^+} = Q_A^+ = \left(1 - \frac{1}{P_{RE}}\right)\left(\frac{\mu_E}{\mu_W}\right)\frac{d}{dY}\left(\frac{U^+}{2}\right)^2 + M_1^+ H_A^+ \qquad (3.4.7)$$

$$\left(\frac{\mu_E}{\mu_W}\right) = 1 + K^2 Y^{+2}\left[1 - \exp\left(-\frac{Y^+\sqrt{\tau^+}}{A^+}\right)\right]^2 \frac{dU^+}{dY^+} \qquad (3.4.8)$$

$$\left(\frac{1}{P_{RE}}\ \frac{\mu_E}{\mu_W}\right) = \frac{1}{P_R} + \frac{K^+ Y^{+2}}{P_{RT}}\left[1 - \exp\left(-\frac{Y^+\sqrt{\tau^+}}{A^+}\right)\right]^2 \frac{dU^+}{dY^+} \qquad (3.4.9)$$

and for the stream function

$$\frac{dW^+}{dY^+} = U^+ \tag{3.4.10}$$

For large values of Y^+, Eqs. (3.4.5) through (3.4.9) simplify to

$$\frac{dU^+}{dY^+} = \frac{\sqrt{\tau}^+}{KY^+} \tag{3.4.11}$$

$$\frac{dH^+}{dU^+} = \frac{P_{RT}Q^+}{\tau^+} \tag{3.4.12}$$

$$\frac{dH_A^+}{dU^+} = (P_{RT} - 1)U^+ + \frac{P_{RT}M^+H_A^+}{\tau^+} \tag{3.4.13}$$

which yield the following analytical solutions for the cases of interest.

CASE I $m^+ = p^+ = 0$ (Flat-Plate, No Bleed)

$$U^+ = \frac{1}{K} \ln (C_5Y^+) \tag{3.4.14}$$

$$W^+ = \frac{1}{K}\left[Y^+ \ln (C_5Y^+) - Y^+\right] + C_6 \tag{3.4.15}$$

$$H_A^+ = (P_{RT} - 1)\frac{U^{+2}}{2} + C_2 \tag{3.4.16}$$

$$H^+ = U^+ + C_3 \tag{3.4.17}$$

CASE II $p^+ = 0,\ m^+ \neq 0$ (Flat-Plate, With Bleed)

$$U^+ = \frac{1}{K}\ln(C_1 Y^+) + \frac{M^+}{4K^2}\left[\ln(C_1 Y^+)\right]^2 \tag{3.4.18}$$

$$W^+ = \frac{Y^+}{K}\left[\ln(C_1 Y^+) - 1\right] + \frac{M^+}{4K^2}\left\{Y^+\left[\ln(C_1 Y^+)\right]^2 - 2Y^+\left[\ln(C_1 Y^+) - 1\right]\right\} + C_4(M^+) \tag{3.4.19}$$

$$H_A^+ = (P_{RT}-1)\left\{\frac{U^{+2}}{2} + \frac{(1+M^+U^+)^{P_{RT}} - \left[1 + P_{RT}M^+U^+ + P_{RT}(P_{RT}-1)(M^+U^+)^2/2\right]}{(1-P_{RT})(2-P_{RT})M^{+2}}\right\} + C_2(1+M^+U^+)^{P_{RT}} \tag{3.4.20}$$

$$H^+ = \frac{1}{M^+}\left\{1 - \exp\left[\ln(1+M^+U^+) + C_3 M^+\right]\right\} \tag{3.4.21}$$

CASE III $M^+ = 0,\ P^+ \geq 0$ (Pressure Gradient, No Bleed)

$$U^+ = \frac{1}{K}\ln(C_5 Y^+) + \frac{2}{K}\left[\sqrt{1+P^+Y^+} - 1\right] - \frac{1}{K}\ln\left[\frac{2+P^+Y^+ + \sqrt{1+P^+Y^+}}{4}\right] \tag{3.4.22}$$

$$W^+ = \frac{1}{K}\left[Y^+\ln(C_5 Y^+) - Y^+\right] + \frac{2}{K}\left[\frac{2}{3P^+}(1+P^+Y^+)^{3/2} - Y^+ - \frac{2}{3P^+}\right] - \frac{2}{K}\left\{Y^+\ln\left(\frac{1+\sqrt{1+P^+Y^+}}{2}\right) - \frac{Y^+}{2} + \frac{\sqrt{1+P^+Y^+}-1}{P^+}\right\} + C_6 \tag{3.4.23}$$

$$H_A^+ = (P_{RT} - 1)\frac{U^{+2}}{2} + C_2 \qquad (3.4.24)$$

$$H^+ = U^+ + C_3 \qquad (3.4.25)$$

Note that for Cases II and III, in the limits as $M^+ \to 0$ and $P^+ \to 0$, Case I is obtained. The constants of integration in Eqs. (3.4.14) through (3.4.25) are obtained by numerically integrating Eqs. (3.4.5) through (3.4.7) out to a value of Y^+ and evaluating the constants by matching with the analytical solutions. It should be noted that since analytical solutions cannot be found for the general case, Case III is used for flows with pressure gradient and bleed.

The analytical solution is used to compute the flow in the inner layer which is matched to the numerical solution for the outer flow at some streamline near the wall. This matching is accomplished by iteratively finding the friction velocity U^* such that Eq. (3.4.18) or Eq. (3.4.22) is satisfied on the streamline where the flow is matched. Once the friction velocity is found the adiabatic wall temperature may be determined by matching the temperatures at the matching streamline using Eq. (3.4.20) or Eq. (3.4.24). If the wall temperature is specified, Eq. (3.4.25) is used to determine the heat flux.

3.5 Classification of Equations

In fluid mechanics, the equations of motion are generally classified as elliptic for inviscid subsonic flow, hyperbolic for inviscid supersonic flow, and parabolic for boundary layer flows. The classification of the equations being solved in the present analysis is required to establish the proper boundary conditions and to evaluate the general properties of the solutions.

The equations of motion to be examined are Eqs. (3.2.31), (3.2.32), (3.2.33), (3.2.35), and (3.2.39) with the stresses and heat fluxes substituted appropriately. Then we have five equations, continuity, three momentum equations, and the energy equation for the five variables, $U_s, U_\phi, U_n, \Pi, \Theta$. If α is the characteristic surface, then according to Ref. 17, the following determinant vanishes on the characteristic surface.

$$D = \begin{vmatrix} U_s & U_\phi & U_n & \Pi & \Theta \\ \alpha_{,s} & 0 & \alpha_n & \psi/\Pi & -\psi/\Theta \\ -C_1\alpha_{,n}^2 & 0 & 0 & C_2\alpha_{,s} & 0 \\ 0 & C_1\alpha_{,n}^2 & 0 & 0 & 0 \\ 0 & 0 & 0 & \alpha_{,n} & 0 \\ C_3\alpha_{,n}^2 & C_3\alpha_{,n}^2 & 0 & -\psi/\Pi & C_4\alpha_{,n}^2 \end{vmatrix} = 0 \qquad (3.5.1)$$

where the subscript notation is used to denote partial derivatives and

$$\psi = U_s\alpha_{,s} + U_s\alpha_{,n} \qquad (3.5.2)$$

$$\begin{aligned} C_1 &= V\left(\frac{\mu_E}{\mu_r}\right) \\ C_2 &= 1/(\gamma M_r^2) \\ C_3 &= \gamma M_r^2 V^2\left(\frac{\mu_E}{\mu_r}\right)/P \\ C_4 &= -\frac{1}{\Pi}\frac{\gamma}{\gamma-1}\frac{V}{N_R P_R}\left(\frac{\mu_E}{\mu_r}\right) \end{aligned} \qquad (3.5.3)$$

Evaluating the determinate, we have

$$D = C_4 C_1^2 P \alpha_{,n}^8 = 0 \tag{3.5.4}$$

Hence all roots are real and equal and the equations of motion derived here are parabolic.

Since the equations of motion are parabolic, the proper boundary conditions can be prescribed. Along the inner and outer walls

$$\begin{aligned} U_{sw} &= U_{\phi w} = 0 \\ U_{nw} &= \mathring{M}_w / P_w \end{aligned} \tag{3.5.5}$$

For the energy equation we have either adiabatic walls or prescribed temperature

$$Q_w = 0 \quad \text{or} \quad \Theta = \Theta_w \tag{3.5.6}$$

Finally, the flow entering the duct $U_s(n)$, $U_\phi(n)$, $\Pi(n)$, $\Theta(n)$ must be specified. The exit flow conditions cannot be specified but must be determined by the solution.

The subcharacteristics (Ref. 18) are determined by the equations of motion minus the diffusion terms and the resulting determinate is given by,

$$D = \begin{vmatrix} \alpha_{,s} & 0 & \alpha_{,n} & \psi/\Pi & -\psi/\Theta \\ P\psi & 0 & 0 & C_2 \alpha_{,s} & 0 \\ 0 & P\psi & 0 & 0 & 0 \\ 0 & 0 & -[P\psi] & C_2 \alpha_n & 0 \\ 0 & 0 & 0 & -\psi & \frac{\gamma}{\gamma-1}\,\psi/\Theta \end{vmatrix} \tag{3.5.7}$$

where the boundary layer assumption has not been made and the term in the bracket is the term that will vanish when the boundary layer assumption is made (i.e., it contains the acceleration terms in the momentum equation). Evaluating the determinate

$$D = \frac{P^3\psi^3}{\gamma M_r^2} \frac{\gamma}{\gamma-1} \left\{ \varepsilon (M_s^2-1)\, a_{,s}^2 + \varepsilon\, 2\, M_s M_n\, a_{,s}\, a_{,n} + (\varepsilon M_n^2 - 1) a_{,n}^2 \right\} \qquad (3.5.8)$$

where

$$\varepsilon = \left[P\psi\right] / (P\psi) \qquad (3.5.9)$$

When the boundary layer assumption is made ($\varepsilon = 0$), the characteristics are real and equal. If $\varepsilon = 1$, the characteristics are imaginary for $M < 1$ and real and distinct for $M > 1$. Thus, it is seen that if the boundary layer assumption is not made, the subcharacteristics have the properties that are usually associated with fluid dynamic flow regimes. It is only the boundary layer assumption which reduces the equations to a parabolic system.

Although the equations of motion are parabolic for subsonic flows, the solutions can be expected to have some properties of elliptic flows since the coordinates were obtained from the solution to an elliptic differential equation (Laplace's equation). Thus, normal pressure gradients required to turn the flow are a function of the curvature of the streamline coordinates and the calculated flow starts to turn upstream of a corner. However, the upstream flow cannot start to turn due to downstream flow separation since the streamline coordinates do not have this information.

For supersonic flow, the equations of motion are still parabolic, but the inviscid portion of the flow should have properties of solutions of hyperbolic equations. Discontinuities, such as shock waves may exist, and turning of the flow at a corner due to an expansion fan may exist in hyperbolic flows. These flows cannot be described well by the present analysis because the streamline coordinate system currently incorporated into the analysis does not accurately describe the curvature of the real streamlines. However, in duct flows for which the turning is more gradual, and for which the Mach number is close to 1.0, reasonable solutions may be possible with the present analysis since the Mach lines are nearly normal to the flow and may be approximated by the potential lines, which are the characteristics of the parabolic equation. In principle, it may be possible to solve the problem for supersonic flow with expansion waves and weak shocks provided an orthogonal coordinate system can be constructed from a supersonic inviscid solution. It should be noted, however, that for strong shock-boundary-layer interaction, the method would require several iterations because the shock location would depend on the boundary layer growth.

3.6 Method of Solution

The equations of motion, Eqs. (3.2.31) through (3.2.35) and Eqs. (3.2.40) and (3.2.41) are solved by the explicit numerical method of Ref. 19. This explicit method was chosen on the basis of its success on the analogous incompressible flow problem described in Ref. 7 after other numerical methods had been tried. With this method, the solution for the dependent variables and their normal derivatives are presumed known from previous calculation or input data up to station S. After some manipulation, these seven equations may be reduced to two equations of the form

$$\frac{\partial}{\partial \eta}\left(\frac{\partial \psi}{\partial S}\right) = F_{\psi}\left[\frac{\partial \psi}{\partial S}, \frac{\partial \Pi}{\partial S}\right] \tag{3.6.1}$$

$$\frac{\partial}{\partial \eta}\left(\frac{\partial \Pi}{\partial S}\right) = F_{\Pi}\left[\frac{\partial \psi}{\partial S}, \frac{\partial \Pi}{\partial S}\right] \tag{3.6.2}$$

These equations are then linear in the unknown dependent variables $\partial\psi/\partial S$ and $\partial\Pi/\partial S$. Thus they can be thought of as two linear ordinary differential equations across the duct which may be solved with the boundary conditions

$$\left(\frac{\partial \psi}{\partial S}\right)_{n=0} = -\frac{G_H}{V_H}\,\mathring{M}_H \tag{3.6.3}$$

$$\left(\frac{\partial \psi}{\partial S}\right)_{n=1} = \frac{G_T}{V_T}\,\mathring{M}_T \tag{3.6.4}$$

Since Eqs. (3.6.1) and (3.6.2) are linear, they may be solved numerically by calculating the homogeneous and particular solutions with the boundary conditions

$$\left(\frac{\partial \psi}{\partial S}\right)_p = -\frac{G_M \mathring{M}_H}{V_H}\;;\quad \left(\frac{\partial \psi}{\partial S}\right)_h = 0$$

$$\left(\frac{\partial \Pi}{\partial S}\right)_p = 0\;;\quad \left(\frac{\partial \Pi}{\partial S}\right)_h = 1.0 \tag{3.6.5}$$

and then adding these solutions to obtain the general solution, that is

$$\frac{\partial \psi}{\partial S} = \left(\frac{\partial \psi}{\partial S}\right)_p + C\left(\frac{\partial \psi}{\partial S}\right)_h \tag{3.6.6}$$

$$\frac{\partial \Pi}{\partial S} = \left(\frac{\partial \Pi}{\partial S}\right)_p + C\left(\frac{\partial \Pi}{\partial S}\right)_h \tag{3.6.7}$$

The constant of integration C, is obtained by satisfying Eq. (3.6.5) at the tip wall, that is

$$\frac{G_T \mathring{M}_T}{V_T} = \left(\frac{\partial \psi}{\partial S}\right)_{n=1} = \left(\frac{\partial \psi}{\partial S}\right)_p + C\left(\frac{\partial \psi}{\partial S}\right)_h \tag{3.6.8}$$

From Eqs. (3.6.5) and(3.6.7) it can be seen that the integration constant is equal to the streamwise pressure gradient on the hub wall. (It is important to note from the above discussion that in the present method of solution the streamwise pressure gradient is obtained by satisfying continuity without the need for iteration.)

In the numerical solution of Eqs. (3.6.1) and (3.6.2) normal derivatives are distorted by the transformation

$$X(\eta) = \partial \eta / \partial \eta \tag{3.6.9}$$

For any dependent variable $\phi(K)$, the normal derivatives are obtained using central differences, that is

$$\left(\frac{\partial \phi}{\partial \eta}\right)_K = \frac{\phi(K+1) - \phi(K-1)}{2\Delta\eta\, X(K)} \tag{3.6.10}$$

where $\Delta\eta$ is equally spaced. The integration of Eqs. (3.6.1) and (3.6.2) takes place using the trapazoid rule, that is

$$\left(\frac{\partial \psi}{\partial S}\right)_{K+1} = \left(\frac{\partial \psi}{\partial S}\right)_K + \frac{\Delta \eta}{2}\left[\frac{F_\psi(K)}{X(K)} + \frac{F_\psi(K+1)}{X(K+1)}\right]$$

$$\left(\frac{\partial \Pi}{\partial S}\right)_{K+1} = \left(\frac{\partial \Pi}{\partial S}\right)_K + \frac{\Delta \eta}{2}\left[\frac{F_\Pi(K)}{X(K)} + \frac{F_\Pi(K+1)}{X(K+1)}\right] \qquad (3.6.11)$$

It is noted that $F_\psi(K+1)$ and $F_\Pi(K+1)$ are not known; however, they are linear functions of $\partial\psi/\partial S$ and $\partial\Pi/\partial S$. Thus

$$F_\psi = A_\psi(K) + B_\psi(K)\left(\frac{\partial \psi}{\partial S}\right)_K + C_\psi(K)\left(\frac{\partial \Pi}{\partial S}\right)_K$$

$$F_\Pi = A_\Pi(K) + B_\Pi(K)\left(\frac{\partial \psi}{\partial S}\right)_K + C_\Pi(K)\left(\frac{\partial \Pi}{\partial S}\right)_K \qquad (3.6.12)$$

Hence, substituting Eq. (3.6.12) into Eq. (3.6.11), $\partial\psi/\partial S$ and $\partial\Pi/\partial S$ at $K = K+1$ are obtained from the relations

$$\left[1 - \frac{2\Delta\eta B_\psi(K+1)}{X(K+1)}\right]\left(\frac{\partial \psi}{\partial S}\right)_{K+1} + \left[-\frac{2\Delta\eta C_\psi(K+1)}{X(K+1)}\right]\left(\frac{\partial \Pi}{\partial S}\right)_{K+1}$$

$$= \left(\frac{\partial \psi}{\partial S}\right)_K + \frac{\Delta \eta}{2}\left[\frac{F_\psi(K)}{X(K)} + \frac{A_\psi(K+1)}{X(K+1)}\right] \qquad (3.6.13)$$

$$\left[-\frac{2\Delta\eta B_\Pi(K+1)}{X(K+1)}\right]\left(\frac{\partial \psi}{\partial S}\right)_{K+1} + \left[1 - \frac{2\Delta\eta C_\psi(K+1)}{X(K+1)}\right]\left(\frac{\partial \Pi}{\partial S}\right)_{K+1}$$

$$= \left(\frac{\partial \Pi}{\partial S}\right)_K + \frac{\Delta \eta}{2}\left[\frac{F_\Pi(K)}{X(K)} + \frac{A_\Pi(K+1)}{X(K+1)}\right] \qquad (3.6.14)$$

The homogeneous solution is then obtained by setting $A_\psi = A_\Pi = 0$.

Once $\partial\psi/\partial S$ and $\partial\Pi/\partial S$ are determined across the duct, the streamwise derivatives of the other variables are found, and integration in the streamwise direction takes place using the second order formula

$$\Pi(S+dS) = \Pi(S-dS) + 2\Delta S\left(\frac{\partial\Pi}{\partial S}\right)_S \tag{3.6.15}$$

A special case exists for the boundary condition evaluated at the axis of symmetry since the equations of motion are singular at the origin. For this case, the solution may be expanded in a series about the origin and evaluated at a control surface with a small radii, that is

$$\begin{aligned} U_S &= U_S(0) + C_1 R^2 \\ U_\phi &= C_2 R \\ \Theta &= \Theta(0) + C_3 R^2 \end{aligned} \tag{3.6.16}$$

where C_1, C_2, C_3 can be evaluated at the first two mesh points.

4.0 GENERAL DESCRIPTION OF COMPUTER PROGRAM

This section is intended to describe the general features of the computer program in sufficient detail so that the program can be run successfully by the average intended user. The first subsection describes what problems can be solved and what problems cannot be solved. It also describes any special care which should be used in exercising the various options. The second and third subsections present a detailed description of the input which is required in the operation of the computer program and the interpretation of the printed output. Since any complicated computer program may fail due to inconsistencies in the input or failure of the theory, the computer program is provided with self-diagnostics which notify the user of the type of failure. The last subsection deals with these program diagnostics as well as helpful hints to correct problems which may be encountered.

4.1 General Features of Program

Program Language

The computer program was written and developed in FØRTRAN V computer language for use on a UNIVAC 1108 computer. A special UARL INCLUDER code was used to generate a new source file to facilitate conversion of the program for operation on an IBM 360 computer. The actual conversion was done by the UARL CØNCUR code which provides a means for converting UNIVAC 1108 CUR tape source elements into IBM 360 card image form. The program was then compiled in FØRTRAN IV and executed on an IBM 360 computer.

Types of Fluids

The fluid may be any compressible gas as defined by its thermodynamic properties R, C_p, C_u, μ, P_{RL}, P_{RT}. If not otherwise specified, the gas is assumed to be air. The reference conditions for the gas properties must be specified at standard sea level conditions.

Types of Flow Situations

Subsonic, turbulent, swirling, or nonswirling flows in axisymmetric ducts may be calculated including flows with radial total pressure distortion. Two-dimensional flows may be calculated by constructing an annular duct in which the inner to outer radius approaches 1.0. When struts are included in the duct, the solution is given for the circumferential average of the flow contained between two adjacent struts.

Duct Geometry Options (IØPT3)

The flow through any axisymmetric duct may be calculated provided that the flow is generally in the axial direction. Duct flows normal to the axis of symmetry, or which reverse direction cannot be calculated due to logic limitations in Subroutine CØØR. Ducts with sharp discontinuities, such as a step, which produce separation also cannot be calculated.

Provision is made in the program to either read the duct coordinates from input data cards (IØPT3=2), or to calculate the duct coordinates analytically (IØPT3 > 4) from a few input duct shape parameters. If the duct coordinates are read from input cards, care should be taken that the input coordinates have sufficient smoothness to calculate the first and second derivatives using numerical finite-difference equations. When the second option is used (IØPT3 > 4), the user must program his own calculation in Subroutine GDUCT. Sample programs (IØPT3=1, 3, 4) are given in Subroutine GDUCT for the users reference. For ducts with no centerbody a zero radius must be specified.

An important restriction to the computer program is that the inlet and exit flow must have no normal pressure gradients produced by streamline curvature although it may have normal pressure gradients due to swirl. Many ducts do not satisfy this requirement; however, these ducts can still be treated if the duct is extended. For curved annular ducts exhausting to atmosphere, the exit flow may have curvature. This phenomena may be simulated by extending the duct to approximate the curvature of the exit flow.

Inlet Flow Options (IØPT1)

The computer program is provided with two methods to describe the inlet flow. When IØPT1=1, the inlet flow is calculated by prescribing the stagnation conditions (P_0, T_0), the inlet Mach number M_1, the swirl angle α_1, and the boundary layer parameters δ^* and n which are the boundary layer displacement thickness and power law velocity profile exponent, respectively. The core flow is then calculated from isentropic flow relations, and boundary layers added using power law velocity profile relations. When stagnation conditions are not specified, the calculation assumes sea level conditions.

When IØPT1=2, the inlet flow is prescribed from input data cards which specify the stagnation pressure P_0, static pressure P, swirl angle α, and stagnation temperature T_0, as a function of the fractional distance across the inlet. This data need not be specified at equidistant points since a linear interpolation is used to specify the data at the mesh points used in the calculation. If experimental data is not used, care should be taken that the data is self-consistent and that it satisfies the radial equilibrium equation. Since the initial growth of the boundary layer is sensitive to the wall shear stress, data describing the boundary layers should be accurately specified. When this is not possible, boundary layers may be added to each wall by specifying δ^* and n. Special care should be exercised in using IØPT1=2 option, with or without the feature of adding in the wall boundary layers. If the stress distribution across the duct is not smooth and realistic, numerical instabilities might originate in the inlet flow and grow rapidly to a point where the calculation is terminated. This may take the form of an unrealistically early separation.

Boundary Conditions (T_w, M_w)

Either the adiabatic wall or the heat transfer case may be calculated. The program assumes adiabatic walls unless the wall temperature is specified. Any wall temperature distribution may be specified, either on input cards when the duct coordinates are read, or calculated when the duct coordinates are calculated. The case of wall bleed may also be treated in a similar manner; wall bleed flow rate is zero, unless otherwise specified.

Force Options (IØPT2)

Subroutine FØRCE is provided with four options (see Flow Chart 7.2.7.1) for calculating the strut force. For IØPT2=1, the strut force is calculated from experimental data in the form of P_0, P, α, T_0 across a control surface just upstream and downstream of the blades. This mode of calculation should be very useful in evaluating the influence of struts on duct flows using experimental measurements. For IØPT2=4, the strut forces are again calculated from experimental data, but this time from exit angle, α_3, and loss coefficient, Z_B, data. Experimental data for turning vanes are more likely to be presented in this form and this option should be useful in evaluating experimental data and developing empirical coefficients. For IØPT2=2, the blade force is calculated from empirical relations contained in Subroutine CASC. For this option, Subroutine CASC produces the section lift and drag coefficients of the strut. For IØPT2=3, the blade force is also predicted from Subroutine CASC. In this case, however, CASC produces the exit turning angle, α_3, and the loss coefficient, Z_B.

Blade Shape Option (ISHAPE)

The blade section lift and drag coefficients, or exit flow angle and loss coefficient, are calculated in Subroutine CASC according to the blade shape index ISHAPE. Since hundreds of blade shapes and turning vanes exist and cannot all be programmed, the user must modify Subroutine CASC for his use. However, as an aid to the user in developing this subroutine, two options have been programmed. For ISHAPE=1, the struts are NACA 5 digit series uncambered airfoils. The output for this option is in the form of section lift and drag coefficients. For ISHAPE=2, empirical relations for turning vanes are programmed. In this case the output of Subroutine CASC is the exit flow angle and loss coefficient.

Failure Modes

In the event of failure in the calculation, the program prints an error message called "diagnostic". These "diagnostics" are in addition to the computer diagnostics and are clearly labeled as such. These "diagnostics" terminate the calculation only when very serious. A list of these "diagnostics" appear in Section 4.4. Included with this list is an identifying number for the "diagnostics", the location (Subroutine), and the immediate cause of the failure. Where possible, suggestions are made to correct the calculation.

Debug Options (IDBGN)

Auxiliary printout which was originally used to debug the computer program is available to the user by setting the appropriate IDBGN option. However, the user must refer to the program listing or compilation to determine the meaning of this printout.

Grid Selection

The grid selection parameters appear on the third input card and are given by DDS, KL, JL, KDS. The number of streamlines including the wall boundaries is given by KL. Good numerical results are obtained with KL = 26. The maximum number of streamlines which can be used is KL=100. The number of streamwise stations is divided into a coarse grid JL and a fine grid which is JL*KDS. The maximum number of streamwise stations in the coarse grid is given by JL=51. There is no limit to the size of the fine grid. Since the numerical method used to integrate the equations of motion is conditionally stable, KDS is an important stability parameter. Good results are obtained with KDS=5. If the solution is numerically unstable KDS should be increased. It should be noted that computing time is directly proportional to KDS. The parameter DDS, distorts the normal coordinate by placing more streamlines near the wall. Increasing DDS, moves the streamline closer to the wall. Good results have been obtained by setting DDS=10.

Separation

Separation is determined when the streamwise component of the wall stress goes to zero. Since the equations become numerically unstable as the wall stress approaches zero, the wall stress is extrapolated ahead two stations. When the extrapolated value of wall stress is less than zero, the calculation is terminated and an appropriate message is printed.

4.2 Description of Input

This subsection describes the loading of input data cards for running the computer program. Care should be taken in loading the program because the input changes depending on the options chosen on the second data card. Multiple cases can be run simply by stacking the cases in order. The last case is followed by two blank cards.

Card No. 1: Title Card

Name	Col.	Format	Comments:
TITLE	1-72	12A6*	Any alpha numeric characters.

Card No. 2: Option Card

Name	Col.	Format	Comments:
IØPT1	1-2	I2	(FLØWIN Option) IØPT=1 The inlet flow is computed by specifying the data on card 5. IØPT=2 The inlet flow is read from 2 x KLL data cards following card 5.
IØPT2	2-4	I2	(FØRCE Option) IØPT2=0 No blades or struts exist in the duct and these cards are not loaded. IØPT2=1 The strut forces are calculated from experimental data on cards 2 x KLL cards following card 9. If IØPT1=2 data cards must be separately loaded. IØPT2=2 The blade force is calculated from CL and CD in Subroutine CASC. IØPT2=3 The blade force is calculated from $\hat{\alpha}_3$ and Z_B in Subroutine CASC. IØPT2=4 The blade force is calculated from KLL input data cards following card 9 with $\hat{\alpha}_3$ and Z_B given.
IØPT3	5-6	I2	(GDUCT Option) IØPT3=1 Calculate a straight annular duct IØPT3=2 Read duct coordinates IØPT3=3 Calculate a straight wall annular diffuser IØPT3=4 Calculate NACA curved wall annular diffuser

*12A6 UNIVAC 1108
18A- IBM 360

Card No. 2: Option Card (Continued)

Name	Col.	Format	Comments:
IØPT4	7-8	I2	Print solution every IOPT4 stations.
IØPT5	9-10	I2	Blade force data input (see IØPT2=1)
IØPT6	11-12	I2	Matching point. If not specified, the matching point for Spalding's solutions is the second mesh point from the wall; otherwise, it is the IØPT6th point from the wall.
IØPT7	13-14	I2	If IØPT7=0, the gas is assumed to be air. If IØPT7≠0, input gas parameters.

Card No. 3: Mesh Parameters

Name	Col.	Format	Comments:
DDS	1-10	F10.3	Mesh distortion parameter (see Section 7.6) Good results are obtained $5 \leq DDS \leq 10$.
KL	11-13	I3	Number of streamlines including wall $2 \leq KL \leq 100$
JL	14-16	I3	Number of streamwise stations, $JL \leq 51$
KDS	17-19	I3	Number of steps per streamwise station (see Section 7.6)
KLL	20-22	I3	Number of streamlines of data input (see IØPT1, IØPT2)

Card No. 4: GDUCT

Name	Col.	Format	Comments:
			These input cards are read in subroutine GDUCT as programmed by the user.

The following duct geometries (designated as IØPT3=1,2,3, and 4) have been programmed:

Card No. 4: (IØPT3=1)

Name	Col.	Format	Comments:
RH1	1-10	F10.0	Hub radius (ft)
RT1	11-20	F10.0	Tip radius (ft)
Z1	21-30	F10.0	Length (ft)
TWH	31-40	F10.0	Hub wall temperature (deg R)
TWT	41-50	F10.0	Tip wall temperature (deg R)
AMWH	51-60	F10.0	Hub wall bleed ($lb/ft^2/sec$)
AMWT	61-70	F10.0	Tip wall bleed ($lb/ft^2/sec$)

Card No. 4: (IØPT3=2)

Name	Col.	Format	Comments:
Z1	1-10	F10.0	Duct length (ft)

Cards Following Card No. 4: (IØPT3=2)

Name	Col.	Format	Comments:
R(1,1,J)	1-80	8F10.0	Tip radius (ft)
R(2,1,J)	1-80	8F10.0	Hub radius (ft)

Card No. 4: (IØPT3=3)

Name	Col.	Format	Comments
RH1	1-10	F10.0	Hub radius (ft)
RT1	10-11	F10.0	Tip radius (ft)
Z1	11-20	F10.0	Duct length (ft)
ZTHRO	20-30	F10.0	Length to throat (ft)

Card No. 4: (IØPT3=3) (Continued)

Name	Col.	Format	Comments:
ANGH	30-40	F10.0	Hub wall angle (deg)
ANGT	30-50	F10.0	Tip wall angle (deg)

Card No. 4: (IØPT3=4)

Name	Col.	Format	Comments:
TWH	1-10	F10.0	Hub wall temperature (deg R)
TWT	11-20	F10.0	Tip wall temperature (deg R)
AMWH	21-30	F10.0	Hub wall bleed ($lb/ft^2/sec$)
AMWT	31-40	F10.0	Tip wall bleed ($lb/ft^2/sec$)

Card No. 5: Inlet Flow Distribution

Name	Col.	Format	Comments:
AMS1	1-10	F10.0	Nominal inlet Mach number
ALP1	11-20	F10.0	Nominal swirl angle at hub (deg to axis)
DSH	21-30	F10.0	Boundary layer displacement thickness on hub wall (ft)
DST	31-40	F10.0	Boundary layer displacement thickness on tip wall (ft)
ANH	41-50	F10.0	Power law exponent for hub boundary layer
ANT	51-60	F10.0	Power law exponent for tip boundary layer

2 x KLL Inlet Flow Cards Following Card 5 (Only if IØPT1=2)

Name	Col.	Format	Comments:
Y	1-10	F10.0	Fractional distance across duct
P_o	11-20	F10.0	Total pressure (lb/ft^2 abs)
P	21-30	F10.0	Static pressure (lb/ft^2 abs)

α	31-40	F10.0	Swirl angle to axis (deg)
T_o	41-50	F10.0	Total temperature (deg R)

The first KLL cards describe the inlet flow. The second KLL cards describe the exit flow. If the exit flow is not known, KLL blank data cards must be used. If $\delta^*_H > 0$ on Card 5.0, boundary layers are added according to card 5.0.

Card No. 6: Blade Data (Only if IØPT2≠0)

Name	Col.	Format	Comments:
ZCL	1-10	F10.0	Axial location of strut centerline (ft) (see Fig. (7.2.8.1))
NB	11-13	I3	Number of struts
ISHAPE	14-16	I3	Blade shape index ISHAPE=1 NACA 5 digit series blade ISHAPE=2 Swirl vane

Card No. 7: Blade Row Geometry Hub (Only if IØPT2≠0)

Name	Col.	Format	Comments:
RCLH	1-10	F10.0	Hub radius at blade centerline (ft)
ALPSH	11-20	F10.0	Chord angle to blade face (deg)
CHØRDH	21-30	F10.0	Chord (ft)
THICKH	31-40	F10.0	Thickness/chord
PHICH	41-50	F10.0	Camber angle (deg) (see Fig. (7.2.2.1))

Card No. 8: Blade Row Geometry Midpoint (Only if IØPT2≠0)

Name	Col.	Format	Comments:
RCLM	1-10	F10.0	Midpoint radius at blade centerline (ft)
ALPSM	11-20	F10.0	Chord angle to blade face (deg)
CHØRDM	21-30	F10.0	Chord (ft)

Card No. 8 (Continued)

Name	Col.	Format	Comments:
THICKM	31-40	F10.0	Thickness/chord
PHICM	41-50	F10.0	Camber angle (deg) (see Fig. (7.2.2.1))

Card No. 9: Blade Row Geometry Tip (Only if IØPT2≠0)

Name	Col.	Format	Comments:
RCLT	1-10	F10.0	Tip radius at blade centerline (ft)
ALPST	11-20	F10.0	Chord angle to blade face (deg)
CHØRDT	21-30	F10.0	Chord (ft)
THICKT	31-40	F10.0	Thickness/chord
PHICT	41-50	F10.0	Camber angle (deg) (see Fig. (7.2.2.1))

2 x KLL Strut Data Cards Following Card 9 (IØPT5≠0, IØPT2=1)

Name	Col.	Format	Comments:
Y	1-10	F10.0	Fractional distance across duct
P_0	11-20	F10.0	Stagnation pressure (lb/ft^2 abs)
P	21-30	F10.0	Static pressure (lb/ft^2 abs)
α	31-40	F10.0	Swirl angle to axis (deg)
T_0	41-50	F10.0	Stagnation temperature (deg R)

The first KLL cards describe the inlet flow to strut row. The second KLL cards describe the exit flow. (see Card 2).

KLL Blade Data Cards Following Card 9 (IØPT5≠0, IØPT2=4)

Name	Col.	Format	Comments:
Y	1-10	F10.0	Fractional distance across duct
α	11-20	F10.0	Swirl angle at exit (deg)
Z_B	21-30	F10.0	Loss coefficient

Card No. 10: Performance Point

Name	Col.	Format	Comments:
PRESO	1-10	F10.0	Inlet stagnation pressure (lb/ft^2 abs)
TEMPO	11-20	F10.0	Inlet stagnation temperature (deg R)
ACI	21-30	F10.0	Clauser constant (0.016)
AKI	31-40	F10.0	Von Karman constant (0.41)
API	41-50	F10.0	Van Driest constant (26.0)
PRTI	51-60	F10.0	Turbulent Prandtl number
PRLI	61-70	F10.0	Laminar Prandtl number

Card No. 11: Specify Gas (Only if IØPT7=1)

Name	Col.	Format	Comments:
CPR	1-10	F10.0	Specific heat at constant pressure (ft^2/sec^2)
CVR	11-20	F10.0	Specific heat at constant volume (ft^2/sec^2)
VISCR	21-30	F10.0	Viscosity ($lb\ sec/ft^2$)

4.3 Description of Output

Title Page

The output presented on this page is self-explanatory except for the following variables

$$m_I = \int_{r_H}^{r_T} g_B \rho U_S \, dr \tag{4.3.1}$$

$$a_I = \int_{r_H}^{r_T} g_B \, dr \tag{4.3.2}$$

$$\bar{P}_I = \frac{1}{M_I} \int_{r_H}^{r_T} g_B \rho U_S P_I \, dr = \text{PRESI} \tag{4.3.3}$$

$$\bar{q}_I = \frac{1}{M_I} \int_{r_H}^{r_T} g_B \rho U_S (1/2 \rho U_I^2) \, dr = \text{DYNPI} \tag{4.3.4}$$

$$\bar{M}_I = \frac{1}{M_I} \int_{r_H}^{r_T} g_B \rho U_S M_I \, dr = \text{MACHI} \tag{4.3.5}$$

$$\text{WFL}\phi = 32.2 \, N_B M_I \tag{4.3.6}$$

$$\text{USR} = M_I / \rho_r / a_I \tag{4.3.7}$$

$$\text{REY} = r_r U_r \rho_r / \mu_r \tag{4.3.8}$$

Wall Conditions Page

This page presents a table of $Z, R_H, \dot{m}_N, \Theta_H, R_T, \dot{m}_T, \Theta_T$ which was calculated in Subroutine GDUCT.

Strut Data Pages(2) (If IØPT2=1)

These pages present the strut data that were read into the program with IØPT2=1. It is written with the same format as the input (see Section 4.2).

Blade Force Variables Pages(2) (If IØPT2≠0)

These pages present the variables $Y, \hat{U}_s, \hat{U}_\phi, \hat{\alpha}, \hat{\Pi}, \hat{\Theta}, \hat{M}, \hat{\Pi}_0, \hat{\Theta}_0, \hat{P}$ across the flow passage at the upstream (station 2) and downstream (station 3) control surface. These flow variables are used to calculate the blade force.

Blade Force Page (If IØPT2≠0)

This page presents a summary of the blade force calculation $Y, G_B, \Xi_s, \Xi_\phi, C_L, C_D, Z_B, I$ across the duct.

Gap Average Flow Page

This page presents the solution for the flow variables across the duct at selected streamwise stations depending on IØPT4. A table of values for $Y, U_s, U_\phi, \alpha, \Pi, \Theta, M, \Pi_0, \Theta_0, C_p$ are given where

$$C_p = (\Pi - \Pi(0,0))/\bar{q}_1 \tag{4.3.9}$$

In addition, the wall values for $Z, \dot{m}, C_{f\phi}, C_{fs}, Q$ are printed, where $C_{f\phi}$ and C_{fs} are defined by

$$C_{f\phi} = \tau_{n\phi}/\bar{q}_1 \tag{4.3.10}$$

$$C_{fs} = \tau_{ns}/\bar{q}_1 \tag{4.3.11}$$

The one-dimensional characteristics of the flow are also given; area ratio a/a_1, Mach number (isentropic flow) M_1, incompressible and compressible flow pressure coefficient CPINC and CPCØMP.

Finally, the following quasi-two-dimensional boundary layer information is given:

THET = θ^*/r_r , Momentum thickness (dimensionless)

H12 = δ^*/θ^* , Shape factor (dimensionless)

REYTH = $\rho_\infty U_\infty \theta^*/\mu_\infty$, Reynolds number based on momentum thickness (dimensionless)

CF = τ_w/q_∞ , Wall friction coefficient (dimensionless)

REC = R_c , Recovery factor (dimensionless)

STAN = St , Stanton number (dimensionless)

These variables are based on boundary layer thickness defined by the maximum velocity in the duct and, therefore, may not be meaningful if swirl, flow distortion, or large normal pressure gradients exist.

IDBGØ Pages

Intermediate printouts which were used to debug the program may be called by setting the debug options IDBGØ=1. IDBGØ may be specified on the option input card. The user should refer to the program listing in each subroutine to determine the printout variables.

IDBGØ	Subroutine	Printout
IDBG1	SPLDC	Tables of $U^+(Y^+), H_\Delta^+(Y^+), H^+(Y^+), W^+(Y^+)$
IDBG2	SPLDC	Table of $C_N(m^+)$, $C_N(P^+)$
IDBG3	FLØWIN	Flow input variables and parameters
IDBG4	STRESS	Table of G(K) and parameters
IDBG5	SØLVE	Tables of DF(K), DHF(K), DPF(K)
IDBG6	CØØR	Tables of Q(K), RH(J), RT(J)
IDBG7	FØRCE	Table of FF(K)

4.4 Description of Failure Modes

The computer program can diagnose the cause of certain failure modes and a printed message of the following form is given.

DIAGNOSTIC NO. ϕ FOR ANNULAR DIFFUSER DECK

The number ϕ identifies the type of failure from the list below.

(1) AMPLUS OR PPLUS OUTSIDE RANGE OF TABLE

This failure occurs in Subroutine CINTP. In attempting to interpolate a value of $C(m^+)$ or $C(p^+)$ from the table, a value of m^+ or p^+ is encountered which is outside the tabulated values. Calculation is then terminated. This failure may occur for small values of U^* as the flow approaches separation.

(2) ITERATION IN FUNCTION USTAR FAILED TO CONVERGE

This failure occurs in Function USTAR and means that Newton's iteration does not converge. Since $U^+(Y^+)$ is a well behaved function with no saddle points or singularities except a logrithmic singularity at $Y^+ = 0$, Newton's method should converge if the input is correct. The possibility of extrapolating to a negative value of U^+ has been anticipated and corrective measures applied. Failure, however, may occur when the numerical integration is numerically unstable, or if $Y^+ < 10$.

(3) AMPLUS CANNOT BE LESS THAN -0.06

This failure mode occurs in Subroutine SPLD because asymptotic solutions do not exist for $m^+ < -0.06$. Calculation is terminated.

(4) ADD STRAIGHT ANNULAR CHANNEL INLET

This failure mode occurs in Subroutine CØØR and represents a warning that the inlet flow must not have a normal pressure gradient. For better results add a straight annular channel inlet. The calculation, however, is not terminated by this failure mode.

(5) WALL CURVATURE TOO LARGE AT STATION (I)

This failure mode occurs in Subroutine CØØR when the wall curvature is too large and the calculation is terminated. This failure frequently occurs when the duct coordinates are discontinuous. Check the calculation in Subroutine GDUCT.

(6) SOLUTION UNSTABLE AT S = (XXX.)

This failure mode occurs in Subroutine SØLVE when the streamwise velocity is negative resulting from numerical instability. The calculation is then terminated. Decreasing the step size (increasing KDS) may improve stability.

(7) BLADE DATA IN ERROR IN FORCE INTERPOLATION ROUTINE

This failure mode occurs in Subroutine FØRCE from failure of the interpolation procedure. This failure can only occur if the input data is wrong.

(8) ITERATION OF BACK PRESSURE CALCULATION FAILS TO CONVERGE

This failure mode occurs in Subroutine FINVIS when the iteration scheme required to compute the back pressure from radial equilibrium of the downstream flow fails to converge. This failure frequently occurs when the loss coefficient is excessively high. Calculation is terminated.

(9) YPLUS LESS THAN 10. IN FUNCTION FUPLUS

This failure mode occurs in Function FUPLUS because the inner layer analytical solutions are not valid for $Y^+ < 10$. This failure sets $U^+ = 0$ and, therefore, the calculation must be terminated. The problem may be corrected by increasing Y^+ at the matching point, by increasing the Reynolds number, or increasing the mesh spacing near the wall.

(10) YPLUS AT MATCHING POINT OUTSIDE BOUNDS

For best results, Y^+ at the matching point must lie between the limits $40 \leq Y^+ \leq 500$. When the calculation is outside these bounds, Y^+ is printed out but the calculation is not terminated.

(11) PROGRAM ASSUMES INLET FLOW HAS CURVATURE

The analysis assumed that the inlet flow duct has no curvature, hence normal pressure gradients are produced only by swirl. Calculation, however, is not terminated.

(12) CRITICAL MACH NUMBER INSTABILITY

This failure mode occurs when the critical Mach number is reached too close to a mesh point. It can be corrected by changing KDS to move the mesh point.

(13) ISHAPE=(I) AND IØPT2=(J) ARE NOT CONSISTENT

The input options are not consistent. See Section 4.2.

5.0 REFERENCES

1. Reneau, L. R., J. P. Johnson, and S. J. Kline: Performance and Design of Straight, Two-Dimensional Diffusers. Transactions of ASME, Journal of Fluid Mechanics, Vol. 89, March 1969, pp. 141-160.

2. Sovran, G. and E. D. Klomp: Optimum Geometries for Rectilinear Diffusers. Fluid Mechanics of Internal Flow, El Sevier Publishing Co., 1967.

3. Fox, R. W. and S. J. Kline: Flow Regime Data and Design Methods for Curved Subsonic Diffusers. Journal of Basic Engineering, Transactions of the ASME, Series D, Vol. 84, No. 3, September 1962, pp. 303-312.

4. Howard, J., H. Henseler, and A. Thornton-Trump: Performance and Flow Regimes for Annular Diffusers. ASME Paper 67, WA/FE-21, 1967.

5. Runstadler, P. W. and R. C. Dean: Straight Channel Diffuser Performance at High Inlet Mach Numbers. Transactions of ASME, Journal of Basic Engineering, Vol. 91, September 1969, pp. 397-422.

6. Anderson, O. L.: A Comparison of Theory and Experiment for Incompressible, Turbulent, Swirling Flows in Axisymmetric Ducts. AIAA Paper No. 72-42, 10th Aerospace Sciences Meeting, January 1972.

7. Anderson, O. L.: Numerical Solutions of Incompressible Turbulent Swirling Flows Through Axisymmetric Annular Ducts. United Aircraft Research Laboratories Report No. H213577-1, March 1968.

8. Pai, S.: Viscous Flow Theory, Vol. I, D. Van Nostrand Co., Inc., Princeton, New Jersey, 1956.

9. Hinze, J. O.: Turbulence. McGraw-Hill Book Co., Inc., New York, New York, 1959.

10. Hoerner, S. J.: Fluid Dynamic Drag. Published by the Author, Midland Park, New Jersey, 1965.

11. Abbott, I. H., A. E. Von Doenhoff, and L. S. Tivers: Summary of Airfoil Data. NACA Report No. 824, 1967.

12. Johnson, I. A. and R. O. Bullock: Aerodynamic Design of Axial Flow Compressors. NASA SP-36, 1965.

13. Smith, A. M. O. and T. Cebici: Numerical Solutions to the Turbulent Boundary Layer Equations. Douglas Aircraft Report No. DAC 33735, May 1967.

14. Schlicting, H.: Boundary Layer Theory. McGraw-Hill Book Co., Inc., New York, New York, 1955.

15. Clauser, F.: The Turbulent Boundary Layer. Advanced Applied Mechanics, Vol. 4, 1956, pp. 1-51.

16. Spalding, D. B. and S. V. Pantankar: Heat and Mass Transfer in Boundary Layers. Morgan-Gampian, London, England, 1967.

17. Courant, R.: Methods of Mathematical Physics, Vol. II. New York, Interscience, 1962.

18. Wang, K. C.: On the Determination of Zones of Influence and Zones of Dependence for Three-Dimensional Boundary Layer Equations. Journal of Fluid Mechanics, Vol. 48, Part II, 1971.

19. Lubard, S. C. and J. A. Schetz: Numerical Solutions of Boundary Layer Problems. University of Maryland Report 67-1, AFSOR 67-2056, September 1967.

20. Chi, S. W. and D. B. Spalding: Influence of Temperature Ratio and Heat Transfer to a Flat Plate Through a Turbulent Boundary Layer. Procedures of 3rd International Heat Transfer Conference (AICHE), II, 1966, pp. 41-49.

21. Copp, M. R.: Effects of Inlet Wall Contour on the Pressure Recovery of a 10 deg 10 inch Inlet Diameter Conical Diffuser. NACA RM L51E11a, September 1951.

22. Wood, C. C. and J. R. Henry: Effects of Shock-Boundary-Layer Interaction on the Performance of a Long and Short Subsonic Annular Diffuser. NACA RM L58A31, 1958.

6.0 LIST OF SYMBOLS

a	Area (ft^2)
A	Area, a/r_r^2 (dimensionless)
A^+	Van Driest constant (26.0)
A^*	Critical area ratio (dimensionless)
b	Chord (ft)
B	Chord, b/r_r (dimensionless)
c	Speed of sound (ft/sec)
c_p	Specific heat pressure ($ft^2/sec^2/deg\ R$)
c_v	Specific heat volume ($ft^2/sec^2/deg\ R$)
C_D	Drag coefficient, $2D/(\rho_2 U_2^2 b)$ (dimensionless)
C_L	Lift coefficient, $2L/(\rho_2 U_2^2 b)$ (dimensionless)
D	Drag/span (lb/ft)
e_{ns}	Streamwise strain (1/sec)
$e_{n\phi}$	Tangential strain (1/sec)
f	Force/area (lb/ft^2)
f	Force/span (lb/ft)
g	Gap between walls (ft)
G	Gap between walls, g/r_r (dimensionless)
g_B	Gap between chord lines (ft)
G_B	Gap between chord lines (dimensionless)
h	Enthalpy (ft^2/sec^2)

H^+ Universal stagnation enthalpy, $(h_{ow}-h_o)\rho_w U^*/q_w$ (dimensionless)

H_A^+ Universal adiabatic stagnation enthalpy, $(h_{oAW}-h_{oA})/(U^*)^2$ (dimensionless)

I Entropy ($ft^2/sec^2/deg\ R$)

L Lift/span (lb/ft)

m Mass flow (slugs/sec)

M Mass flow, $m/(N_B r_r^2 \rho_r U_r)$ (dimensionless)

$\mathring{m}$ Mass flow/area ($slugs/ft^2/sec$)

m^+ Universal mass flow parameter, $\mathring{m}_w/(\rho_w U^*)$ (dimensionless)

$\mathring{M}$ Mass flow/area, $\mathring{m}/(\rho_r U_r)$ (dimensionless)

M Mach number, U/C (dimensionless)

M_s Streamwise Mach number (dimensionless)

n Normal coordinate (dimensionless)

η Normal coordinate, $n/(r_r V_r)$ (dimensionless)

N_B Number of struts (dimensionless)

N_R Reynolds number, $r_r \rho_r U_r/\mu_r$ (dimensionless)

p Pressure (lb/ft^2)

p^+ Universal pressure gradient parameter, $\frac{\mu_w}{\rho_w U^+}\ \frac{1}{\rho_w U^{+2}}\ \frac{dp}{dx}$ (dimensionless)

P_R Prandtl number, $\left(\frac{\mu C_p}{\lambda}\right)$ (dimensionless)

P_{RT} Prandtl number turbulent, $\left(\frac{\mu C_p}{\lambda}\right)_T$ (dimensionless)

q Heat flux, $-\lambda \frac{\partial T}{\partial Y}$ ($lb/ft/sec$)

$\overline{q}_1$ Average inlet dynamic pressure (lb/ft^2)

Q Heat flux, $q/(\rho_r U_r c_p T_r)$ (dimensionless)

Q^+ Universal heat flux, q/q_w (dimensionless)

Q_A^+	Universal heat flux (adiabatic), $\dot{q}/(\rho_w U^{*3})$ (dimensionless)
r	Radius (ft)
R_c	Recovery factor, Eq. (3.2.35) (dimensionless)
R	Radius, r/r_r (dimensionless)
$\mathcal{R}$	Gas constant ($ft^2/sec^2/deg\ R$)
s	Streamwise coordinate (dimensionless)
S	Streamwise coordinate, $s/(r_r V_r)$ (dimensionless)
S_t	Stanton number (dimensionless)
t	Blade thickness (ft)
T	Temperature (deg R)
T^+	Universal temperature, $c_p T/u^{*2}$ (dimensionless)
u_s	Streamwise velocity (ft/sec)
u_n	Normal velocity (ft/sec)
u_ϕ	Tangential velocity (ft/sec)
u	Magnitude of velocity (ft/sec)
u_B	Blade velocity (ft/sec)
u^*	Friction velocity, $\sqrt{\tau_w/\rho_w}$ (ft/sec)
U_s	Streamwise velocity, U_s/U_r (dimensionless)
U_n	Normal velocity, U_n/U_r (dimensionless)
U_ϕ	Tangential velocity, U_ϕ/U_r (dimensionless)
U	Magnitude of velocity, U/U_r (dimensionless)
U_B	Blade velocity, U_B/U_r (dimensionless)

U^+	Universal velocity, U/U^* (dimensionless)
U^*	Friction velocity, U^*/U_r (dimensionless)
v	Metric scale coefficient (dimensionless)
V	Metric scale coefficient, v/v_r (dimensionless)
W^+	Stream function inner layer (dimensionless)
$\forall$	Volume (ft^3)
x	Distance along streamline (ft)
y	Distance normal to wall (ft)
z	Axial distance (ft)
X	Distance along streamline, x/r_r (dimensionless)
Y	Distance normal to wall, y/r_r (dimensionless)
Y^+	Universal distance from wall, $y\rho_w u^*/\mu_w$ (dimensionless)
Z	Axial distance, z/r_r (dimensionless)
Z_B	Loss coefficient (dimensionless)
α	Swirl angle to axis (deg)
α_s	Chord angle to axis (deg)
γ	Ratio of specific heats, c_p/c_v (dimensionless)
δ	Boundary layer thickness (ft)
δ^*	Displacement thickness (ft)
Δ	Boundary layer thickness, δ/r_r (dimensionless)
Δ^*	Displacement thickness, δ^*/r_r (dimensionless)
E_{ns}	Streamwise strain, $r_r e_{ns}/u_r$ (dimensionless)
$E_{n\phi}$	Tangential strain, $r_r e_{n\phi}/u_r$ (dimensionless)

η	Transformed normal coordinate (dimensionless)
H	Blade/force area $r_r f/(\rho_r u_r^2)$ (dimensionless)
θ	Angle of streamline to axis (deg)
θ^*	Momentum thickness (ft)
Θ	Temperature ratio, T/T_r (dimensionless)
Θ^*	Momentum thickness, θ^*/T_r (dimensionless)
I	Entropy, $(I-I_r)/\mathcal{R}$ (dimensionless)
κ	Von Karman constant (0.41)
λ	Thermal conductivity (lb/sec/deg R)
μ	Viscosity (slugs/ft/sec)
Ξ	Blade force/span, $f/(r_r \rho_r u_r^2)$ (dimensionless)
Π	Pressure ratio, p/p_r (dimensionless)
ρ	Density (slugs/ft^3)
ρ_s, ρ_n	Radius of curvature (ft)
P	Density ratio, ρ/ρ_r (dimensionless)
P_s, P_n	Radius of curvature (dimensionless)
σ	Solidity, b/g_B (dimensionless)
Σ_{ns}	Streamwise stress, $\tau_{ns}/(\rho_r u_r^2)$ (dimensionless)
$\Sigma_{n\phi}$	Tangential stress, $\tau_{n\phi}/(\rho_r u_r^2)$ (dimensionless)
τ_{ns}	Streamwise stress (lb/ft^2)
$\tau_{n\phi}$	Tangential stress (lb/ft^2)
τ^+	Stress, τ/τ_w (dimensionless)

ϕ	Tangential coordinate (radians)
ϕ_c	Camber angle (deg)
ϕ_B	Blade dissipation function ($lb/sec/ft^2$)
Φ_B	Blade dissipation function (dimensionless)
χ	Clauser constant (0.016) (dimensionless)
X	Normal coordinate transform, $d\eta/dn$ (dimensionless)
ψ	Stream function (slugs/ft)
Ψ	Stream function (dimensionless)

Subscripts

o	Stagnation conditions
1	Inlet conditions
2	Upstream of strut
3	Downstream of strut
A	Adiabatic
E	Effective turbulent
H	Hub conditions
I	Incompressible conditions
M	Midspan conditions
r	Reference conditions*

*Reference conditions are based on standard sea level atmosphere conditions for all thermodynamic quantities. The reference radius r_r is the inlet outer radius, and the velocity is the mean inlet velocity.

$_T$	Tip conditions
$_w$	Wall conditions
$_\infty$	Free stream or edge of boundary layer

Superscripts

$\bar{}$	Mean or average quantity
$\wedge$	Variables for blade force calculation
$'$	Deviation from mean quantity

7.0 APPENDIX A: DETAILED PROGRAM DESCRIPTION

A detailed description of the computer program is given in this section. The subroutines and external functions are described individually. A list of FØRTRAN variables and DIMENSION FØRTRAN variables in blank common are given as well as a source listing and a set of functional flow charts.

The subroutines and external functions are all described with the same format using the name of the subroutine with its argument list given as a title. A list of options and FØRTRAN symbols used only in the named subroutine are then given. Any special or additional theory used in the subroutine is presented but well known numerical methods are not described. Figures and Flow Charts appear with the subroutine.

Subroutine GDUCT, CASC, and FTHIK, which generate the duct shape, and calculate the strut lift and drag coefficient, and blade thickness distribution, respectively, have special status since they must be written by the user. Sample calculations are given, and the user should examine carefully the flow charts for these subroutines.

7.1 Main Program

Object Control input/output.

Options All options described in Section 4.2.

List of Symbols All variables in blank CØMMØN.

Theory

The MAIN program serves as an executive program to read input according to selected options and write the appropriate output. In addition, it computes or sets fixed data which is used for any case that may be calculated such as calling Subroutine SPLD which computes the constants for the inner layer solution. Finally, the MAIN program calls Subroutine SØLVE which does the actual computation. The flow chart is shown in Fig. 7.1.1.

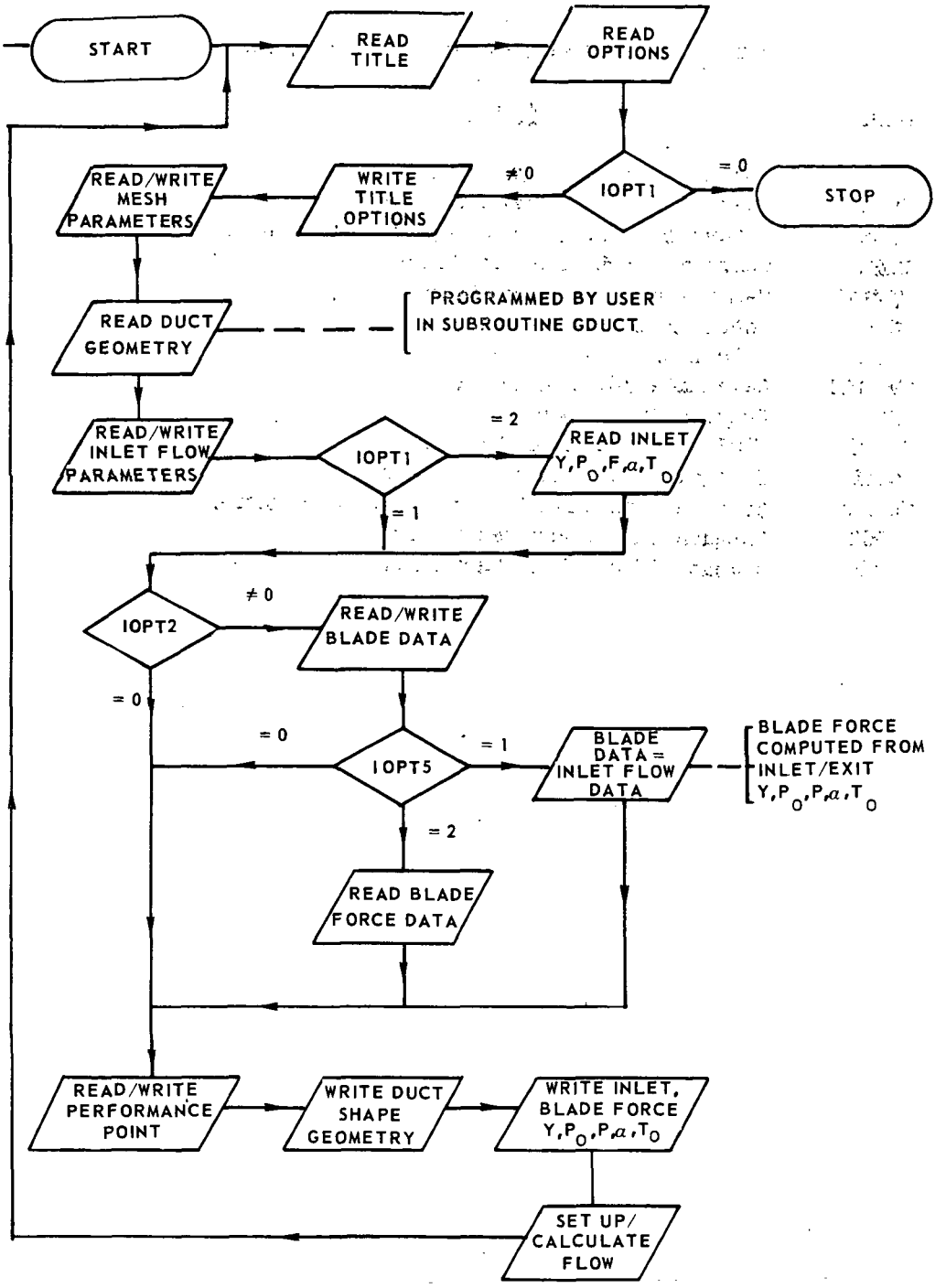

FIG. 7.1.1-FLOW CHART MAIN PROGRAM.

7.2 List and Description of Subroutines

	Name	Object
7.2.1	BL2D	Compute Boundary Layer Parameters
7.2.2	CASC	Compute Strut Performance
7.2.3	CINTP	Interpolate Table of Asymptotic Constants
7.2.4	CØØR	Compute Coordinate Functions
7.2.5	FINVIS	Calculate Strut Back Pressure
7.2.6	FLØWIN	Setup Inlet Flow
7.2.7	FØRCE	Calculate Strut Force
7.2.8	GBLADE	Calculate Blade Geometry
7.2.9	GDUCT	Compute Duct Shape
7.2.10	SLETE	Find Strut Control Surfaces
7.2.11	SØLVE	Integrate Equations of Motion
7.2.12	SPLDC	Compute Constants for Inner Layer Solution
7.2.13	STRESS	Compute Stress and Heat Flux
7.2.14	VARB	Compute Blade Force Variables

7.2.1 Subroutine BL2D

Object Compute Boundary Layer Parameters

Options

II=1	Calculate Hub Boundary Layer	
=2	Calculate Tip Boundary Layer	
III=1	Curve Fit	$Y = PU/(P_\infty U_\infty)$
=2	Curve Fit	$Y = U/U_\infty$

List of Symbols

AMF	$= M_\infty$	, Free stream Mach number (dimensionless)
AN1,AN2	$= n_1, n_2$	, Velocity Profile Power Law Exponent (dimensionless)
BLØCK	$= B_c = \left[\Delta_H^* R_H + \Delta_T^* R_T\right]/A$	, Blockage factor (dimensionless)
CF1	$= C_f = \Sigma_w/(1/2\, P_\infty U_\infty^2)$	, Wall Friction Coefficient (dimensionless)
DSH1	$= \Delta_H^* = \int_0^{\Delta H}\left[1 - \frac{PU_s}{PU_\infty}\right]dy$	, Displacement thickness hub (dimensionless)
DST1	$= \Delta_T^* = \int_0^{\Delta T}\left[1 - \frac{PU_s}{P_\infty U_\infty}\right]dy$	, Displacement thickness tip (dimensionless)
D1	$= \Delta^*/\Delta_1$	, Displacement thickness ratio (dimensionless)
D2	$= \Theta^*/\Delta_1$	, Momentum thickness ratio (dimensionless)
H12	$= H_{12} = \Delta^*/\Theta^*$	, Shape factor (dimensionless)
QF	$= q_\infty = 1/2\, P_\infty U_\infty^2$	, Free-stream dynamic pressure (dimensionless)
QW	$= Q\omega$	, Wall heat flux (dimensionless)
RCALC	$= R_C = \left[\Theta_w\Theta_\infty - 1\right]/\left(\frac{\gamma-1}{2} M_\infty^2\right)$	, Recovery factor (dimensionless)
REYTH	$= R_{e\theta} = P_\infty U_\infty \Theta^*/\frac{\mu_\infty}{\mu_r}$	, Reynolds number (dimensionless)
RF	$= P_\infty$	, Free-stream density (dimensionless)
STAN	$= Q_W/\left[P_\infty U_\infty(\Theta_w - \Theta_{WA})\right]$	, Stanton number (dimensionless)
TF	$= \Theta_\infty$	, Free-stream temperature (dimensionless)

THET $= \Theta^* = \int_0^{\Delta} \frac{PU_S}{PU_\infty}\left[1 - \frac{U_S}{U_\infty}\right] dY$, Momentum thickness (dimensionless)

TW $= \Theta_W$, Wall temperature (dimensionless)

TWA $= \Theta_{WA} = \left[1 + P_{RL}^{1/3} \frac{\gamma - 1}{2} M_\infty^2\right]\Theta_\infty$, Adiabatic wall temperature (dimensionless)

UF $= U_\infty$, Free-stream velocity (dimensionless)

XB $= \overline{X}$, Average X (dimensionless)

YB $= \overline{Y}$, Average Y (dimensionless)

Theory

When the boundary layers are very thin, it is difficult to integrate the flow variables accurately. Therefore, a power law is fitted to the solution of the form

$$PU/(P_\infty U_\infty) = (Y/\Delta_1)^{1/n_1} \qquad (7.2.1.1)$$

and

$$U/U_\infty = (Y/\Delta_1)^{1/n_2} \qquad (7.2.1.2)$$

which with logrithmic differentiation become

$$\ln(y/\Delta_1) = n_1 \ln\left[(PU)/(P_\infty U_\infty)\right] \qquad (7.2.1.3)$$

or

$$\ln(y/\Delta_2) = n_2 \ln\left[U/U_\infty\right] \qquad (7.2.1.4)$$

Letting

$$X = \ln(Y/\Delta_1) \text{ or } \ln(Y/\Delta_2) \text{ (The choice dependent upon III)} \qquad (7.2.1.5)$$

and

$$Y = \ln\left[PU_s/P_\infty U_\infty\right] \text{ or } \ln\left[U_s/U_\infty\right] \qquad (7.2.1.6)$$

a least square fit

$$Y = \bar{Y} + b(X - \bar{X}) \qquad (7.2.1.7)$$

is used to determine $n_1, n_2, \Delta_1, \Delta_2$. Finally,

$$\Delta^*/\Delta_1 = 1/(1+n_1) \qquad (7.2.1.8)$$

and

$$\Theta^*/\Delta_2 = \left(\frac{\Delta_2}{\Delta_1}\right)^{1/n_1}\left[\frac{n_1}{1+n_1} - \frac{n_1}{1+n_1+n_1/n_2}\right] \qquad (7.2.1.9)$$

7.2.2 Subroutine CASC (Argument List)

Object Compute Strut Performance

Options

ISHAPE=1 NACA 5 digit Series Airfoil
=2 Flow Turning Vane

List of Symbols (Argument List)

ALPH3	$= \hat{\alpha}_3$	, Exit Flow angle (deg)
ALPS	$= \alpha_s$	, Chord angle to axis (deg)
ALP1	$= \hat{\alpha}_2$	, Inlet flow angle (deg)
AMACH	$= \hat{M}_2$	, Inlet Mach number (dimensionless)
BCHØRD	$= B$	, Chord (dimensionless)
CD	$= C_D$	, Drag coefficient (dimensionless)
CL	$= C_L$	, Lift coefficient (dimensionless)
PHIC	$= \phi_c$	, Camber angle (deg)
SØLD	$= \sigma = B/G_B$	, Solidity (dimensionless)
TM	$= t_M$	, Blade thickness (dimensionless)
ZLØSS	$= Z_B$	, Loss coefficient (dimensionless)

Theory

This subroutine computes the blade or strut section performance. Since many strut shapes are possible (Refs. 10 and 11), only two shall be described here for illustrative purposes.

ISHAPE=1

The subsonic performance of isolated airfoils is given in Ref. 11. Selecting the NACA 5 digit uncambered airfoils and applying the Prandtl-Glauert rule

$$\left(\frac{dC_L}{d\alpha}\right)_0 = 0.109 - 0.0256 \frac{t_M}{B} \frac{1}{\sqrt{1-\hat{M}_2^2}} \qquad (7.2.2.1)$$

$$C_L = \left(\frac{dC_L}{d\alpha}\right)_0 \frac{(\hat{\alpha}_2 - \alpha_s)}{\sqrt{1-\hat{M}_2^2}} \qquad (7.2.2.2)$$

$$C_D = 0.0075 - 0.00382\, C_L^2 \qquad (7.2.2.3)$$

ISHAPE=2

For turning vanes of high solidity, it is assumed that the exit flow angle is equal to the metal angle and that the loss coefficient is given by the stator cascade losses of Ref. 12. Then

$$\hat{\alpha}_3 = \alpha_s - \phi_c/2 \qquad (7.2.2.4)$$

$$D = \left[1 - \frac{\cos\hat{\alpha}_2}{\cos\hat{\alpha}_3}\right] + \frac{\cos\hat{\alpha}_2}{2\sigma}\left[\tan\hat{\alpha}_2 - \tan\hat{\alpha}_3\right] \qquad (7.2.2.5)$$

$$\Phi_D = 0.005 + 0.005\,(D/4)^{4.28} \qquad (7.2.2.6)$$

$$Z_B = \Phi_D \frac{2\sigma}{\cos\hat{\alpha}_3}\left[\frac{\cos\hat{\alpha}_2}{\cos\hat{\alpha}_3}\right]^2 \qquad (7.2.2.7)$$

Input/Output

The input to this subroutine comes in the argument list and is given by $\hat{\alpha}_2$, α_s, $\hat{M}_2$, B, ϕ_c, t_M, σ ISHAPE, IØPT2, NØPT5. The output is also in the argument list and is either C_L, C_D, or $\hat{\alpha}_3$, Z_B. It is noted that IØPT2 and ISHAPE must be compatable. The sign convention for determining this force is shown in Fig. 7.2.2.1 and the flow chart for this subroutine is given in Fig. 7.2.2.2.

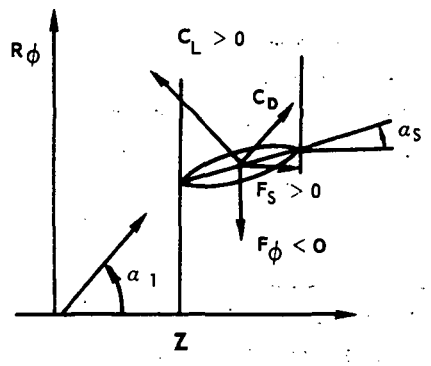

1. a DECELERATING FLOW

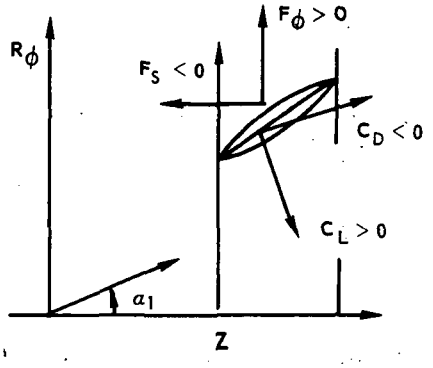

1. b ACCELERATING FLOW

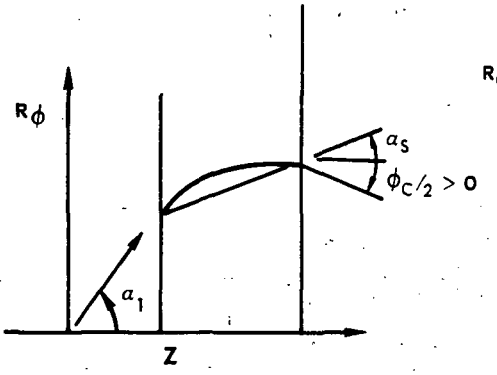

1. c DECELERATING FLOW

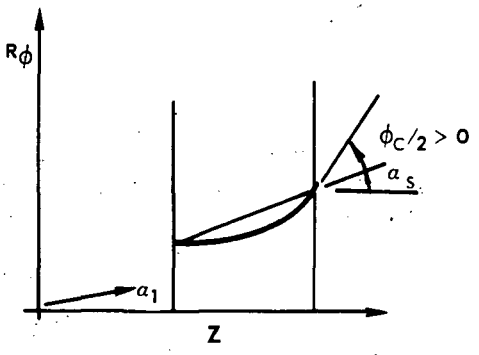

1. d ACCELERATING FLOW

FIG. 7.2.2.1 -SIGN CONVENTION BLADE FORCES.

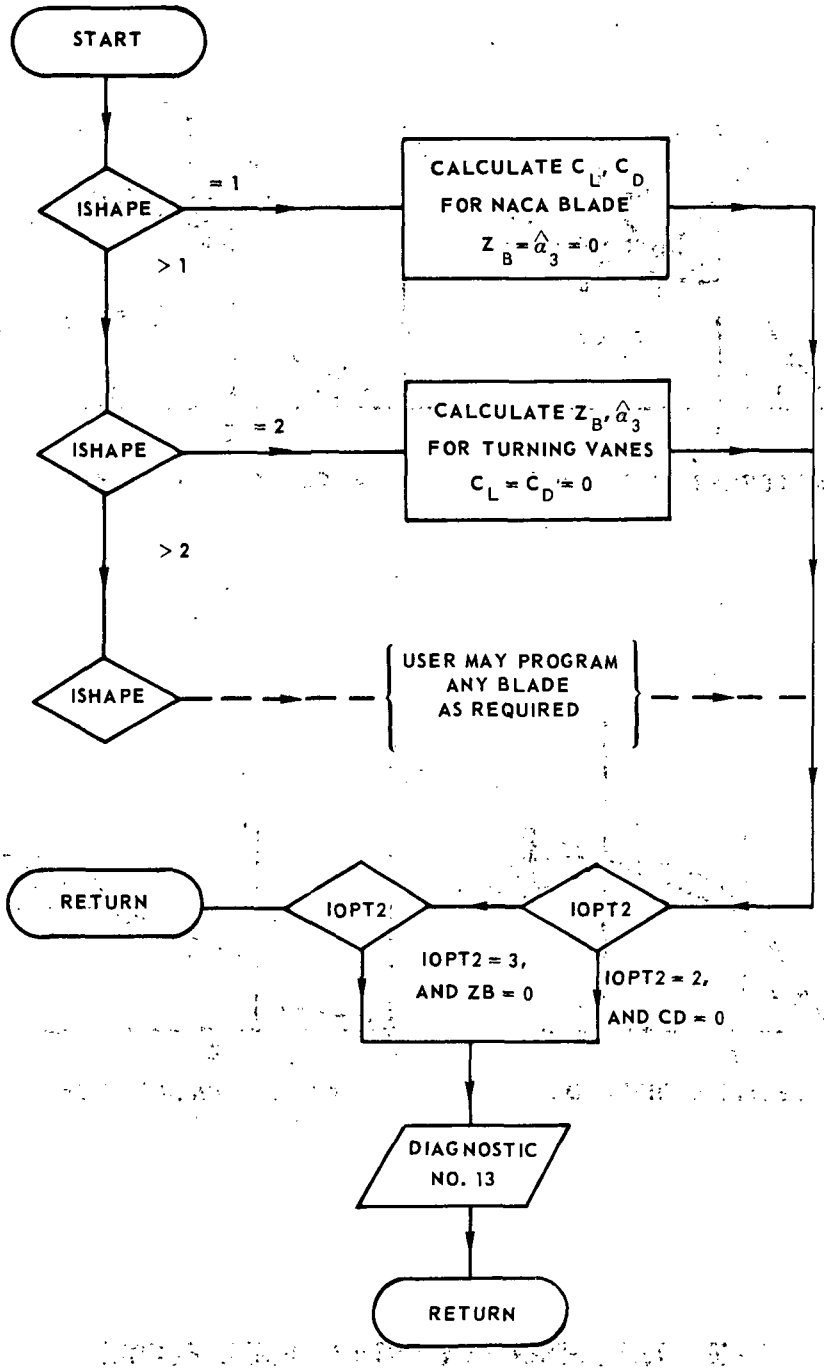

FIG. 7.2.2.2-FLOW CHART FOR SUBROUTINE CASC.

7.2.3. Subroutine CINTP

Object Interpolate Table of Asymptotic Constants

Options

IF($1 \leq LO \leq LM-2$) Calculate Constants
IF($LO \leq 1$. OR. $LO > LM-2$) Stop Calculations

List of Symbols

AMPLUO = m_0^+	,	First value of interpolation for m^+ (dimensionless)
LO	,	Index of first value of interpolation
PLUSO = p_0^+	,	First value of interpolation for p^+ (dimensionless)
X	,	Fractional distance (dimensionless)

Theory

Newton's forward differencing interpolation formula is used since it involves only tabulated values. Let

$$x = (m^+ - m_0^+)/\Delta m^+ \qquad (7.2.3.1)$$

$$= (p^+ - p_0^+)/\Delta p^+ \qquad (7.2.3.2)$$

Then for three successive tabulated points (f_0, f_1, f_2) for any tabulated function f

$$f = f_0 + (f_1 - f_0)x + (f_2 - 2f_1 + f_0)x(x-1)/2 \qquad (7.2.3.3)$$

with the restiction for best accuracy that

$$x \leq 1 \qquad (7.2.3.4)$$

7.2.4 Subroutine CØØR(KSS,JSS)

Object Compute Coordinate Functions

Options

NØPT3=1 Compute and Store Coordinates
=2 Compute Coordinate Functions

List of Symbols

A1 $= R_T(J+1) - R_T(J-1)$

A2 $= R_T(J+1) - 2R_T(J) + R_T(J-1)$

A5 $= Y_H + Y_T$, Sum of metric scale coefficients (dimensionless)

A6 $= V_H / V_T$, Ratio of metric scale coefficients (dimensionless)

B1 $= R_H(J+1) - R_H(J-1)$

B2 $= R_H(J+1) - 2R_H(J) + R_H(J+1)$

C $= C$, Constant in χ transformation (dimensionless)

C1 $= \left(\frac{dR_H}{dZ} + \frac{dR_T}{dZ}\right)/2$, Mean wall slope at J-1 (dimensionless)

C2 $= Z_T - Z_H$, at J-1 (dimensionless)

C3 $= R_T - R_H$, at J-1 (dimensionless)

C4 $= \left(\frac{dR_H}{dZ} + \frac{dR_T}{dZ}\right)/2 + \frac{Z_T - Z_H}{R_T - R_H}$, Slope difference at J-1 (dimensionless)

D1 $= \left(\frac{dR_H}{dZ} + \frac{dR_T}{dZ}\right)/2$, at J+1 (dimensionless)

D2 $= Z_T - Z_H$, at J+1 (dimensionless)

D3 $= R_T - R_H$, at J+1 (dimensionless)

D4 $= \left(\frac{dR_H}{dZ} + \frac{dR_T}{dZ}\right)/2 + \frac{Z_T - Z_T}{R_T - R_H}$, Slope difference at J+1 (dimensionless)

DZ $= \Delta Z$, Step size (dimensionless)

RH1 $= R_H$, Wall radius at s hub (dimensionless)

RH2 $= dR_H/dZ$, Wall slope at s hub (dimensionless)

RH3 $= d^2R_H/dZ^2$, Wall second derivative at s hub (dimensionless)

RT1 $= R_T$, Wall radius at s tip (dimensionless)

RT2 $= dR_T/dZ$, Wall slope at s tip (dimensionless)

RT3 $= d^2R_T/dZ^2$, Wall second derivative at s tip (dimensionless)

YT $= Y_T$, Duct height at s (dimensionless)

ZH $= Z_H$, Axial location of hub wall at s (dimensionless)

ZT $= Z_T$, Axial location of tip wall at s (dimensionless)

Theory

An approximate potential flow solution can be constructed for ducts where the meridonal plane curvature and divergence of the duct is not too large (see Section 3.1). This solution for the coordinates must be known in terms of n and s rather than R and Z since these are the independent variables.

Through each mesh point on the hub contour a straight line is passed through the tip contour such that its slope satisfies the condition

$$\frac{dR_M}{dZ} = \frac{1}{2}\left[\frac{dR_H}{dZ} + \frac{dR_T}{dZ}\right] = -\frac{Z_T - Z_H}{R_T - R_H} \qquad (7.2.4.1)$$

where R_T and Z_T are the intersections as shown in Fig. 7.2.4.1. This straight line then approximates the potential line. Since the metric scale coefficient is the potential flow velocity, it follows that

$$V_M = \frac{V_H + V_T}{2} = \frac{1}{Y_T} \qquad (7.2.4.2)$$

$$\frac{V_H}{V_T} = \frac{\Delta X_T}{\Delta X_H} \qquad (7.2.4.3)$$

The streamwise coordinate, from Eq. (3.1.8) is

$$S = \int_0^X V dX \tag{7.2.4.4}$$

The normal coordinate is transformed in the following manner so as to place more streamlines near the wall

$$n = \frac{1}{2} + \tan^{-1}\left[2 \tan \frac{C}{2} \left(2 - \frac{1}{2}\right)\right] \frac{1}{C} \tag{7.2.4.5}$$

The constant C is a mesh distortion parameter which can be varied between the limits

$$0 < C < \pi \tag{7.2.4.6}$$

The coordinate functions are constructed as follows

$$R(n,s) = R_H(s) + \left[R_T(s) - R_H(s)\right] \cdot n \tag{7.2.4.7}$$

and

$$Z(n,s) = Z_T(s) + \left[Z_T(s) - Z_H(s)\right] \cdot n \tag{7.2.4.8}$$

For the special case of no centerbody, the following transformation is used

$$n = \tan^{-1}\left[(\tan c)\, \eta\right]/c \tag{7.2.4.9}$$

$$\frac{d\eta}{dn} = \frac{c}{\tan c \cos^2(cn)} \qquad (7.2.4.10)$$

$$\frac{d^2\eta}{dn^2} = \frac{2c^2}{\tan c} \frac{\sin(cn)}{\cos^3(cn)} = \frac{2c \sin}{\cos} \qquad (7.2.4.11)$$

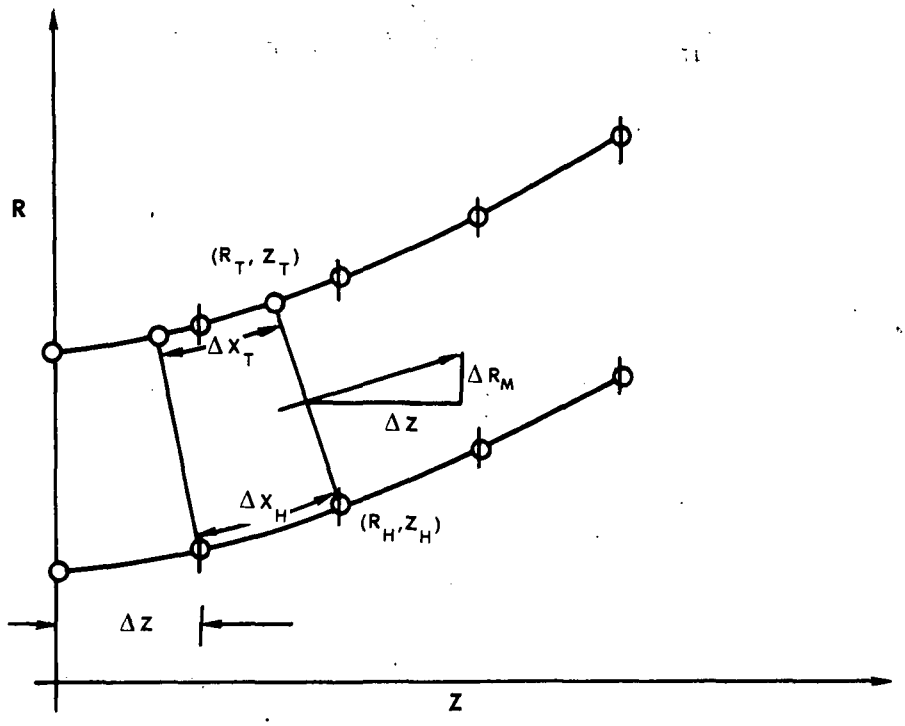

FIG. 7.2.4.1-CONSTRUCTION OF COORDINATES.

7.2.5 Subroutine FINVIS(LØPT)

Object Calculate Strut Back Pressure

Options

LØPT=1 Input Upstream Flow
=2 Calculate $\hat{\Pi}_3(0)$ from $\hat{\alpha}_3, Z_B$
=3 Calculate Downstream Flow
=4 Calculate $\hat{\Pi}_3(0)$ from C_L, C_D

List of Symbols

DPXIC	$= \Delta\Pi$	, Increment in back pressure (dimensionless)
EPS	$= \epsilon$	, Convergence criteria (dimensionless)
KIMH,KIMT	=	, Index for end points; hub, tip (dimensionless)
PIH1	$= \hat{\Pi}_3^{(I)}(0)$	, Iterative guess for back pressure (dimensionless)
PIH2	$= \hat{\Pi}_3^{(I+1)}(0)$	, Iterative guess for back pressure (dimensionless)
PIMIN	$= \Pi_M$	, Minimum total pressure (dimensionless)
PSIHH	$= \hat{\psi}_3(0)$	, Stream function at hub (dimensionless)
PSIHT	$= \hat{\psi}_3(1)$	, Stream function at tip (dimensionless)
PSIH1	$= \hat{\psi}_3^{(I)}(1)$	, Iterative solution of $\hat{\psi}$ at tip (dimensionless)
PSIH2	$= \hat{\psi}_3^{(I+1)}(1)$	, Iterative solution of $\hat{\psi}$ at tip (dimensionless)

Theory

This subroutine calculates the upstream and downstream flow variables needed to determine the blade force and dissipation function, as shown in the flow chart (Fig. 7.2.5.1)

LØPT=1

The upstream flow is assumed to be equal to the computed flow at the upstream control surface. In the annulus boundary layer, the variables are set equal to their value at the boundary layer displacement height (see Section 3.3).

LØPT=2

The downstream back pressure $\hat{\Pi}_3(0)$, is determined by integrating Eq. (3.3.30) and Eq. (3.3.31) using a third order Runge-Kutta integration. The initial value $\hat{\Pi}_3(0)$ must be determined iteratively (see flow chart, Fig. 7.2.5.2). A pressure increment $\Delta\Pi$ is estimated from the minimum total pressure $\hat{\Pi}_M$ as follows

$$\Delta\Pi = \hat{\Pi}_M / 50 \tag{7.2.5.1}$$

Then guesses for the hub wall pressure are obtained from

$$\hat{\Pi}_3(0) = \hat{\Pi}_M + (A\Pi)(ITER) \tag{7.2.5.2}$$

Successive guesses are made for $\hat{\Pi}_3(0)$ with $\Delta\Pi$ increments, until the tip boundary condition $\hat{\psi}_3(1)$ is bounded by successive guesses $\hat{\psi}_3^{(i-1)}(1)$, $\hat{\psi}_3^{(i-2)}(1)$. Then using Newton's method

$$\hat{\Pi}_3(0) = \hat{\Pi}_3^2(0) + \frac{\hat{\psi}_3(1) - \hat{\psi}_3^1(1)}{\hat{\psi}_3^{(2)}(1) - \hat{\psi}_3^{(1)}(1)} \left[\hat{\Pi}_3^{(2)}(0) - \hat{\Pi}_3^{(1)}(0)\right] \tag{7.2.5.3}$$

Convergence occurs when

$$\left| \left(\hat{\Pi}_3^{(2)}(0) - \hat{\Pi}_3^{(1)}(0)\right) / \hat{\Pi}_3^{(2)}(0) \right| < \epsilon \tag{7.2.5.4}$$

LØPT=3

When $\hat{\Pi}_3(\eta)$ is known, then the downstream flow can be determined since $\hat{\Pi}_{03}(\eta)$ and $\hat{\Theta}_3(\eta)$ is known (Eqs. (7.2.7.1) through (7.2.7.7)).

LØPT=4

This option integrates Eq. (3.3.28) and Eq. (3.3.29) using a third order Runge-Kutta integration. Subroutine VARB is used to get the integrands for the given flow variables. An iterative procedure similar to LØPT=2 option is used to determine $\hat{\Pi}_3(0)$.

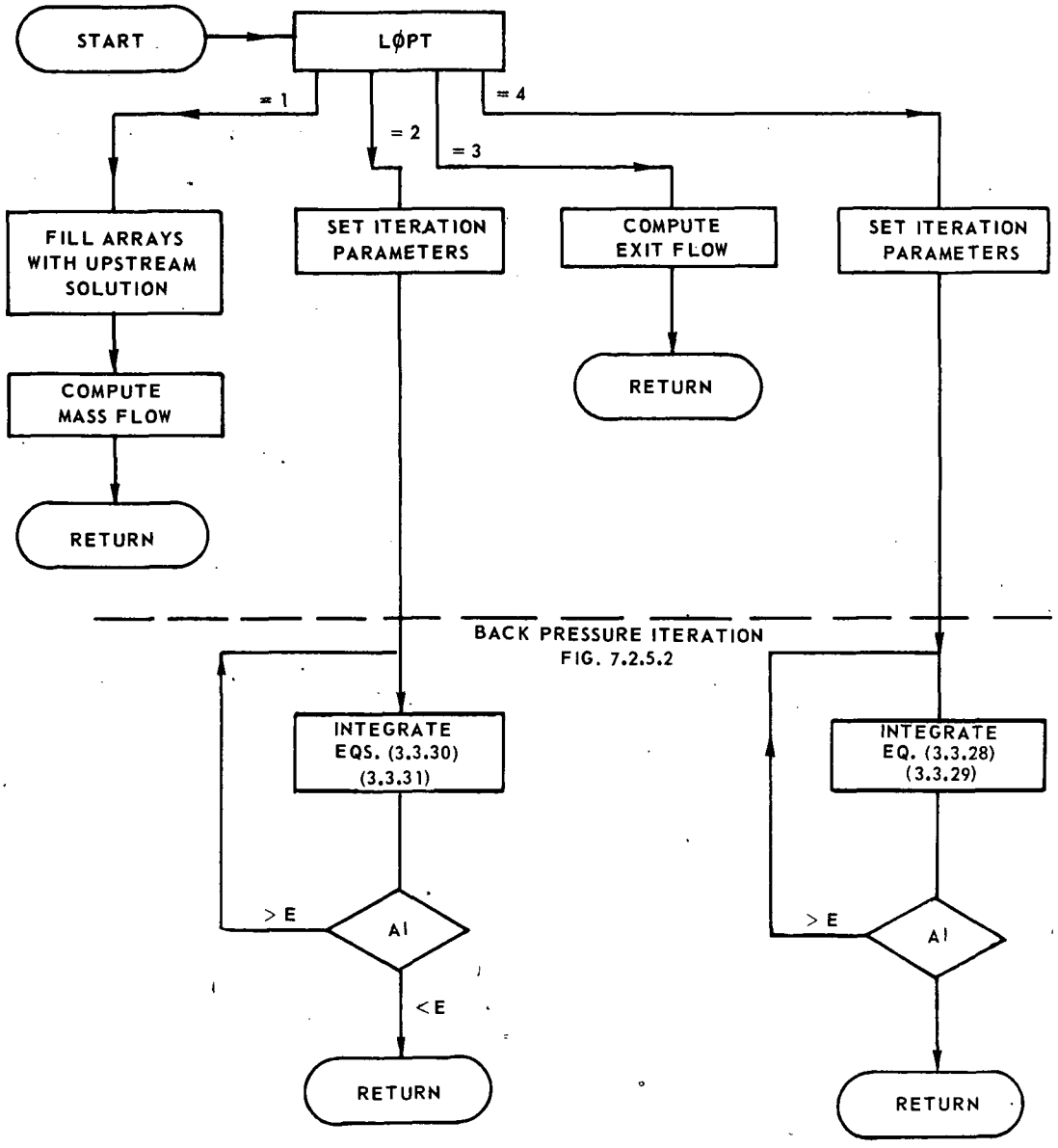

FIG. 7.2.5.1–FLOW CHART FOR SUBROUTING FINVIS.

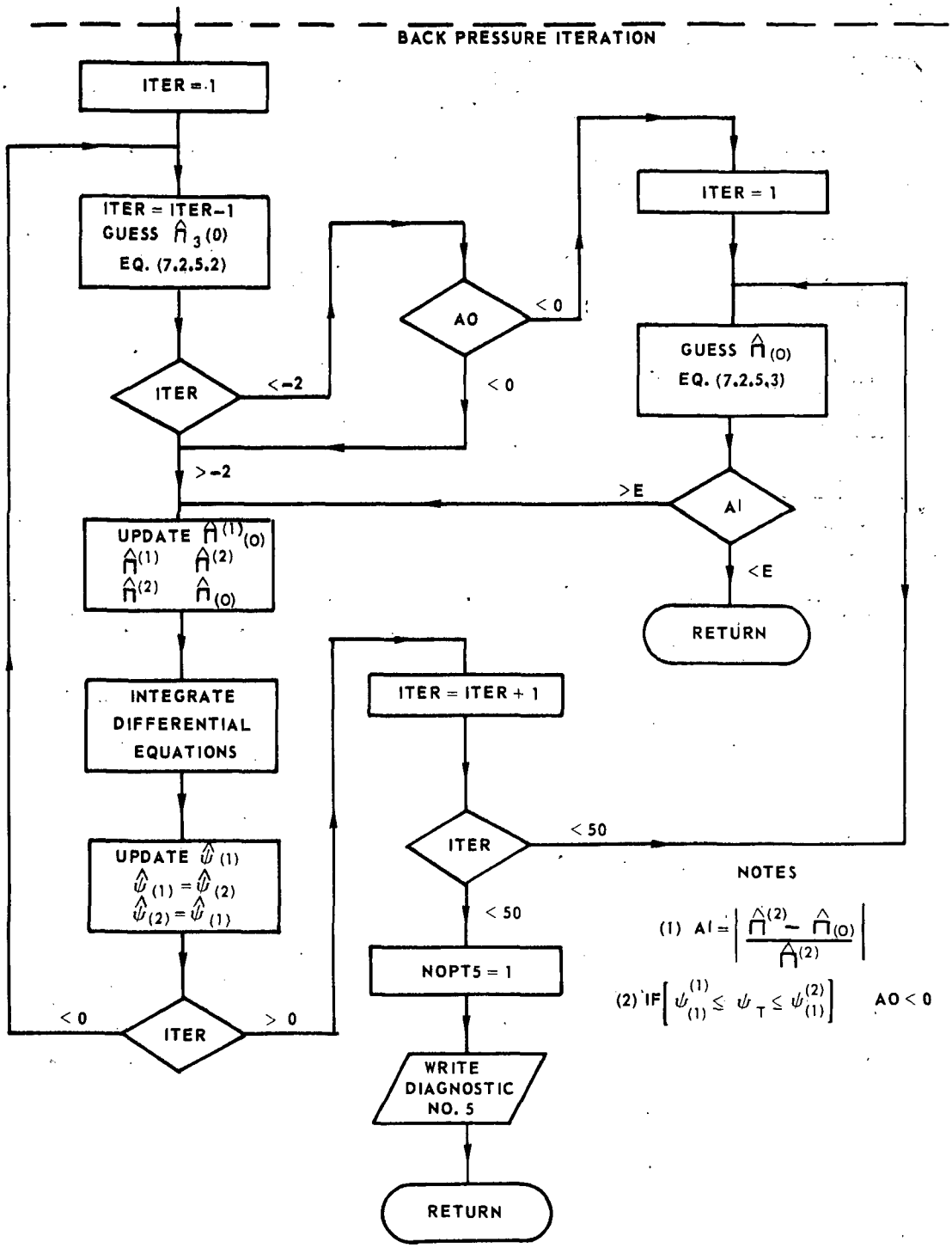

FIG. 7.2.5.2.-FLOW CHART FOR BACK PRESSURE ITERATION LOOP IN SUBROUTINE FINUIS.

7.2.6 Subroutine FLØWIN

Object Set Up Inlet Flow

Options

IØPT1=1 Compute Inlet Flow
IF ($T_0 = 0$) $P_0 = P_r$ and $T_0 = T_r$

IØPT1=2 Read Inlet Flow
IF ($\delta^* > 0$) Add boundary layers specified
IF ($T_0 > 10.$) Normalize with T_r and P_r

List of Symbols

BINP(I,J,K), Interpolated from BINPUT(IH,J,L)

Theory IØPT1=1

For this option the free-stream flow is assumed to be isentropic with a constant free-stream Mach number M_s and wall boundary layers defined by power law velocity profiles. Since the swirling flow must be in radial equilibrium, Eq. (3.2.39) must be satisfied together with the isentropic flow relations, Eqs. (3.2.51) and (3.2.52). Neglecting curvature in the meridonal plane

$$\frac{\partial \Pi}{\partial n} = \frac{\gamma}{R} \frac{\partial R}{\partial n} \Pi M_\phi^2 \qquad (7.2.6.1)$$

where

$$M_\phi^2 = M^2 - M_s^2 \qquad (7.2.6.2)$$

$$M^2 = \frac{2}{\partial - 1}\left[\left(\frac{\Pi_0}{\Pi}\right)^{\frac{\gamma-1}{\gamma}} - 1\right] \qquad (7.2.6.3)$$

Equation (7.2.6.1) can be integrated with

$$M(0) = M_S / \cos(\alpha_H) \tag{7.2.6.4}$$

and

$$\frac{\Pi_o}{\Pi(0)} = \left[1 + \frac{\gamma-1}{2} M(0)^2\right] \frac{\gamma}{\gamma-1} \tag{7.2.6.5}$$

as initial conditions using Runge-Kutta method.

For a given displacement thickness and velocity profile power law, wall boundary layers can be added, assuming collateral boundary layers, such that α is unchanged. Then

$$\Delta = (1+n)\Delta^* \tag{7.2.6.6}$$

$$\frac{U}{U_\infty} = \left(\frac{y}{\Delta}\right)^{1/n_2} \tag{7.2.6.7}$$

and

$$\frac{\Theta}{\Theta_\infty} = 1 + \sqrt[3]{P_{RL}} \frac{\gamma-1}{2} M_\infty^2 \left[1 - \left(\frac{U}{U_\infty}\right)^2\right] + \frac{\Theta_w - \Theta_{AW}}{\Theta_\infty} \left[1 - \frac{U}{U_\infty}\right] \tag{7.2.6.8}$$

Finally, the inlet mass flow and reference velocity are determined as follows

$$u_r = \frac{N_B}{A} \int_0^1 \frac{G}{V} P U_s \frac{d\eta}{X} \tag{7.2.6.9}$$

$$\dot{w} = g \rho_r u_r a_r A \tag{7.2.6.10}$$

Theory IØPT1=2

For this option, the input flow is calculated from experimental input data. The input variables selected are spanwise location, total pressure, static pressure, flow angle, and total temperature, since these are the primary measured variables. A simple linear interpolation is used so that for any variable ϕ,

$$\phi(Y(\eta)) = \phi(Y_1) + \left[\phi(Y_2) - \phi(Y_1)\right]\left[Y(\eta) - Y_1\right] \qquad (7.2.6.11)$$

The flow variables are calculated from Eqs. (7.2.7.1) through (7.2.6.7).

If ($T_0 > 10$), it is assumed that pressure and temperature are given in PSF and deg R, respectively, and the flow is normalized accordingly. If δ^* is given, it is assumed that boundary layers should be added accordingly to the velocity profile power law above. Finally, the weight flow and reference velocity are determined from Eqs. (7.2.6.9) and (7.2.6.10).

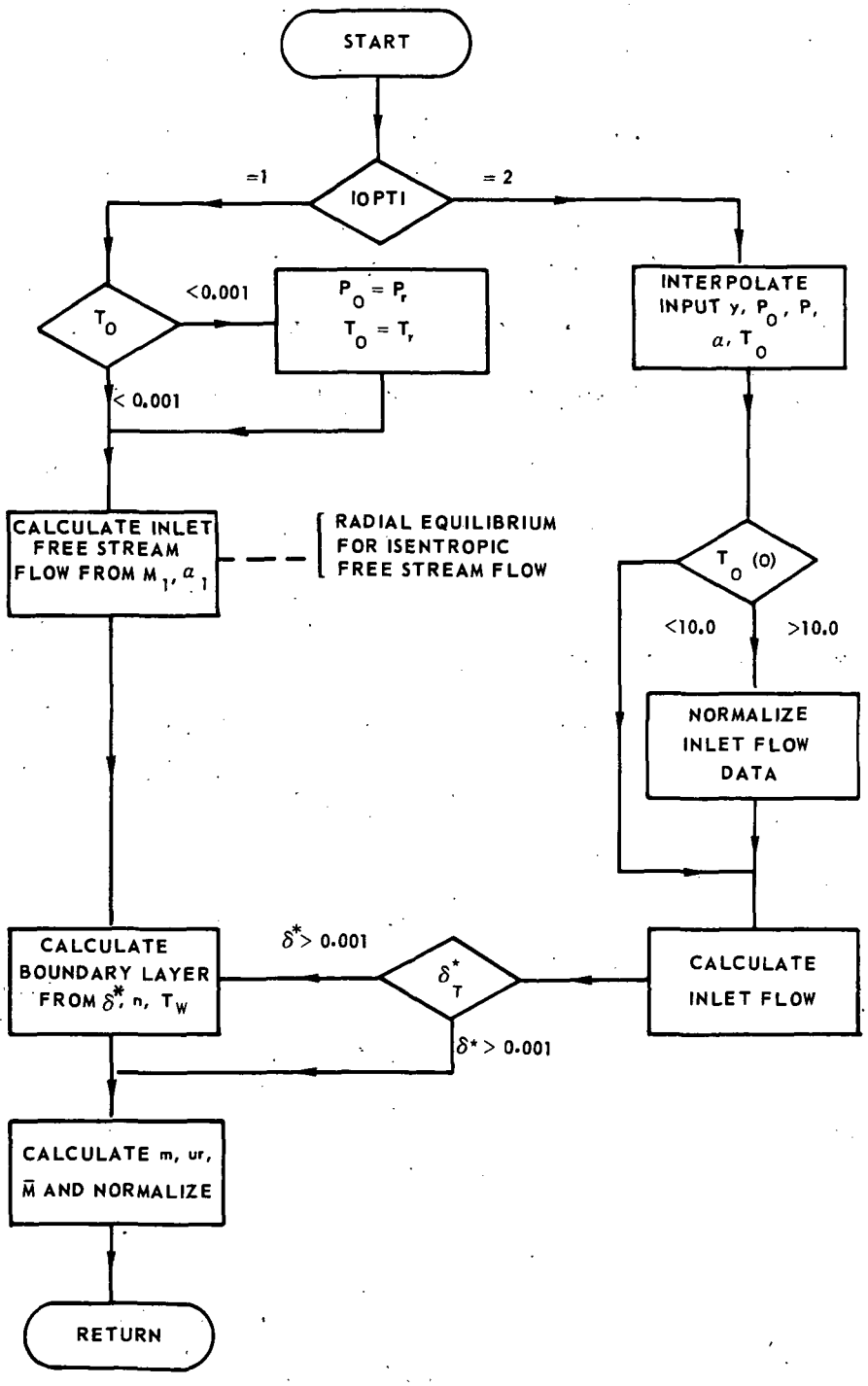

FIG. 7.2.6.1-FLOW CHART FOR SUBROUTINE FLØWIN.

7.2.7 Subroutine FØRCE(LØPT)

Object Compute Blade Force

Options

LØPT=1 Compute Blade Force/Span
=2 Compute Local Blade Force

IØPT2=1 Use Experimental Data
=2 Use Isolated Airfoil Predicted C_L and C_D
=3 Use Cascade Predicted Z_B and α_2
=4 Use Input Z_B and α_2

List of Symbols

AINPT(I,J,K), Interpolated From AINPUT(I+1,J,L)

Theory LØPT=1

The theory is given in Section 3.3 and a flow chart in Fig. 7.2.7.2.

IØPT2=1

This option computes the strut force from experimental blade element data taken just upstream and downstream of the strut. If $y, \Pi_0, \Pi, \Theta_0, \alpha$ are measured at the two locations, we have

$$\hat{M} = \left\{\frac{2}{\gamma-1}\left[\left(\frac{\Pi_0}{\Pi}\right)^{\frac{\gamma-1}{\gamma}} - 1\right]\right\}^{1/2} \tag{7.2.7.1}$$

$$\hat{\Theta} = \hat{\Theta}_0\left(\frac{\hat{\Pi}}{\hat{\Pi}_0}\right)^{\frac{\gamma-1}{\gamma}} \tag{7.2.7.2}$$

$$\hat{P} = \hat{\Pi}/\hat{\Theta} \tag{7.2.7.3}$$

$$\hat{U} = \frac{\hat{M}}{M_r}\sqrt{\hat{\Theta}} \tag{7.2.7.4}$$

$$\hat{I} = \frac{\gamma}{\gamma-1}\ln\hat{\Theta} - \ln\hat{\Pi} \tag{7.2.7.5}$$

$$\hat{U}_s = \hat{U}\cos\hat{\alpha} \tag{7.2.7.6}$$

$$\hat{U}_\phi = \hat{U}\sin\hat{\alpha} \tag{7.2.7.7}$$

The strut force is computed from Eqs. (3.3.18) and (3.3.19) and the losses from Eqs. (3.3.22) and (3.3.23). Since the experimental measurements do not necessarily occur on streamlines used for computing, a linear interpolation is used to obtain AINPT from AINPUT.

IØPT2=2

If the solidity is small, then the blade or strut force can be calculated from isolated airfoil data in which C_L and C_D are presented for various blade shapes and incidence angles. When this is possible we have, from Eqs. (3.3.25) and (3.3.26)

$$\Xi_\sigma = -G_B\hat{P}_2\hat{U}_2^2\sigma\left[-C_L\sin\hat{\alpha}_2 + C_D\cos\hat{\alpha}_2\right] \tag{7.2.7.8}$$

$$\Xi_\phi = -G_B\hat{P}_2\hat{U}_2^2\sigma\left[-C_L\cos\hat{\alpha}_2 + C_D\sin\hat{\alpha}_2\right] \tag{7.2.7.9}$$

IØPT2=3

If the solidity is large, then the blade forces must be obtained from cascade data because the blade or struts no longer act as isolated airfoils. Since these correlations are usually given for Z_B and α_2, Eqs. (3.3.30) and (3.3.31) are used to satisfy mass flow and radial equilibrium using Subroutine FINVIS. The force is calculated from Eqs. (3.3.18) and (3.3.19).

IØPT2=4

This option is the same as IØPT2=3 except that Z_B and α_2 are obtained from experimental data input.

LØPT=2

This option provides the local blade force once the blade force per unit span is calculated. Obtaining the blade force per unit span from Eqs. (3.3.20) and (3.3.21), the local blade force is determined as follows.

$$H_s = \frac{\Xi_s}{G_B (Z_{TE} - Z_{LE})} \qquad (7.2.7.10)$$

$$H_\phi = \frac{\Xi_\phi}{G_B (Z_{TE} - Z_{LE})} \qquad (7.2.7.11)$$

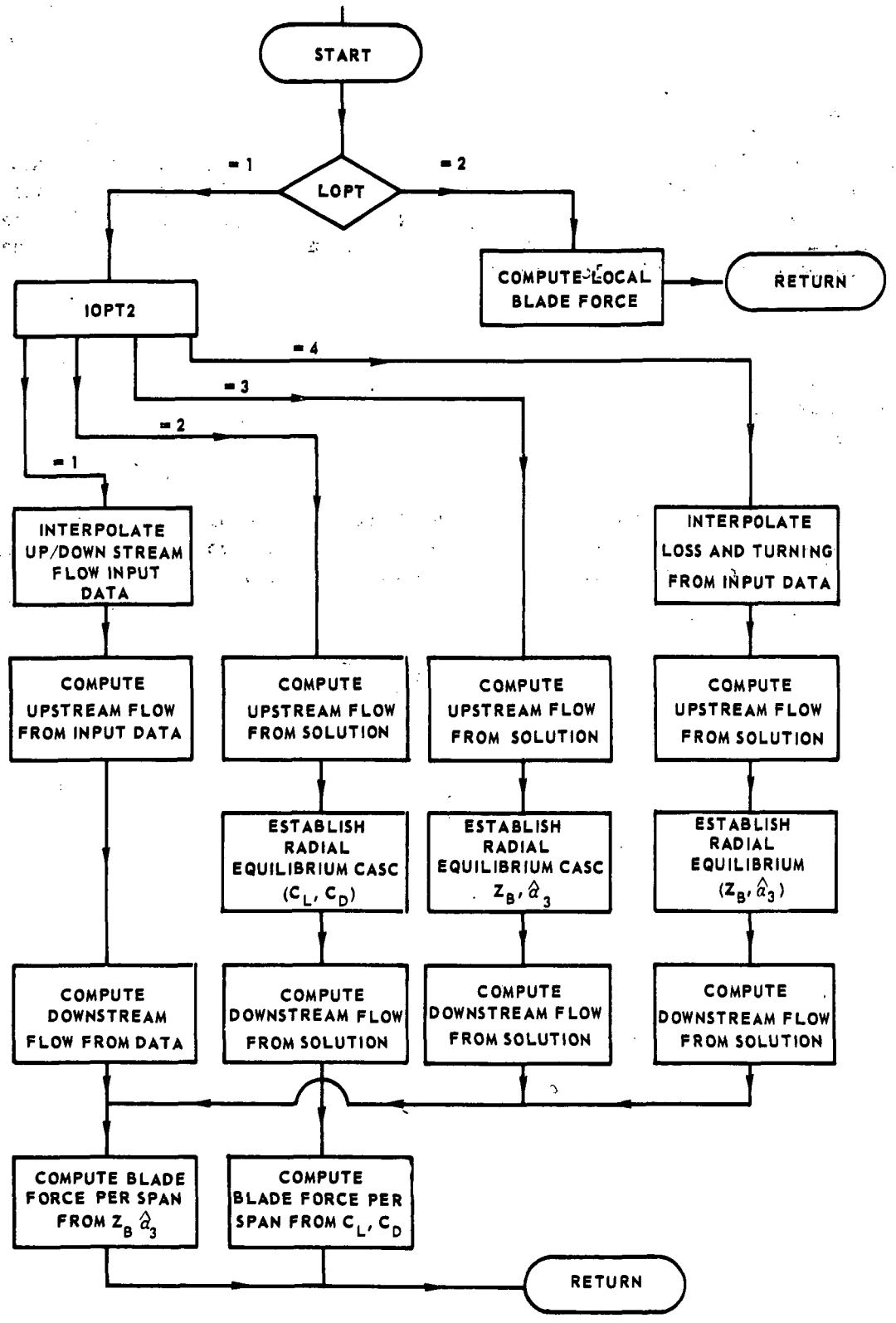

FIG. 7.2.7.1-FLOW CHART FOR SUBROUTINE FORCE.

7.2.8 Subroutine GBLADE(KK,LØPT)

Object Compute Blade Geometry

Options

LØPT=1 Compute Blade Centerline Properties
=2 Compute Local Properties

List of Symbols

RR = Y_{CL} , Fractional distance along blade centerline (dimensionless)

THICKN = t_M , Maximum blade thickness (dimensionless)

ZBAR = $\bar{Z}$, Fractional distance along chord line (dimensionless)

KK = Index of spanwise station

Theory

If three points are given for any blade parameter along the blade centerline, a parabolic fit is used to interpolate any intermediate point (see Fig. 7.2.8.1). Thus, for any parameter ϕ

$$Y_{CL} = \frac{R - R_{CLH}}{R_{CLT} - R_{CLH}} \qquad (7.2.8.1)$$

and

$$\phi = \phi_H + (4\phi_M - 3\phi_H - \phi_T)Y_{CL} + (2\phi_H + 2\phi_T - \phi_M)Y_{CL} \qquad (7.2.8.2)$$

In addition, along the chord line projected to the (r,z) plane a given thickness distribution may be applied, according to ISHAPE, using Function FTHICK.

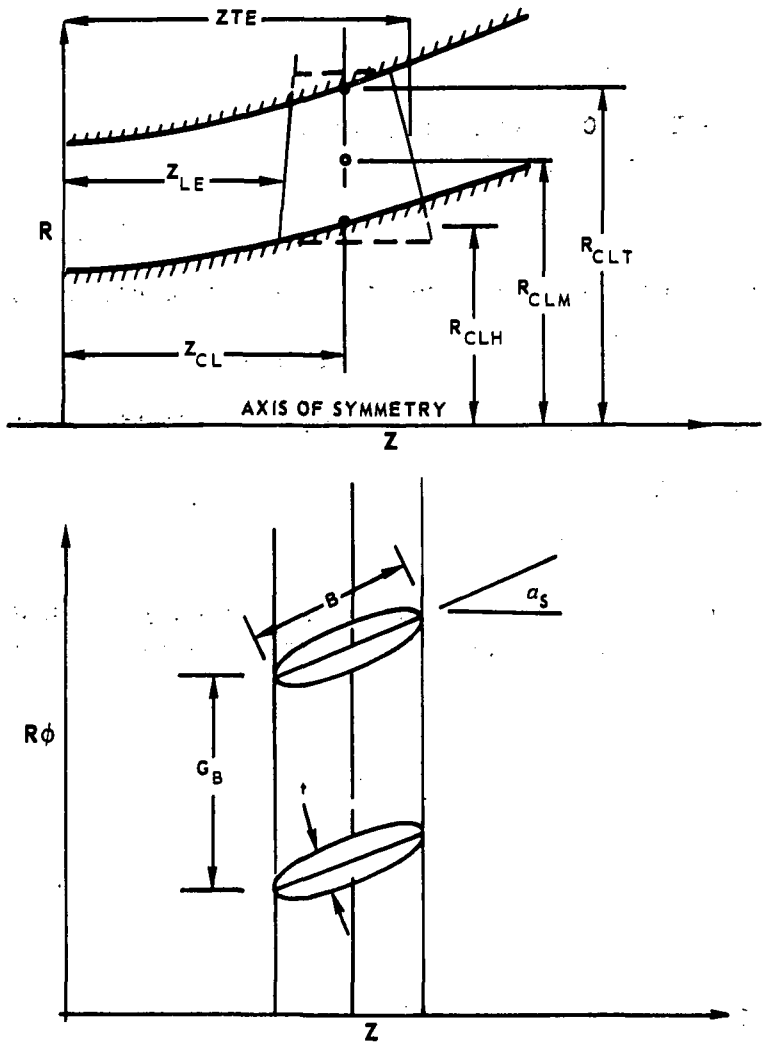

FIG. 7.2.8.1-BLADE GEOMETRY.

7.2.9 Subroutine GDUCT

Object Compute Duct Shape

Options

IØPT3=1 Straight Annular Duct
=2 Read Duct Shape
=3 Straight-Wall Diffuser
=4 NACA Curved-Wall Diffuser

List of Symbols

(As needed by user.)

Theory

This subroutine is used to prescribe the duct shape $r_H(Z), r_T(Z)$, wall bleed $\dot{m}_H(Z), \dot{m}_T(Z)$, and wall temperature $T_H(Z), T_T(Z)$, as required. Since these functions are input, the user programmer may write a subroutine for this purpose or read the required information according to IØPT3. In addition, the subroutine computes the reference radius and normalizes the variables r and T. The variable $\dot{m}$ is normalized in Subroutine FLØWIN when u_r is calculated.

Input/Output

The user may program any duct shape and wall boundary conditions as required. In addition to any input the programmer may write in this subroutine, the programmer has available the number of streamwise mesh points JL. The output of this subroutine must be (R(I,K,J), I=1,3; K=1,2, J=1,JL) and Z1. Note that all variables are normalized as shown in the sample subprogram described in the Subroutine GDUCT listing and that equally spaced spanwise stations are used. The flow chart (Fig. 7.2.9.1) should be followed in programming.

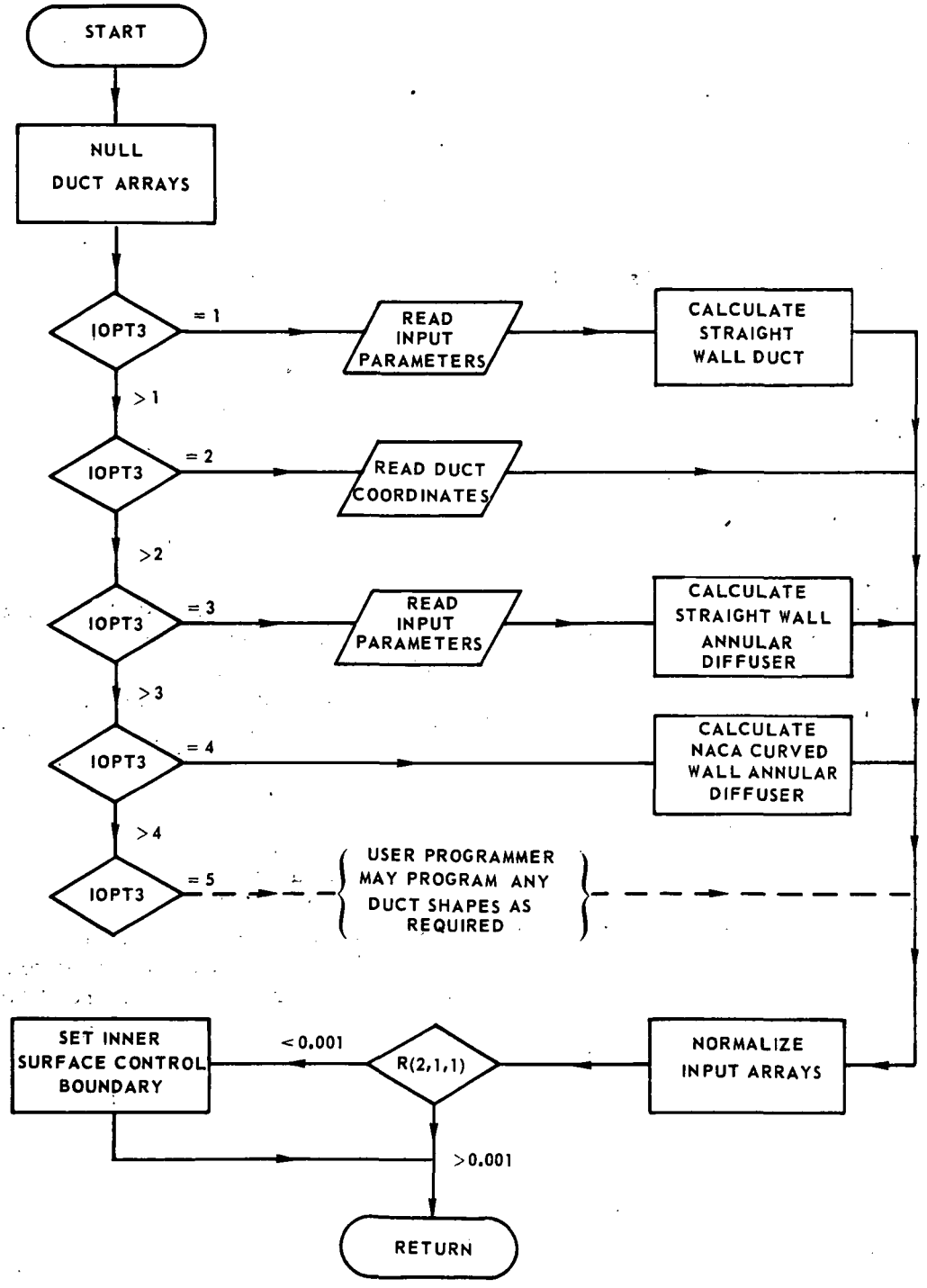

FIG. 7.2.9.1.-FLOW CHART FOR SUBROUTINE GDUCT.

7.2.10 Subroutine SLETE(KSSLE,KSSTE)

Object Find Strut Control Surfaces

Options

None.

List of Symbols

KSSLE,KSSTE, Leading edge and trailing edge index
SLE,STE , Leading and trailing edge coordinate (dimensionless)
ZLEH,ZLET , Axial distance hub leading and trailing edge (dimensionless)
ZTEH,ZTET , Axial distance tip leading and trailing edge (dimensionless)

Theory

The intersection of the leading and trailing edge of the blade with the hub and tip casing are obtained from Subroutine GBLADE. Then the coordinates of the hub and tip boundaries are searched until the proper value of streamwise coordinate S for the leading edge and trailing edge of the blade are found. The coordinate index KSSLE is located just upstream of the blade and the coordinate KSSTE is located just downstream of the blade.

7.2.11 Subroutine SØLVE

Object Integrate Equations of Motion

Options

IØPT4, Print every IØPT4 Station

List of Symbols

AAR $= A/A_1$, Area ratio (dimensionless)

AARS $= A/A^* = \frac{1}{M_I}\left[\frac{1+\frac{\gamma-1}{2}M_I^2}{\frac{\gamma-1}{2}}\right]^{\frac{\gamma+1}{2(\gamma-1)}}$, Critical area ratio (dimensionless)

ALPHA $= \alpha$, Swirl angle (deg)

AMACHI $= M_I$, Inviscid flow Mach number (dimensionless)

C $= \partial\Pi(0)/\partial S$, Constant of integration (dimensionless)

CFSH $= C_{fSH} = \tau_{sn}(0)/\bar{q}_1$, Streamwise wall friction coefficient hub (dimensionless)

CFST $= C_{fST} = \tau_{sn}(1)/\bar{q}_1$, Streamwise wall friction coefficient tip (dimensionless)

CFPH $= C_{f\phi H} = \tau_{\phi n}(0)/\bar{q}_1$, Tangential wall friction coefficient hub (dimensionless)

CFPT $= C_{f\phi T} = C_{\phi n}(1)/\bar{q}_1$, Tangential wall friction coefficient tip (dimensionless)

CPINC $= C_{PI} = 1-(A_1/A)^2$, Incompressible pressure coefficient (dimensionless)

CPCOMP $= C_{PC} = \left[\Pi_I(s)-\Pi_I(0)\right]/\left[\Pi_{OI}(0)-\Pi_I(0)\right]$, Compressible pressure coefficient (dimensionless)

PRCOEF $= C_p = (P-P(0))/\bar{q}_1$, Local pressure coefficient (dimensionless)

QKK $= \bar{q}_1/(1/2\,\rho_T u_r^2)$, Average inlet dynamic pressure (dimensionless)

Theory

The equations of motion in Section 3.2 are integrated numerically according to the procedures described in Section 3.6. The flow chart is given in Fig. 7.2.11.1.

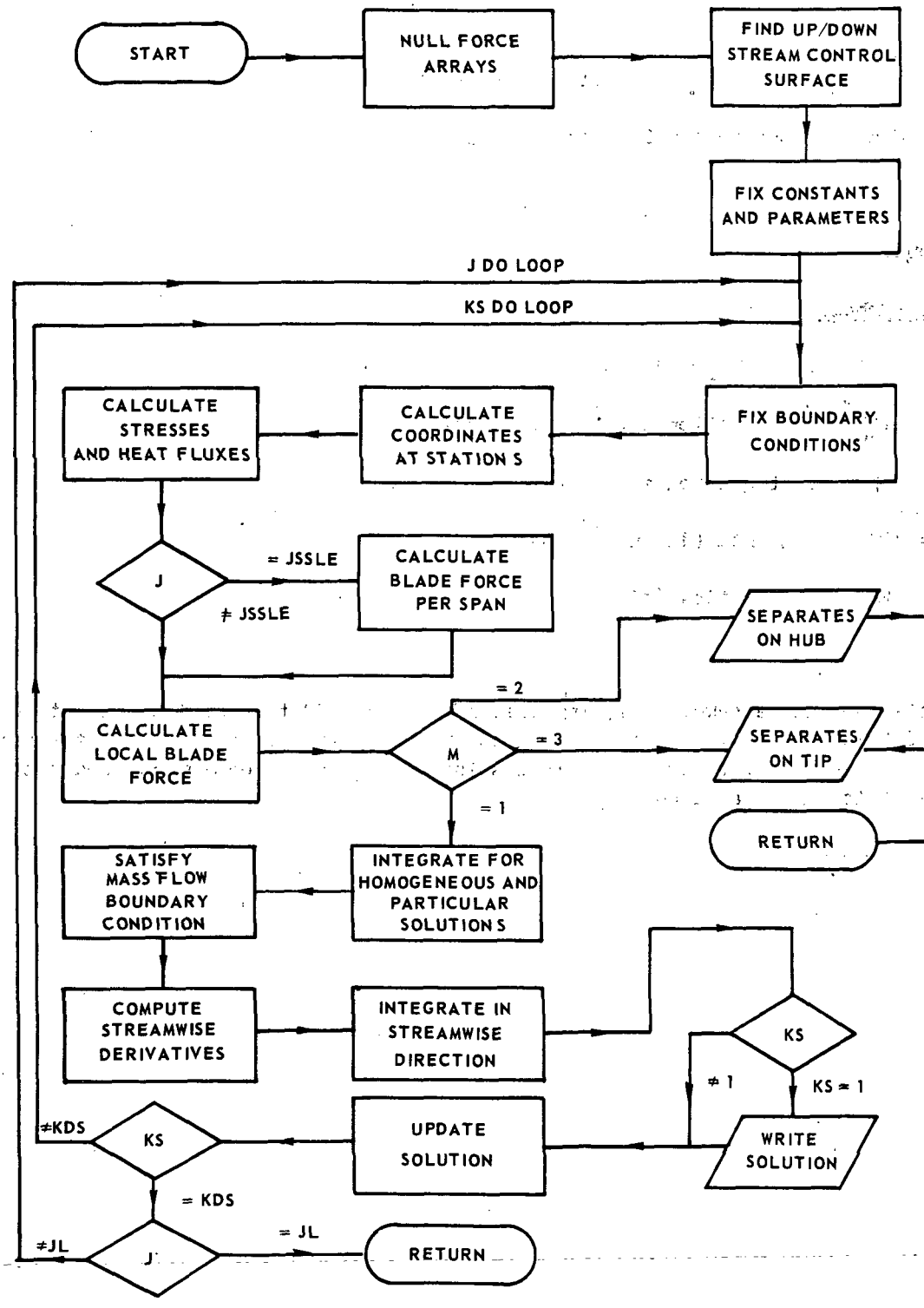

FIG. 7.2.11.1.-FLOW CHART FOR SUBROUTINE SØLVE.

7.2.12 Subroutine SPLDC

Object Compute Constants for Inner Layer Solution

Options

None.

List of Symbols

UU(1) = U^+ , Velocity (dimensionless)

UU(2) = H_A^+ , Stagnation enthalpy (dimensionless)

UU(3) = H^+ , Stagnation enthalpy (dimensionless)

UU(4) = Y^+ , Length (dimensionless)

UU(5) = W^+ , Mass flow (dimensionless)

Theory

This subroutine numerically integrates Eqs. (3.4.5) through (3.4.7) out to a value of Y_M^+ using a third order Runge-Kutta method. At the value of Y_M^+, the numerical solutions are matched to the analytical solutions given in Section 3.4 and the constants of integration are evaluated.

7.2.13 Subroutine STRESS

Object Compute Stress and Heat Flux

Options

NØPT2=1 Adiabatic Wall
=2 Nonadiabatic Wall
NØPT1=1 $P^+ = m^+ = 0$
=2 $P^+ \neq 0,\ m^+ = 0$
=3 $P^+ = 0,\ m^+ \neq 0$
NØPT6=1 Centerbody
=2 No centerbody

List of Symbols

AMPH,AMPT	=	m_H^+ , m_T^+	, Mass flow bleed hub, tip (dimensionless)
AMUO	=	$(\mu_E/\mu_r)_\infty$	, Free-stream eddy viscosity (dimensionless)
AMUM	=	$(\mu/\mu_r)_\infty$	, Free-stream molecular viscosity (dimensionless)
AWH,AWT	=	α_{WH}, α_{WT}	, Wall swirl angle hub, tip (dimensionless)
DELO	=	Δ^*_∞	, Mean displacement thickness (dimensionless)
KMM			, Index for maximum velocity (dimensionless)
PPH,PPT	=	P_H^+ , P_T^+	, Pressure gradient hub, tip (dimensionless)
QWH,QWT	=	Q_H , Q_T	, Wall heat flux hub, tip (dimensionless)
RHØM	=	P_M	, Mean free-stream density (dimensionless)
SKMH,SKMT	=	$\Sigma_{WH} , \Sigma_{HT}$	, Wall stress hub, tip (dimensionless)
SWH,SWT	=	$\Sigma(KMH), \Sigma(KMT)$	, Wall stress matching point (dimensionless)
TWH,TWT	=	Θ_{WH}, Θ_{WT}	, Wall temperature (dimensionless)
UM	=	U_∞	, Maximum free-stream velocity (dimensionless)
USTARH,USTART	=	U_H^*, U_T^*	, Friction velocity hub, tip (dimensionless)

Theory

The inner layer solution is a function of $U^*(S)$. Since the inner layer solution does not correct for dU^*/dS, U_s and ψ are continuously updated to match the inner and outer layer mass flows.

The normal derivatives, stresses, and heat flux are computed using central differences in the core flow. For the inner layer solution, derivatives are obtained analytically from FUPLUS and FHPLUS.

7.2.14 Subroutine VARB(PI3,AX,BX,K,IX)

Object Compute Blade Force Variables

Options

IX = 1,2,3 Steps in third order Runge-Kutta method.

List of Symbols

AX = $d\hat{\Pi}_3/d\eta$, Normal pressure gradient (dimensionless)

BX = $d\hat{\psi}_3/d\eta$, Normal mass flow gradient (dimensionless)

IX , Runge-Kutta index (dimensionless)

K , Streamwise station (dimensionless)

PI3 = $\hat{\Pi}_3$, Downstream static pressure (dimensionless)

RHØ3 = $\hat{P}_3$, Downstream density (dimensionless)

TH3 = $\hat{\Theta}_3$, Downstream temperature (dimensionless)

UPHI3 = $\hat{U}\phi_3$, Downstream swirl velocity (dimensionless)

US3 = $\hat{U}_{s3}$, Downstream streamwise velocity (dimensionless)

Theory

When IØPT2=2, the blade force is known, but the loss and exit angle are not known. This subroutine calculates the integrands for Runge-Kutta integration of Eqs. (3.3.28) and (3.3.29). For a given $\hat{\Pi}_3$, we have for iteration i,

$$\hat{M}_3 = \hat{M}_3^{(i-1)} \tag{7.2.14.1}$$

$$\hat{\Theta}_3 = \hat{\Theta}_{02} / \left[1 + \frac{\gamma - 1}{2} \hat{M}_2^2\right] \tag{7.2.14.2}$$

$$\hat{P}_3 = \hat{\Pi}_3 / \hat{\Theta}_3 \qquad (7.2.14.3)$$

$$\hat{U}_{S3}^2 - \hat{U}_{S2}\left[1 - \frac{\hat{P}_2}{\hat{P}_S}\right]\hat{U}_{S3} - \frac{2}{\hat{P}_S}\left[\frac{\Xi_S}{G} - \frac{\hat{\Pi}_3 - \hat{\Pi}_2}{\gamma M_r^2}\right] - \frac{\hat{P}_2}{\hat{P}_3}\hat{U}_{S2}^2 = 0 \qquad (7.2.14.4)$$

$$\hat{U}_{\phi 3} = \hat{U}_{\phi 2} + \frac{2\,\Xi_\phi}{G_B\left[\hat{P}_3\hat{U}_{S3} + \hat{P}_2\hat{U}_{S2}\right]} \qquad (7.2.14.5)$$

$$\hat{M}_3^{(i-1)} = M_r\left[\hat{U}_{S3}^2 + \hat{U}_{\phi 3}^2\right]^{1/2} / \hat{\Theta}_3^{1/2} \qquad (7.2.14.6)$$

7.3 List of External Function Subroutines

	Name	Object
7.3.1	AMU	Compute Molecular Viscosity
7.3.2	FHPLUS	Compute Thermodynamic Functions of Inner Layer
7.3.3	FUPLUS	Compute Functions of Inner Layer
7.3.4	QWALL	Compute Wall Heat Flux
7.3.5	SPLD	Functions for Calculating Inner Layer
7.3.6	TAWALL	Compute Adiabatic Wall Temperature
7.3.7	USTAR	Compute Friction Velocity
7.3.8	FTHIK	Compute Blade Thickness

7.3.1 Function AMU(T)

Object Compute Molecular Viscosity

Options

None

List of Symbols

AMU = μ/μ_r, Ratio of Molecular Viscosity (dimensionless)

T = Θ , Static Temperature Ratio (dimensionless)

Theory

The molecular viscosity is computed according to Sutherland's formula (Ref. 14). The working fluid is assumed to be air. Accordingly,

$$\frac{\mu}{\mu_r} = \Theta^{3/2} \frac{1 + 198.0/T_r}{\Theta + 198.0/T_r} \qquad (7.3.1)$$

7.3.2 Function FHPLUS(YPLUS,UPL,DUPL,T,DT,SQ,LL)

Object Compute Thermodynamic Functions of Inner Layer

Options

NØPT1=1 $p^+ = 0,\ m^+ = 0$
=2 $p^+ \neq 0,\ m^+ = 0$
=3 $p^+ = 0,\ m^+ \neq 0$

NØPT2=1 Adiabatic Wall
=2 Nonadiabatic Wall

LL =1 FHPLUS = $T_W^+ - T_A^+$ or $T_W^+ - T^+$
=2 FHPLUS = dT_A^+/dY^+ or dT^+/dY^+
=3 FHPLUS = Q_A^+ or Q^+
=4 FHPLUS = dQ_A^+/dY^+ or dQ^+/dY^+

List of Symbols

DT = dT^+/dY^+ , Derivative of temperature (dimensionless)

DUPL = dU^+/dY^+ , Derivative of velocity (dimensionless)

FHPLUS , See option list (dimensionless)

UPL = U^+ , Universal velocity dimensionless)

SQ = $\dfrac{Q}{(\gamma-1)M_r^2 P_W U^{*3}}$, Heat flux parameter (dimensionless)

T = $T_W - T^+$, Temperature difference (dimensionless)

YPLUS = Y^+ , Universal distance from wall (dimensionless)

Theory

An analytical solution exists for the thermodynamic functions for the inner layer as given in Section 3.4. Therefore, the function and its derivatives are known analytically according to the appropriate options.

7.3.3 Function FUPLUS(UST,YA,LL)

Object Compute Functions of Inner Layer Solution

Options

NØPT1=1 $p^+ = 0, m^+ = 0$
=2 $p^+ \neq 0, m^+ = 0$
=3 $p^+ = 0, m^+ \neq 0$

LL =1 FUPLUS = dU^+/dY^+
=2 FUPLUS = U^+
=3 FUPLUS = (μ_E/μ_W)
=4 FUPLUS = W^+

List of Symbols

FUPLUS = – , See Option List (dimensionless)

USTA = U^+ , Friction Velocity (dimensionless)

YA = Y , Distance from Wall (dimensionless)

Theory

An analytical solution for the inner layer $U^+(Y^+)$ is known from Section 3.4. Therefore, the solution and all its derivatives are known analytically. This function subroutine calculates the required functions according to the options listed above.

7.3.4 Function QWALL(TW,U,USTA,RØW)

Object Compute Wall Heat Flux

Options

NØPT2=1 Adiabatic Wall
=2 Nonadiabatic Wall

IF (R(1,3,J) > 0.001) NØPT2 = 2 For Outer Walls
IF (R(2,3J) > 0.001) NØPT2 = 2 For Inner Walls

List of Symbols

T = Θ , Static temperature at matching point (dimensionless)

TW = Θ_w , Wall static temperature (dimensionless)

QWALL = $-Q_w$, Heat flux (dimensionless)

U = U , Magnitude of absolute velocity at matching point (dimensionless)

USTA = U^* , Friction velocity (dimensionless)

RØW = P , Density at the wall (dimensionless)

Theory

If the wall static temperature is specified, then the program assumes that the wall heat flux should be calculated. Since the flow conditions are known at the matching point, and the friction velocity is known, the enthalpy H^+ can be calculated from Eq. (3.4.25). The heat flux is then given by

$$Q_w = \left[\Theta_w - \left(\Theta + \frac{\gamma-1}{2} M_r^2 U^2\right)\right] \frac{P_w U^*}{H^+} \qquad (7.3.4.1)$$

7.3.5 Function SPLD(Y,U,H,I,AM,AK,AA,PL,PT)

Object Provide Functions for Calculating Inner Layer

Options

I =1 SLPD = $dU^+(m^+)/dY^+$
=2 SLPD = dH_A^+/dY^+
=3 SLPD = dH^+/dY^+
=4 SLPD = ——
=5 SLPD = $dU^+(P^+)/dY^+$

List of Symbols

AA = A^+ , Van Driest constant (dimensionless)

AK = κ , Von Karman constant (dimensionless)

AM = m^+ OR p^+ , Mass flow or pressure gradient depending on I (dimensionless)

H = H_A^+ OR H^+ , Stagnation enthalpy depending on I (dimensionless)

PL = P_{RL} , Laminar Prandtl number (dimensionless)

PT = P_{RT} , Turbulent Prandtl number (dimensionless)

SPLD , See option list (dimensionless)

U = U^+ , Universal velocity (dimensionless)

Y = Y^+ , Universal distance (dimensionless)

Theory

This function subroutine provides the required integrands for integrating Eqs. (3.4.5), (3.4.6), and (3.4.7) using a third order Runge-Kutta method.

7.3.6 Function TAWALL(T,U,USTA)

Object Find Adiabatic Wall Temperature

Options

NØPT2=1 Adiabatic Wall
=2 Nonadiabatic Wall

IF (R(1,3,J) ≤ 0.001) NØPT2 = 1 For Outer Wall
IF (R(2,3,J) ≤ 0.001) NØPT2 = 1 For Inner Wall

List of Symbols

T = Θ , Static temperature at matching point (dimensionless)

TAWALL = Θ_W , Adiabatic wall static temperature (dimensionless)

U = U , Magnitude of velocity at matching point (dimensionless)

USTA = U^* , Friction velocity (dimensionless)

Theory

If the wall static temperature is not specified, then the program assumes that the adiabatic wall temperature should be calculated. Since the flow conditions are known at the matching point and the friction velocity is known, the wall temperature is obtained from the relation

$$\Theta_{AW} = \Theta + (\gamma - 1) M_r^2 \left[\frac{U^2}{2} + U^{*2} H_A^+ \right] \qquad (7.3.6.1)$$

where H_A^+ is determined from Eqs. (3.4.16) or (3.4.20).

7.3.7 Function USTAR(KB,YB)

Object Find Friction Velocity

Options

NØPT1=1 $p^+ = 0, m^+ = 0$
=2 $p^+ \neq 0, m^+ = 0$
=3 $p^+ = 0, m^+ \neq 0$

$p^+ \geq 0$; IF($p^+ < 0$) $p^+ = 0$

$m^+ \geq -0.06$; IF ($m^+ < -0.06$) $m^+ = -0.06$

List of Symbols

DFE	=	dF/dU^*	, Derivative of error function (dimensionless)
DUPLUS	=	dU^+/dY^+	, Derivative of velocity (dimensionless)
EE	=	F^+/U^+	, Error (dimensionless)
FE	=	F^+	, Error function (dimensionless)
EPS	=	ϵ	, Error tolerance (dimensionless)
ITERL			, Maximum number of iterations permitted (dimensionless)
KB			, Matching point (dimensionless)
UPLUS	=	U^+	, Universal velocity at matching point (dimensionless)
USTA	=	$U^{*(i)}$	, Guess for friction velocity (dimensionless)
USTAR	=	U^*	, Friction velocity (dimensionless)
YB	=	Y	, Distance from wall (dimensionless)

Theory

The friction velocity is obtained by matching the inner layer analytical solution to the numerical solution at the point KB at a distance YB from the wall. This matching requires an iterative procedure since Eqs. (3.4.14), (3.4.18), or (3.4.22) are too complex to solve for U^*. The slope of the function $U^+(Y^+)$ is always known analytically so Newton's method is chosen. Let

$$U^+ = U / U^+ \tag{7.3.7.1}$$

$$Y^+ = \frac{N_R \, P_W}{(\mu_W / \mu_r)} U^* Y \tag{7.3.7.2}$$

$$P^+ = \frac{1}{\gamma N_R M_r^2} \left(\frac{\mu_W}{\mu_r}\right) \frac{V}{P_W U^{*3}} \left(\frac{\partial \Pi}{\partial S}\right)_W \tag{7.3.7.3}$$

$$m^+ = \frac{\dot{m}}{P_W U^*} \tag{7.3.7.4}$$

Then an error function is defined as

$$F^+(U^*) = U^+(Y^+) - U / U^* \tag{7.3.7.5}$$

and

$$\frac{dF^+}{dU^+} = \frac{N_R \, P_W}{(\mu_W / \mu_r)} Y \frac{dU^+}{dY^+} + \frac{U}{U^{*2}} \tag{7.3.7.6}$$

The iteration proceeds by setting

$$U^{*(i-1)} = U^{*(i)} - F(U^{*2}) / dF(U^{*(i)}) / U^{*(i)} \tag{7.3.7.7}$$

Convergence occurs when

$$\left|\frac{F}{J^{*(i)}}\right| < \epsilon \qquad (7.3.7.8)$$

7.3.8 Function FTHIK(Z,IS,LØP)

Object Compute Blade Thickness Distribution

Options

IS=ISHAPE Blade Shape Index
LØP=1 FTHIK = t/c
=2 FTHIK = d(t/c)/d(x/c)

List of Symbols

Z = X/C , Fractional Chordwise Distance (dimensionless)

Theory

A parabolic arc thickness distribution of the form

$$\frac{t}{c} = 4\left[\left(\frac{x}{c}\right)-\left(\frac{x}{c}\right)^2\right] \qquad (7.3.8.1)$$

is assumed for IS=1.

7.4 List of DIMENSION Variables in Blank COMMON

AINPUT(1,J,K) = Y , Spanwise location (dimensionless)

AINPUT(2,J,K) = Π_0 , Total pressure (lb/ft^2 abs)

AINPUT(3,J,K) = Π , Static pressure (lb/ft^2 abs)

AINPUT(4,J,K) = α , Swirl angle (deg to axis)

AINPUT(5,J,K) = Θ_0 , Total temperature (deg R)

J = 1 , Upstream of blade row (dimensionless)

J = 2 , Downstream of blade row (dimensionless)

K = 1,KLL , Number of spanwise stations

BINPUT(1,J,K) = Y , Spanwise location (dimensionless)

BINPUT(2,J,K) = Π_0 , Total pressure (lb/ft^2 abs)

BINPUT(3,J,K) = Π , Static pressure (lb/ft^2 abs)

BINPUT(4,J,K) = α , Swirl angle (deg to axis)

BINPUT(5,J,K) = Θ_0 , Total temperature (deg R)

J = 1 , Inlet flow

J = 2 , Exit flow

K = 1,KLL , Number of spanwise stations

CONST(1,L) $C_1(m^+)$, Velocity (dimensionless)

CONST(2,L) $C_2(m^+)$, Adiabatic stagnation enthalpy (dimensionless)

CONST(3,L) $C_3(m^+)$, Nonadiabatic stagnation enthalpy (dimensionless)

CONST(4,L) $C_4(m^+)$, Stream function (dimensionless)

CONST(5,L) $C_5(p^+)$, Velocity (dimensionless)

CONST(6,L) $C_6(p^+)$, Stream function (dimensionless)

CNST(I) = CØNST(J,L) , Interpolate values between L, L+1

L =1,20

DF(J,K) = $\partial F(J,2,K)/\partial S$, Streamwise derivatives (dimensionless)

DHF(1,K) = $(\partial\psi/\partial S)_H$, Homogeneous solution for stream function (dimensionless)

DHF(2,K) = $(\partial\Pi/\partial S)_H$, Homogeneous solution for static pressure (dimensionless)

DPF(1,K) = $(\partial\psi/\partial S)_P$, Particular solution for stream function (dimensionless)

DPF(2,K) = $(\partial\Pi/\partial S)_P$, Particular solution for static pressure (dimensionless)

K = 1,KL , Number of streamlines

F(1,I,K) = ψ , Stream function (dimensionless)

F(2,I,K) = U_S , Streamwise velocity (dimensionless)

F(3,I,K) = U_ϕ , Swirl velocity (dimensionless)

F(4,I,K) = Π , Static pressure (dimensionless)

F(5,I,K) = I , Entropy (dimensionless)

F(6,I,K) = Θ , Static temperature (dimenionless)

F(7,I,K) = P , Density (dimensionless)

I = 1 , Inlet conditions

= 2 , S =S

= 3 , S =S + dS

K = 1, KL , Number of streamlines

FF(1,I,K) = $\hat{M}$, Inviscid Mach number (dimensionless)

FF(2,I,K) = $\hat{\Pi}$, Inviscid static pressure (dimensionless)

FF(3,I,K) = $\hat{\Theta}$, Inviscid static temperature (dimensionless)

FF(4,I,K) = $\hat{\Theta}_0$, Inviscid total temperature (dimensionless)

FF(5,I,K) = $\hat{\Pi}_0$, Inviscid total pressure (dimensionless)

FF(6,I,K) = $\hat{P}$, Inviscid density (dimensionless)

FF(7,I,K) = $\hat{U}_s$, Inviscid streamwise velocity (dimensionless)

FF(8,I,K) = $\hat{U}_\phi$, Absolute swirl velocity (dimensionless)

FF(9,I,K) = $\hat{W}_\phi$, Relative swirl velocity (dimensionless)

FF(10,I,K) = $\hat{U}_B$, Blade velocity (dimensionless)

FF(11,I,K) = $\hat{\alpha}$, Absolute angle to axis (deg)

FF(12,I,K) = $\hat{\beta}$, Relative angle to axis (deg)

FF(13,I,K) = $\hat{I}$, Inviscid flow entropy (dimensionless)

FF(14,I,K) = $\hat{U}$, Magnitude of relative inviscid flow velocity (dimensionless)

FF(15,1,K) = $\hat{Z}_B$, Loss coefficient (dimensionless)

FF(15,2,K) = $\Delta\hat{I}_B$, Blade entropy rise (dimensionless)

FF(16,I,K) = $\hat{\psi}$, Stream function (dimensionless)

FF(17,1,K) = C_L , Lift coefficient(dimensionless)

FF(17,2,K) = C_D , Drag coefficient (dimensionless)

I = 1 , Upstream of blade row

= 2 , Downstream of blade row

K = 1, KL , Number of streamline

FG(1,K) = α , Inlet swirl angle (deg)

FG(2,K) = Π_o , Inlet stagnation pressure (dimensionless)

FG(3,K) = Θ_o , Inlet stagnation temperature (dimensionless)

FG(4,K) = M , Inlet Mach number (dimensionless)

FG(5,K) = P_o , Inlet stagnation density (dimensionless)

FG(6,K) = U , Inlet magnitude of velocity (dimensionless)

K = 1, KL , Number of streamlines

FØRC(1,K) = H_s , Streamwise force/area (dimensionless)

FØRC(2,K) = H_ϕ , Swirl force/area (dimensionless)

FØRC(3,K) = Ξ_s , Streamwise force/span (dimensionless)

FØRC(4,K) = Ξ_ϕ , Swirl force/span (dimensionless)

FØRC(5,K) = Φ_B , Blade dissipation /area (dimensionless)

K = 1,KL , Number of streamline (dimensionless)

G(1,K) = μ_E / μ_r , Ratio of turbulent to reference molecular viscosity (dimensionless)

G(2,K) = $\sum_{sn}$, Streamwise stress (dimensionless)

G(3,K) = $\sum_{\phi n}$, Tangential stress (dimensionless)

G(4,K) = $\partial U_s / \partial n$, Normal derivative of streamwise velocity (dimensionless)

G(5,K) = $\partial U_\phi / \partial n$, Normal derivative of swirl velocity (dimensionless)

G(6,K) = $\partial \sum_{sn} / \partial n$, Normal derivative of streamwise stress(dimensionless)

G(7,K) = $\partial \sum_{\phi n} / \partial n$, Normal derivative of tangential stress (dimensionless)

G(8,K) = $U_\phi - U_B$, Relative velocity (dimensionless)

G(9,K) = U , Magnitude of relative velocity (dimensionless)

G(10,K) = E_{sn} , Streamwise rate of strain (dimensionless)

G(11,K) = $E_{\phi n}$, Tangential rate of strain (dimensionless)

G(12,K) = $\partial \Theta / \partial n$, Normal derivative of static temperature (dimensionless)

G(14,K) = $\partial I / \partial n$, Normal derivative of entropy (dimensionless)

G(15,K) = Q , Heat flux (dimensionless)

G(16,K) = $\partial Q / \partial n$, Normal derivative of heat flux (dimensionless)

Q(1,K)= R , Radius (dimensionless)

Q(2,K) = Z , Axial Distance (dimensionless)

$Q(3,K) = \partial R/\partial \eta$, Normal derivative of radius (dimensionless)

$Q(4,K) = \partial R/\partial S$, Streamwise derivative of radius (dimensionless)

$Q(5,K) = \partial^2 R/\partial \eta/\partial S$, Second derivative of radius (dimensionless)

$Q(6,K) = V$, Metric scale coefficient (dimensionless)

$Q(7,K) = \partial V/\partial \eta$, Curvature of potential line (dimensionless)

$Q(8,K) = \partial V/\partial S$, Curvature of streamline (dimensionless)

$Q(9,K) = \partial^2 V/\partial \eta/\partial S$, Second derivative of metric scale coefficient (dimensionless)

$Q(10,K) = Y$, Physical distance across duct (dimensionless)

$Q(11,K) = Y/Y_T$, Fractional distance across duct (dimensionless)

$Q(12,K) = A$, Area between ajacent streamlines (dimensionless)

$Q(13,K) = G$, Gap between blade surfaces (dimensionless)

$Q(14,K) = \partial G/\partial \eta$, Normal derivative of blade surface (dimensionless)

$Q(15,K) = \partial G/\partial S$, Streamwise derivative of blade surface (dimensionless)

$Q(16,K) = \partial \eta/\partial \eta$, Transform of normal coordinate (dimensionless)

$Q(17,K) = \partial^2 \eta/\partial \eta^2$, Second derivative (dimensionless)

$Q(18,K) = \eta$, Normal coordinate (dimensionless)

$Q(19,K) = \eta$, Transformed normal coordinate (dimensionless)

$K = 1,KL$, Number of streamlines (dimensionless)

$R(1,1,J) = R_T(Z_J)$, Radius of hub (dimensionless)

$R(2,1,J) = R_H(Z_J)$, Radius of tip (dimensionless)

$R(1,2,J) = \dot{m}_T(Z_T)$, Mass flow of tip bleed (dimensionless)

$R(2,2,J) = \dot{m}_H(Z_J)$, Mass flow of hub bleed (dimensionless)

$R(1,3,J) = \Theta_H(Z_J)$, Wall temperature of tip (dimensionless)

$R(2,3,J) = \Theta_T(Z_J)$, Wall temperature of hub (dimensionless)

$R\emptyset(1,K) = R$, Radius (dimensionless)

$R\emptyset(2,K) = dR/dZ$, Derivative of radius (dimensionless)

$R\emptyset(3,K) = d^2R/dZ^2$, Second derivative of radius (dimensionless)

$R\emptyset(4,K) = Z$, Axial distance (dimensionless)

$R\emptyset(5,K) = V$, Metric scale coefficient (dimensionless)

$R\emptyset(6,K) = dY/dS$, Derivative of metric scale coefficient (dimensionless)

$R\emptyset(7,K) = Y_T$, Distance across duct (dimensionless)

$R\emptyset(8,K) = S$, Streamwise coordinate (dimensionless)

$R\emptyset(9,K) = \dot{m}$, Mass flow bleed (dimensionless)

$R\emptyset(10,K) = \Theta_W$, Wall temperature (dimensionless)

$R\emptyset S(I) \equiv R\emptyset(I,K)$

Note: 3 arrays defined where $\emptyset$ takes on the value H, M, T

$\phi = H$, Hub Wall

M , Mean line

T , Tip wall

7.5 List of Variables in Blank COMMON

ACHI = χ , Clauser constant (0.016)

ACHAPPA = κ , von Karman constant (0.41)

ALP1 = α_1 , Hub swirl angle (deg)

ALPHS = α_S , Stagger angle to axis (deg)

ALPSH = α_H , Hub stagger angle to axis (deg)

ALPSM = α_M , Midpoint stagger angle to axis (deg)

ALPST = α_T , Tip stagger angle to axis (deg)

AMACH1 = $\bar{M}_1$, Average inlet Mach number (dimensionless)

AMACHR = M_r , Reference Mach number (dimensionless)

AMS1 = M_{S1} , Hub Mach number for input (dimensionless)

AMPLUS = m^+ , Mass flow bleed parameter (dimensionless)

ANH,ANT = n_H, n_T , Power law profile (dimensionless)

APLUS = A^+ , van Driest constant (26.0)

APRES1 = $\bar{P}_1$, Average inlet static pressure (dimensionless)

AREAR = a_r , Reference area (ft^2)

CHORD = B , Strut chord local (dimensionless)

CHORDH = B_H , Strut chord Hub (dimensionless)

CHORDM = B_M , Strut chord midpoint (dimensionless)

CHORDT = B_T , Strut chord tip (dimensionless)

CPR = c_{pr} , Specific heat at constant pressure (5997.0 $ft^2/sec^2/deg$ R)

CPV = c_{pv} , Specific heat at constant volume (3283.0 $ft^2/sec^2/deg$ R)

DDS , Mesh distortion parameter ($1. < DDS \leq 10.$)

DETA = $\Delta\eta$, Step size in Normal coordinate (dimensionless)

DMPLUS = Δm^+ , Step size in asymptotic constant table (m^+) (dimensionless)

DPLUSM = ΔP^+ , Step size in asymptotic constant table (p^+) (dimensionless)

DSH,DST = Δ^*_H, Δ^*_T , Displacement thickness hub, tip (dimensionless)

DS = AS , Streamwise step size between stations (dimensionless)

DSS = dS , Streamwise step size (dimensionless)

DYNP1 = q_1 , Average inlet dynamic pressure (dimensionless)

EP = , 2.7182818

GAMMA = γ , Ratio of specific heats (1.4)

GAP = G , Gap between blades (dimensionless)

GASR = R , Gas constant (1714.0 $ft^2/sec^2/$ deg R)

GMR1 = $(\gamma - 1) M_r^2$

GMR2 = γM_r^2

GRAVR = g , Gravitational constants (32.2 ft/sec^2)

ISHAPE , Blade shape parameter (dimensionless)

JL , Number of streamwise stations (dimensionless)

KDS , Number of streamwise steps/station (dimensionless)

KL , Number of streamlines (dimensionless)

KLL , Number of input streamlines (dimensionless)

KLMH , Hub matching point - inner layer (dimensionless)

KMT , Tip matching point - inner radius (dimensionless)

LM , Size of table of constants for inner layer (dimensionless)

LMM , Midpoint of table of constants for inner layer (dimensionless)

NB , Number of struts (dimensionless)

PHIC = ϕ_C , Blade camber (deg)

PHICH = ϕ_{CH} , Blade camber - hub (deg)

PHICM = ϕ_{CM} , Blade camber - midpoint (deg)

PHICT = ϕ_{CT} , Blade camber - tip (deg)

PPLUS = p^+ , Pressure gradient parameter (dimensionless)

PI = Π , 3.1415926

PRESSR = p_r , Reference static pressure (PSF)

PRL = p_{RL} , Prandtl Number laminar 0.70

PRT = p_{RT} , Prandtl number turbulent 0.72

RADR = r_r , Reference radius (ft)

REY = N_r , Reynolds number (dimensionless)

RCLH = R_{CLH} , Hub radius of blade centerline (dimensionless)

RCLM = R_{CLM} , Midpoint radius of blade center (dimensionless)

RCLT = R_{CLT} , Tip radius of blade centerline (dimensionless)

RHOR = ρ_r , Reference density (slugs/ft^3)

SL = S_L , Length of duct in streamline coordinates (dimensionless)

SNDR = c_r , Reference speed of sound 1116.0 (ft/sec)

SOLD = σ , Solidity (dimensionless)

TEMPR = T_r , Reference temperature (deg-RANKIN)

THICK = t , Local blade thickness (dimensionless)

THICKH = t_H , Blade thickness hub (dimensionless)

THICKM = t_M , Blade thickness midpoint (dimensionless)

THICK = t_T , Blade thickness tip (dimensionless)

THIKM	=	t/B	, Maximum thickness/chord (dimensionless)
TI	=		, (01745329 radians/deg)
USR	=	u_r	, Reference radius (dimensionless)
VISCR	=	μ_r	, Reference molecular viscosity (0.370×10^{-6})
WFLO	=	ω	, Weight flow (lb/sec)
YPLUSM	=	Y_M^+	, Matching point for table of asymptotic constants (dimensionless)
ZCL	=	Z_{CL}	, Axial distance to blade centerline (dimensionless)
ZLE	=	Z_{LE}	, Blade leading edge (dimensionless)
ZTE	=	Z_{TE}	, Blade trailing edge (dimensionless)
Z1	=	Z_1	, Duct axial length (dimensionless)

7.6 Description of Mesh Geometry

Since the numerical solution of turbulent boundary layer equations is required, the mesh points for the normal coordinate are not distributed uniformly across the duct, but crowded near the duct walls. This nonuniform distribution of mesh points is accomplished with the $\eta(n)$ transformation given by Eq. (7.2.4.5) in Subroutine CØØR. Thus the actual calculation is done in an $(\eta(n),S)$ coordinate system.

The (η,S) coordinate system is shown in Fig. (7.6.1). It consists of KL uniformly distributed mesh points on the normal coordinate and JL uniformly distributed mesh points in the streamwise direction. Since the explicit numerical integration method used in this report is conditionally stable, the coordinate in the streamwise direction usually requires a finer mesh then specified by JL. Thus the JL mesh points can further divide by KDS. Therefore

$$\eta = \Delta\eta\,(K-1) \qquad K = 1, KL \tag{7.6.1}$$

and

$$S = \Delta S\,(J-1) + dS\,(KS-1) \qquad J = 1, JL\,;\; KS = 1, KDS \tag{7.6.2}$$

The transformation $\eta(n)$ involves a parameter C which can be related to the distortion of mesh points by

$$C = \frac{\Pi\ DDS}{1+DDS} \tag{7.6.3}$$

where

$$DDS \cong \left(\frac{\Delta n}{\Delta\eta}\right)_w \tag{7.6.4}$$

Finally, it is noted that matching the inner layer solution with the numerical solution occurs at KMH and KMT.

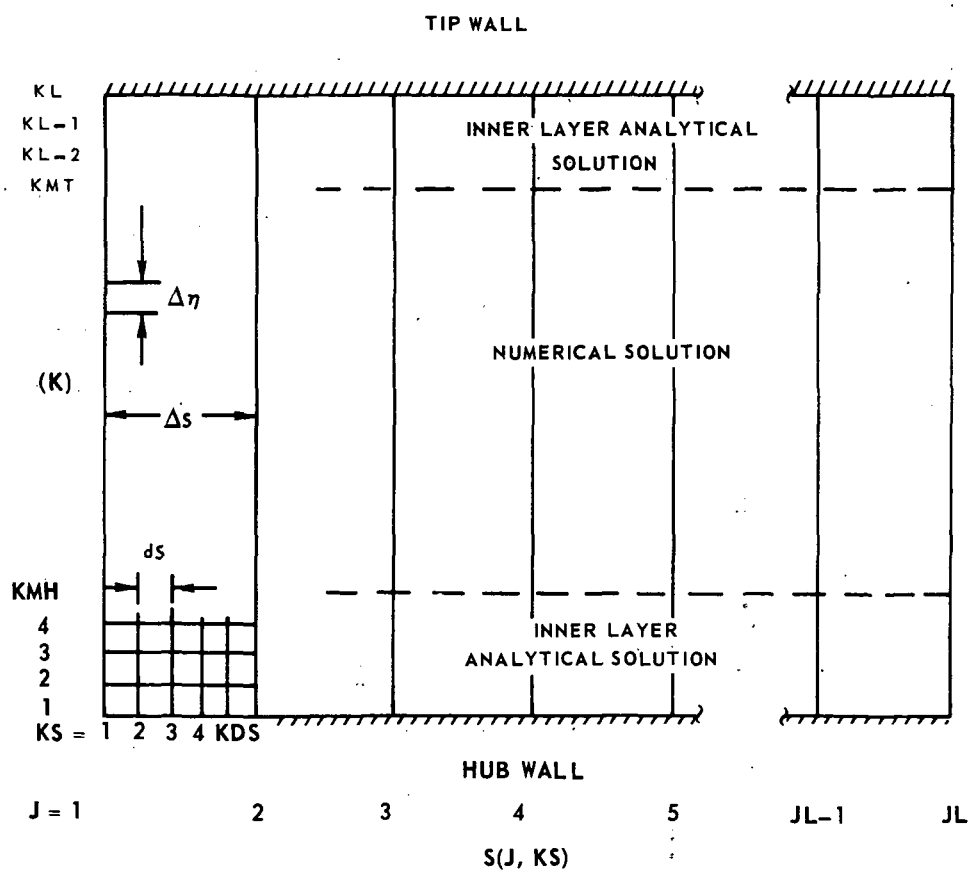

FIG. 7.6.1-(η,S) MESH GEOMETRY.

8.0 APPENDIX B: SAMPLE TEST CASES

A number of test cases are shown in this section to illustrate the various options available in the computer program and to test the accuracy of the calculation by comparison with experimental data where possible. Included with the write-up is an input data sheet used to set up the problem.

8.1 Boundary Layer in Entrance Region of Circular Pipe

This case illustrates use of the computer program to obtain the development of the boundary layer in the inlet region of a circular pipe where the streamwise pressure gradient is small and the boundary layer is thin. The calculated wall friction coefficients as a function of Reynolds number based on momentum thickness for $M_\infty = 0.1$ with different values for von Karman constant κ are plotted in Fig. 8.1.1 and compared with the wall friction laws obtained from Ref. 14. Calculated wall friction coefficients and recovery factors as a function of Reynolds number based on momentum thickness for a range of Mach numbers are plotted in Fig. 8.1.2. The computed wall friction coefficients are compared with the correlations of Ref. 20.

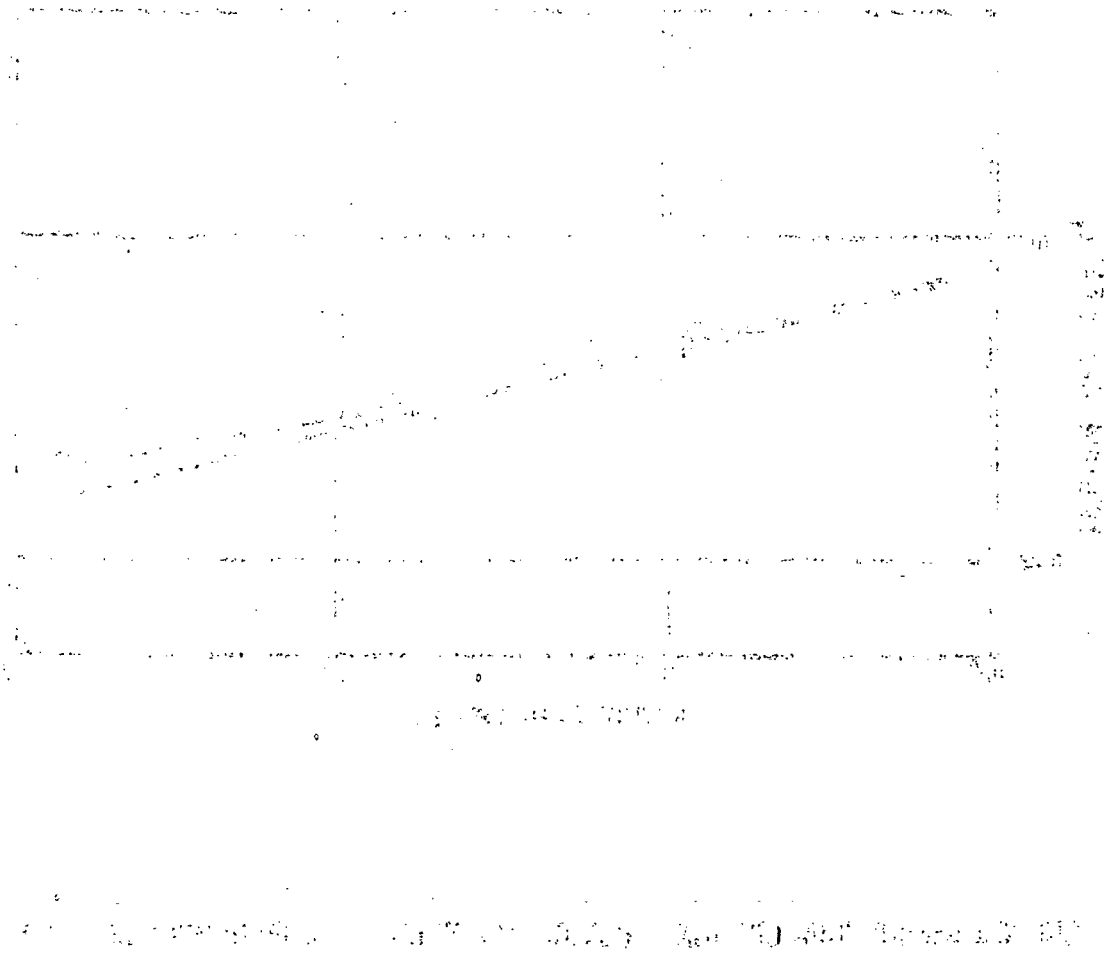

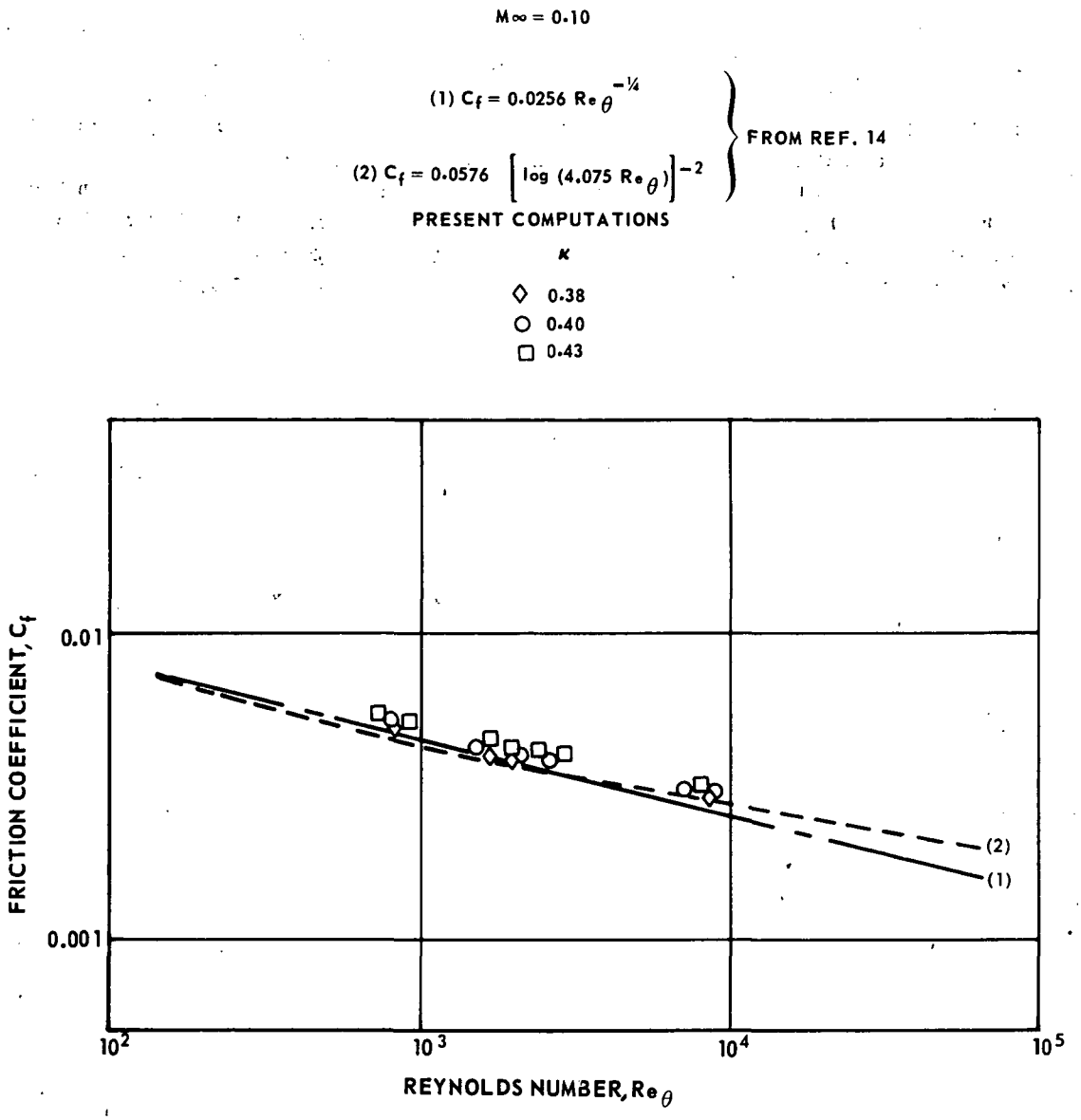

FIG. 8.1.1–VARIATION OF SKIN FRICTION COEFFICIENT WITH REYNOLDS NUMBER.

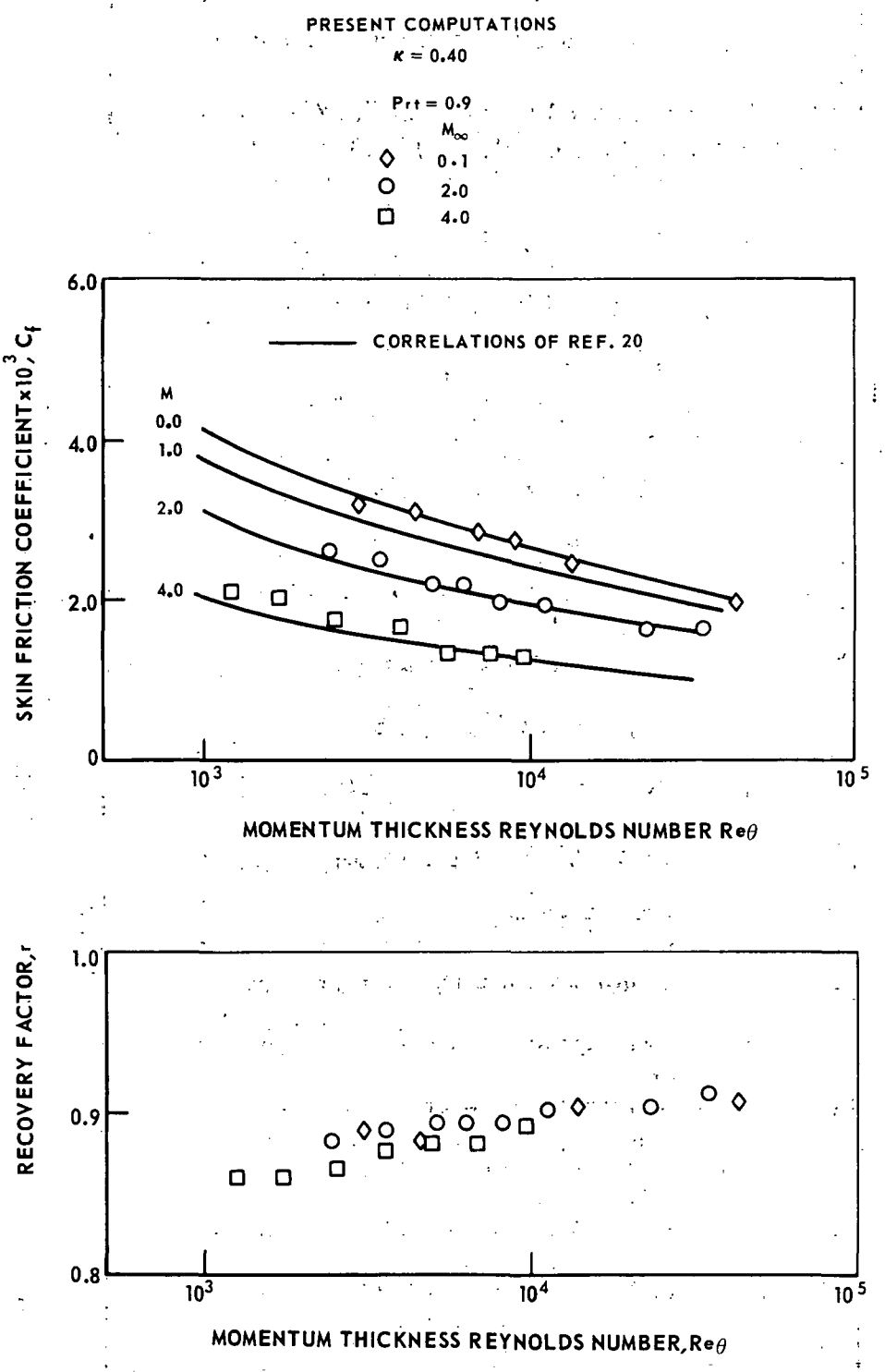

FIG. 8.1.2–VARIATION OF SKIN FRICTION COEFFICIENT AND RECOVERY FACTOR WITH REYNOLDS NUMBER.

UAC CODING FORM #3

ENGINEER ______ MAIL ADDRESS ______ EXTENSION ______

TITLE ______ ANALYST ______ SHEET ______ OF ______

JOB NO. ______ ACCT. NO. ______ W. O. NO. ______

```
ENTRANCE REGION OF CIRCULAR PIPE ADIABATIC WALL
 1
   5.0     26 26  5
   .0        1.0        10.
   MS1       .0                 .01                 7.
 PRESO      519.              AKAPPA

   MS1 = .10    PRESO = 6317.6   AKAPPA = .38
         2.0            4234.0            .40
         4.0            2117.0            .43
                         458.7
```

8.2 Conical Pipe Diffuser

The computed effect of compressibility on the performance of a subsonic conical pipe diffuser is shown in Fig. 8.2.1 and compared with the experimental data from Ref. 21. The solutions are in good agreement with the experimental data showing the increase in pressure recovery with increasing Mach number as well as a drop in pressure at the diffuser throat. This trend is also indicated by the data in Ref. 5. Shown also on Fig. 8.2.1 is the incompressible solution for this diffuser obtained from the numerical procedure described in Ref. 6. These results follow the trend in pressure recovery with Mach numbers; however, the trend in the predicted separation point with Mach number is not consistent with that for the present compressible solutions. This may be partially explained by the fact that the compressible solution tends to calculate slightly higher wall friction coefficients than measured experimentally (see Fig. 8.1.1).

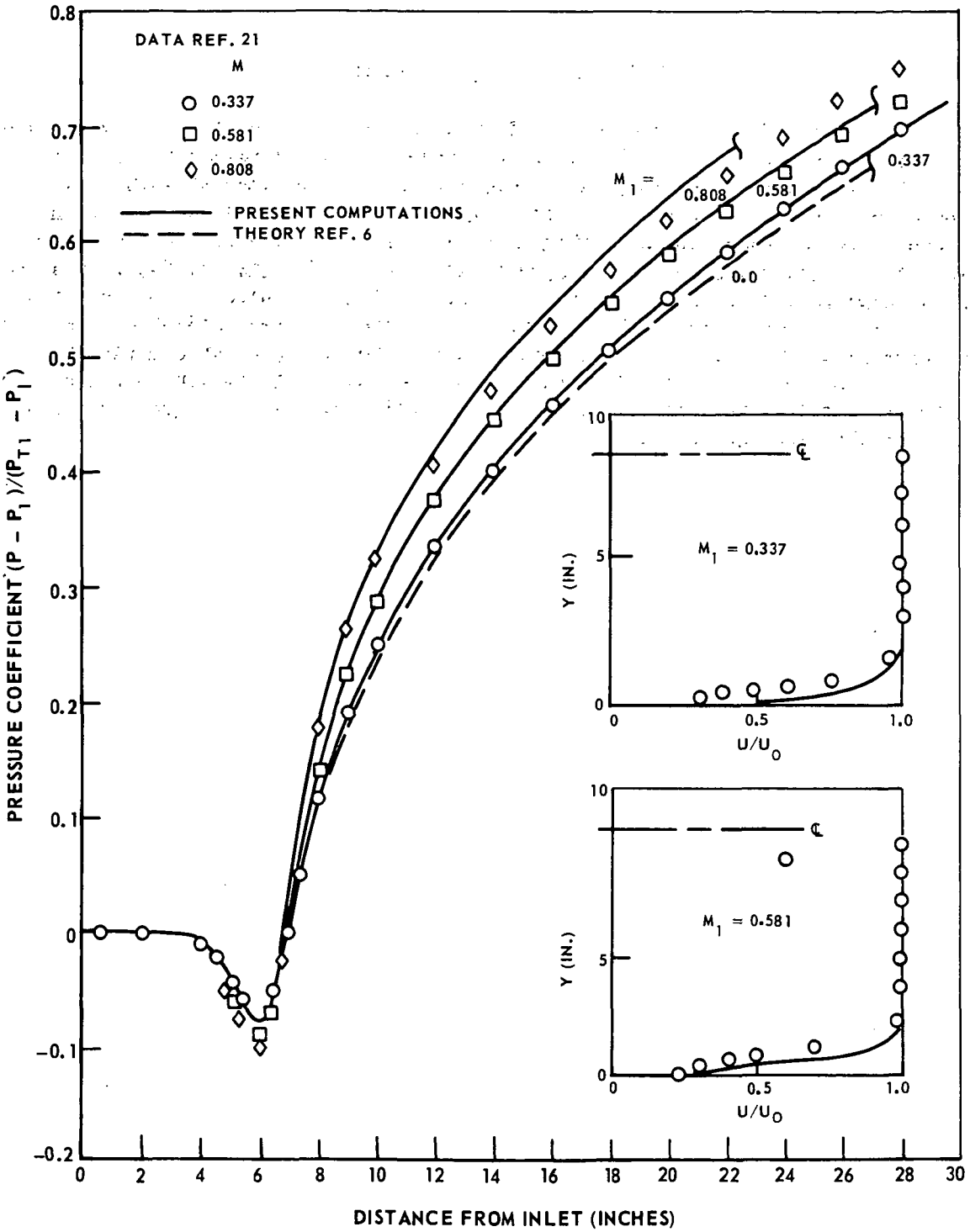

FIG. 8.2.1–EFFECT OF INLET MACH NUMBER ON PRESSURE COEFFICIENT IN A 10° CONICAL DIFFUSER.

UAC CODING FORM #3

ENGINEER _____ MAIL ADDRESS _____ EXTENSION _____

TITLE _____ ANALYST _____ SHEET _____ OF _____

JOB NO. _____ ACCT. NO. _____ W. O. NO. _____

```
SUBSONIC CONICAL DIFFUSER   NACA  RM L51E11A , 1951
1   3
   5.      26 26   5
   .0          .4167      2.467      .5          .0          5.0
   MS1         .0                    .0025                  7.0
         BLANK CARD

   MS1 =  .337
          .581
          .808
```

140

8.3 Annular Diffuser

The computed pressure coefficients for a curved-wall annular diffuser are presented in Fig. 8.3.1 for two different inlet Mach numbers ($M_1 = 0.47$ and $M_1 = 0.75$) and compared with the data of Ref. 22. The predicted pressure recoveries are in good agreement with the experimental data and the trend of increasing pressure recovery with increasing inlet Mach number is again demonstrated. It should be noted that the computed wall pressure coefficients presented in Fig. 8.3.1 are not those obtained directly from the computer output but were corrected to allow direct comparison with the experimental data which is based on a dynamic pressure obtained from a free-stream Mach number rather than a weight-flow-averaged Mach number.

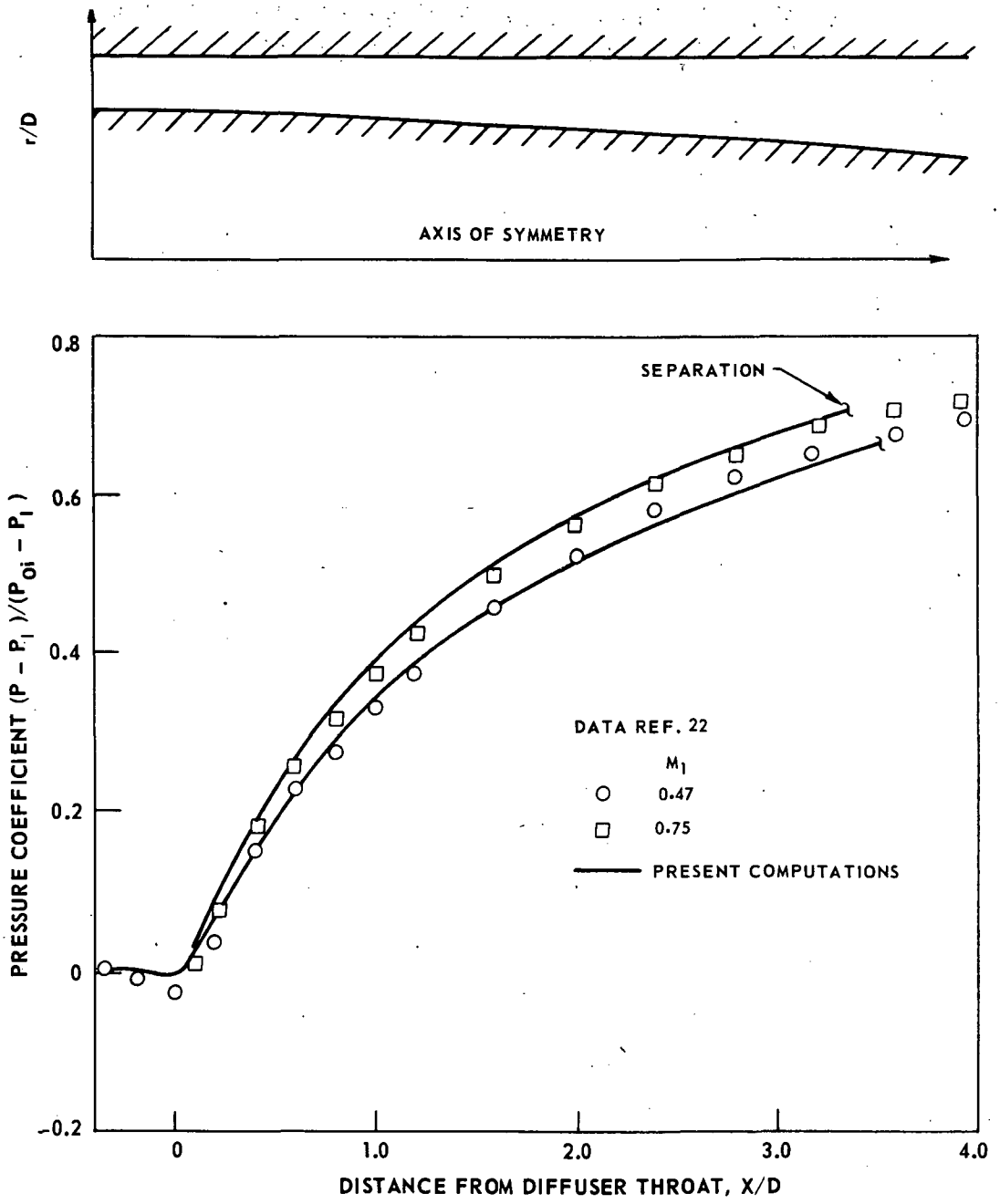

FIG. 8.3.1 – EFFECT OF INLET MACH NUMBER ON PRESSURE COEFFICIENT FOR AN ANNULAR DIFFUSER.

UAC CODING FORM #3

ENGINEER _____ MAIL ADDRESS _____ EXTENSION _____

TITLE _____ ANALYST _____ SHEET _____ OF _____

JOB NO. _____ ACCT. NO. _____ W. O. NO. _____

```
CURVED WALL ANNULAR DIFFUSER  NACA RM L58A31  APRIL 1958
 1  3  3
    5.0          26 26  .5
                BLANK CARD
MS1                .0          .002        .002        7.          7.
                BLANK CARD

                MS1 =  :47
                       :75
```

8.4 Curved-Wall Diffuser With Struts

The computed pressure recovery coefficients for the NASA curved-wall diffuser ($M_1 = 0.47$) described in Ref. 22 and Section 8.3 were recalculated with the addition of two streamline struts placed in the diffuser as shown in Fig. 8.4.1. These streamline-struts were NASA 5 digit series uncambered airfoil sections with a one foot chord and 20 percent thickness-to-chord ratio. The primary effect of these struts is to lower the static pressure coefficient in the region of the strut due to the increased flow Mach number. There has also been a slight loss in pressure coefficient due to the blade loss. It should be noted that the solution does not account for the slight additional flow blockage due to the strut boundary layer growth. In addition, the increased losses due to the interaction of the strut boundary layer with the annulus wall boundary layer are not taken into account.

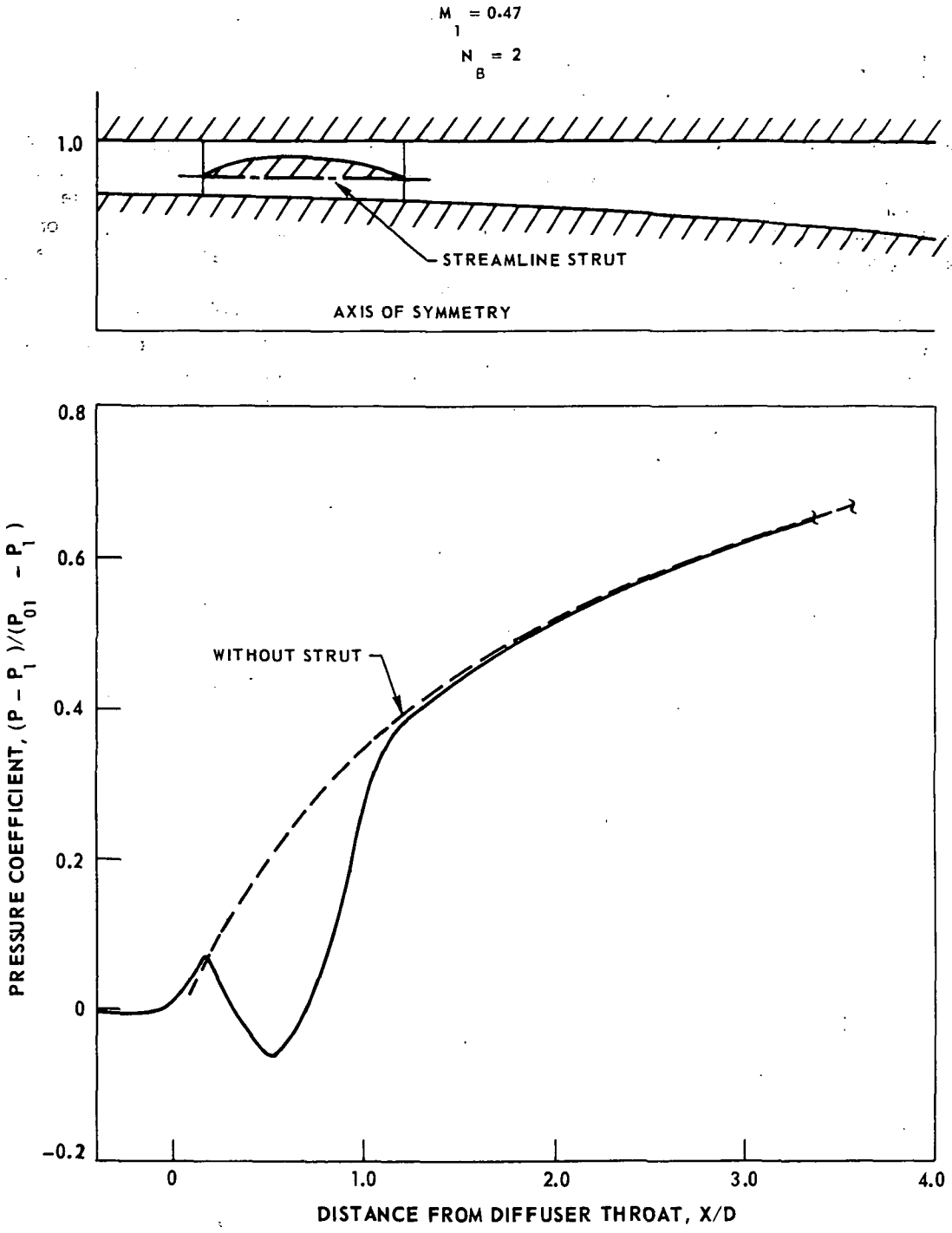

FIG. 8.4.1. – COMPUTED STATIC PRESSURE DISTRIBUTION IN AN ANNULAR DIFFUSER WITH STREAMLINE STRUTS.

UAC CODING FORM #3

ENGINEER _____ MAIL ADDRESS _____ EXTENSION _____

TITLE _____ ANALYST _____ SHEET _____ OF _____

JOB NO. _____ ACCT. NO. _____ W. O. NO. _____

```
CURVED WALL DIFFUSER WITH STRUTS
 133
   5.0      26 26  5
          BLANK CARD
  .47       .0        .002      .002      7.        7.
   1.0      2  1
           .0              1.        .2        .0
           .0              1.        .2        .0
           .0              1.        .2        .0
          BLANK CARD
```

8.5 Curved-Wall Annular Duct With Bleed

In Section 8.3, the flow through an annular diffuser at $M_1 = 0.47$ was found to separate at a distance $X/D = 3.5$ (see Fig. 8.3.1). This separation occurred on the tip wall. Since blowing tends to promote separation and suction tends to delay separation, a solution was obtained for blowing on the hub wall and suction on the tip wall with bleed rates on each wall of 0.02 $lb/sec/ft^2$. Since there is essentially no net change in mass flow with and without bleed for this diffuser, a comparison of the velocity distributions can be made without compensating for differences in mass flow. This comparison, shown in Fig. 8.5.1, indicates that the hub boundary layer is blown out from the wall and the tip boundary layer is sucked in towards the wall. In addition, the computations predicted that separation on the tip wall was delayed to $X/D = 3.7$.

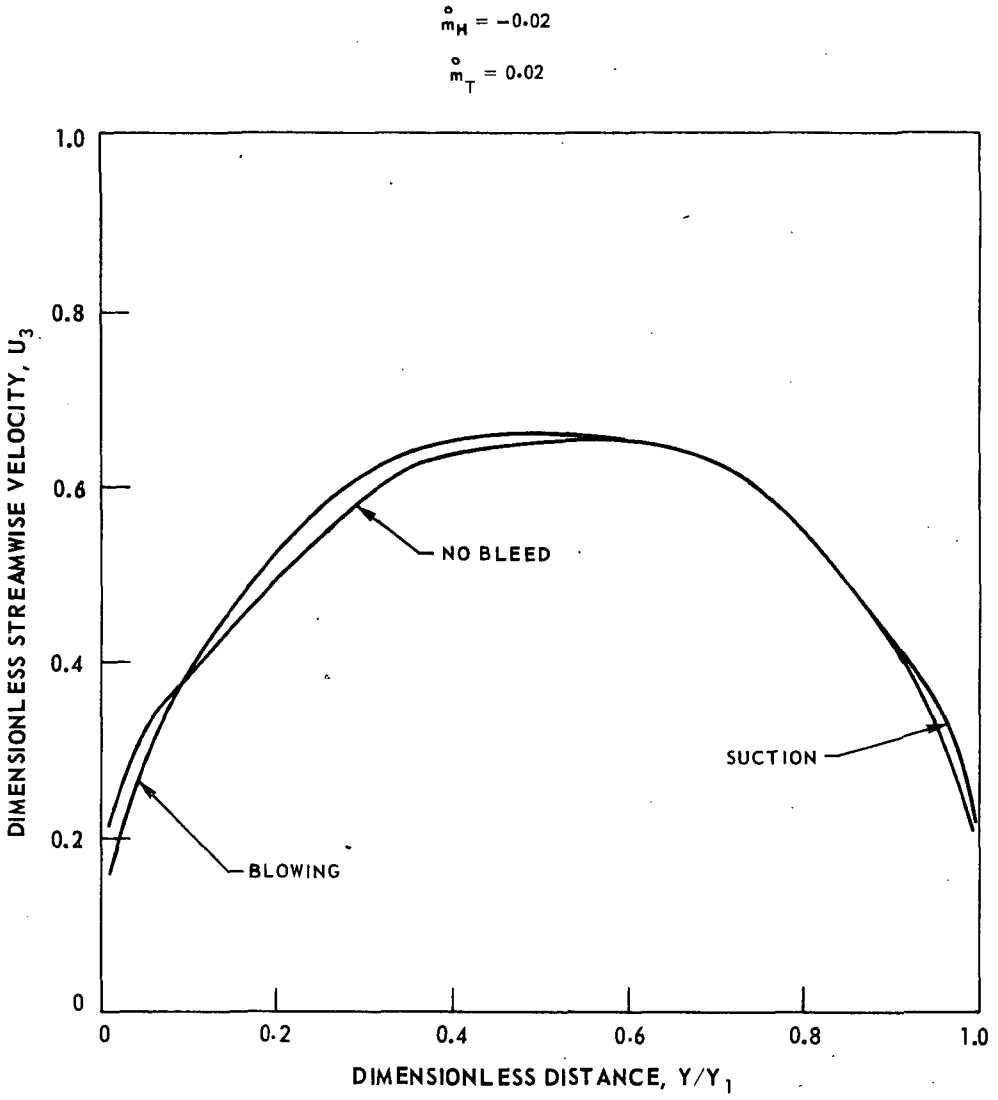

FIG. 8.5.1. – VELOCITY DISTRIBUTIONS IN A CURVED-WALL DIFFUSER WITH BLOWING AND SUCTION.

UAC CODING FORM #3

ENGINEER ______ MAIL ADDRESS ______ EXTENSION ______

TITLE ______ ANALYST ______ SHEET ____ OF ____

JOB NO. ______ ACCT. NO. ______ W. O. NO. ______

```
CURVED WALL DIFFUSER WITH BLEED
 1 3 3
   5.0     26 26  5
                      .02       -.02
  .47       .0        .002      .002      7.        7.
            BLANK CARD
```

NATIONAL AERONAUTICS AND SPACE ADMINISTRATION
WASHINGTON, D.C. 20546

OFFICIAL BUSINESS
PENALTY FOR PRIVATE USE $300

SPECIAL FOURTH-CLASS RATE BOOK

POSTAGE AND FEES PAID
NATIONAL AERONAUTICS AND SPACE ADMINISTRATION
451

U.S.MAIL

POSTMASTER: If Undeliverable (Section 158 Postal Manual) Do Not Return

"The aeronautical and space activities of the United States shall be conducted so as to contribute . . . to the expansion of human knowledge of phenomena in the atmosphere and space. The Administration shall provide for the widest practicable and appropriate dissemination of information concerning its activities and the results thereof."

—NATIONAL AERONAUTICS AND SPACE ACT OF 1958

NASA SCIENTIFIC AND TECHNICAL PUBLICATIONS

TECHNICAL REPORTS: Scientific and technical information considered important, complete, and a lasting contribution to existing knowledge.

TECHNICAL NOTES: Information less broad in scope but nevertheless of importance as a contribution to existing knowledge.

TECHNICAL MEMORANDUMS: Information receiving limited distribution because of preliminary data, security classification, or other reasons. Also includes conference proceedings with either limited or unlimited distribution.

CONTRACTOR REPORTS: Scientific and technical information generated under a NASA contract or grant and considered an important contribution to existing knowledge.

TECHNICAL TRANSLATIONS: Information published in a foreign language considered to merit NASA distribution in English.

SPECIAL PUBLICATIONS: Information derived from or of value to NASA activities. Publications include final reports of major projects, monographs, data compilations, handbooks, sourcebooks, and special bibliographies.

TECHNOLOGY UTILIZATION PUBLICATIONS: Information on technology used by NASA that may be of particular interest in commercial and other non-aerospace applications. Publications include Tech Briefs, Technology Utilization Reports and Technology Surveys.

Details on the availability of these publications may be obtained from:

SCIENTIFIC AND TECHNICAL INFORMATION OFFICE

NATIONAL AERONAUTICS AND SPACE ADMINISTRATION

Washington, D.C. 20546